A study of the influence of thermal drying on physical coal properties

MJG Badenhorst

12016918

Dissertation submitted in fulfilment of the requirements for the degree *Master of Engineering* at the Potchefstroom Campus of the North-West University

Supervisor: **Prof. Q.P. Campbell**

November 2009

ABSTRACT

One of the major issues facing the coal industry today is the decline in economically recoverable reserves, especially in the Witbank / Mpumalanga region of South Africa. This necessitates a critical review of alternate coal sources. One such source was identified as previously discarded and currently arising coal fines. It is well known that great value lies within these fines, but that the high moisture content associated with fine coal leads to thermal inefficiencies, handling problems and increased transport cost. This study will investigate thermal drying as a feasible solution to effectively remove this moisture.

During thermal drying coal is fed into a high temperature environment; this can influence the physical and mechanical properties of the coal. The effects include swelling, caking, cracking, loss of water, loss of volatiles, and many more. These effects are investigated by means of thermogravimetric analysis, scanning electron microscopy with a heating stage, proximate analysis and mercury intrusion. Coal samples with an average particle size of 500 μm were selected for this study. It was found that:

- The rate of moisture loss up to temperatures between 150 and 200°C is at a maximum where after the rate declines up to temperatures between 350 and 450°C when primary devolatilisation initiates.
- No visual changes in the coal are observed up to temperatures between 350 and 450°C.
- A limited amount of volatiles evolve at a constant rate up to 250°C; this is not significant enough to decrease the calorific value of the coal.
- Porosity changes in the coal are observed from temperatures as low as 250°C.

Thermal drying was found to be a feasible alternative to currently employed drying methods with 150°C selected as the optimal drying temperature. A thermal drying plant is proposed with recommendations for future work needed to realise such a plant.

Keywords: Coal, Properties, Thermal, Drying, Vitrinite, Inertinite

OPSOMMING

Een van die grootste probleme in die hedendaagse steenkool industrie is die vermindering van ekonomies herwinbare reserwes, veral in die Witbank / Mpumalanga streke van Suid Afrika. Dit noodsaak ‘n kritiese oorsig van alternatiewe steenkool bronne. Een so ‘n bron is geïdentifiseer as voorheen verwerpte en huidige voortspruitende fyn steenkool. Dit is alom bekend dat die fyn steenkool baie waardevol is maar dat die hoë vog inhoud verbonde aan fyn steenkool lei tot termiese ondoeltreffendheid, hanteringsprobleme en ‘n toename in vervoerkoste. Hierdie studie sal termiese droging ondersoek as ‘n lewensvatbare oplossing om hierdie vog effektief te verwyder.

Gedurende termiese droging word steenkool gevoer na ‘n hoë temperatuur omgewing wat die fisiese en meganiese eienskappe van die steenkool kan beïnvloed. Die gevolg sluit swelling, koeking, kraking, verlies van water, verlies van vlugtige spesies en vele meer in. Hierdie gevolge word ondersoek deur middel van termogravimetriese analise, elektron skanderings mikroskopie met ‘n verhitter, samestellings analise en kwik indringing. Steenkool monsters met ‘n gemiddelde deeltjie grootte van 500 μm is gekies vir die studie. Daar is gevind dat:

- Die tempo van vog verlies tussen temperature van 150 en 200°C ‘n maksimum is waarna die tempo afneem tot temperature tussen 350 en 450°C wanneer primêre ontvlugtiging begin.
- Geen visuele veranderinge in die steenkool word waargeneem tot temperature tussen 350 en 450°C nie.
- ‘n Beperkte hoeveelheid vlugtige spesies onttrek teen ‘n konstante tempo tot ‘n temperatuur van 250°C. Dit is egter nie genoeg om die kaloriewaarde van die steenkool te beïnvloed nie.
- Porositeitsveranderinge in die steenkool word waargeneem van temperature so laag as 250°C.

Daar is gevind dat termiese droging ‘n geskikte alternatief vir huidige drogings metodes is met 150°C aangewys as die optimale drogings temperatuur. ‘n Termiese drogings aanleg word voorgestel met aanbevelings vir verdere studies benodig om so aanleg te verwesenlik.

Sleutelwoorde: Steenkool, Eienskappe, Termiese, Droging, Vitriniet, Inertiniet

ACKNOWLEDGMENTS

I would like to thank the School for Chemical and Mineral Engineering at the North-West University as well as my sponsor, COALTECH 2020, for giving me the opportunity and financial support to complete the research in this study.

In particular I would like to thank my study leader, Prof. Quentin Campbell for his guidance, insight and support throughout this study.

I would also like to thank the personnel at the School for Chemical and Mineral Engineering who made available the facilities and equipment required for this research.

To my parents, daughters and particularly my wife Riki, thank you for believing in me, for all your support and encouragement.

To God be the glory for the ability and inspiration I received to complete this work.

TABLE OF CONTENTS

ABSTRACT **1**
OPSOMMING 2
ACKNOWLEDGMENTS **3**
TABLE OF CONTENTS **4**
FIGURES – SHORT LIST **7**
GRAPHS **9**
TABLES **10**
NOMENCLATURE **11**
1. INTRODUCTION **12**
1.1 Introduction and motivation 12
1.2 Objectives 13
1.3 Scope of investigation 13
2. LITERATURE SURVEY **15**
2.1 Introduction 15
2.2 The future of coal; renewable energy and the hydrogen economy 16
2.2.1 Renewable energy 16
2.2.2 Hydrogen economy 17
2.3 Properties of coal 18
2.3.1 The nature of coal 18
2.3.2 Types of water associated with coal 19
2.3.3 Reasons for dewatering fine coal 19
2.4 Other research and results 20
2.4.1 Fragmentation behaviour during heating 21
2.4.2 Thermal behaviour during heating 23
2.4.3 Mass loss during heating 24
2.4.4 Volatile evolution during heating 25
2.4.5 Chemical and structural changes during heating 27
2.4.6 Swelling and plasticity 29
2.4.7 The pore structure of coal 30
2.4.8 Catalytic effect of impurities 30
2.5 Mechanisms proposed by others 31
2.6 Different drying methods 34
2.6.1 Steam drying 34
2.6.2 Vacuum drying 35
2.6.3 Hydrothermal dewatering 35

2.6.4 Air-drying 36
2.6.5 Gas flow drying 37
2.6.6 Drying by supercritical CO_2 with methanol as entrainer 37
2.7 Industrial thermal dryers 37
2.7.1 Cabinet dryers 37
2.7.2 Calciners 38
2.7.3 Conveyor dryers 38
2.7.4 Flash dryers 39
2.7.5 Fluid bed dryers 40
2.7.6 Indirect dryers 40
2.7.7 Infrared dryers 43
2.7.8 Rotary dryers 43
2.7.9 Specialized dryers – microwave dryers 44
2.7.10 Spray dryers 45
2.8 Spontaneous combustion 46
3. METHODS AND PROCEDURES 47
3.1 Introduction 47
3.2 Experimental procedures and tests 47
3.2.1 Crushing and separation techniques 48
3.2.2 TGA (thermogravimetric analyser) experiments 49
3.2.3 SEM (scanning electron microscope) 50
3.2.4 Nitrogen furnace with proximate analysis 51
3.2.4.1 Nitrogen furnace and preparation of coal samples 51
3.2.4.2 Proximate analysis 53
3.2.5 Mercury intrusion 57
4. RESULTS AND DISCUSSION 60
4.1 Introduction 60
4.2 TGA results 61
4.2.1 TGA results for the WB2 coal 61
4.2.2 TGA results for the WB4 coal 62
4.2.3 TGA results for the TS coal 63
4.2.4 TGA results for the GG coal 64
4.2.5 TGA results for the NV coal 65
4.2.6 Discussion of TGA results 65
4.3 SEM results 66
4.3.1 SEM results for the WB2 coal 66
4.3.2 SEM results for the WB4 coal 73

4.3.3 SEM results for the TS coal 78
4.3.4 SEM results for the GG coal 82
4.3.5 SEM results for the NV coal 90
4.3.6 Discussion of SEM results 96
4.4 Proximate analysis results 96
4.4.1 Proximate analysis results for the WB2 coal 97
4.4.2 Proximate analysis results for the WB4 coal 99
4.4.3 Proximate analysis results for the TS coal 101
4.4.4 Proximate analysis results for the GG coal 103
4.4.5 Proximate analysis results for the NV coal 105
4.4.6 Discussion of proximate analysis results 107
4.5 Mercury intrusion results 108
4.5.1 Mercury intrusion results for the WB2 coal 108
4.5.2 Mercury intrusion results for the WB4 coal 110
4.5.3 Mercury intrusion results for the NV coal 112
4.5.4 Discussion of mercury intrusion results 114
5. PLANT PROPOSAL 115
5.1 Feasibility of a thermal drying plant 115
5.2 Development of a thermal drying process 117
5.3 Calculation of energy requirement 119
6. CONCLUSIONS 123
6.1 Introduction 123
6.2 Conclusions and discussion 123
6.3 Recommendations for further research 125
APPENDIX A: SEM sample photos 126
APPENDIX B: Moisture content graphs 134
APPENDIX C: Tabulated proximate analysis results 138
APPENDIX D: Tabulated mercury intrusion results 144
BIBLIOGRAPHY 147

FIGURES – SHORT LIST

Figure 2.2.1(a): Representation of the world fuel shares for energy consumption in 2006 16
Figure 2.2.1(b): Potential of various energy sources as compared to global energy needs 17
Figure 2.4.1: Graphical representation of the fragmentation model prop. by Dacombe *et al.* ... 22
Figure 2.5.1: Graphical representation of the mechanism proposed by Jarvinen *et al.* 32
Figure 2.7.1: Illustration of a cabinet dryer 37
Figure 2.7.2: Illustration of a calciner 38
Figure 2.7.3: Illustration of conveyor dryers 38
Figure 2.7.4: Illustration of flash dryers 39
Figure 2.7.5: Illustration of fluid bed dryers 40
Figure 2.7.6.1: Illustration of a drum dryer 41
Figure 2.7.6.2: Illustration of a paddle dryer 42
Figure 2.7.6.3: Illustration of a steam tube dryer 42
Figure 2.7.7: Illustration of a infrared dryer 43
Figure 2.7.8: Illustration of rotary dryers 44
Figure 2.7.10: Illustration of spray dryers 45
Figure 3.2.1: Illustr. of crush. & sep. tech. to sep. coal samp. into their size and maceral frac. 48
Figure 3.2.2: Illustration of the thermogravimetric analyser 49
Figure 3.2.3: Illustration of the scanning electron microscope 51
Figure 3.2.4.1: Preparation of the proximate analysis samples in the nitrogen furnace 52
Figure 3.2.4.2.1: Vacuum oven - apparatus used to determine moisture content 54
Figure 3.2.4.2.2: Volatile oven - apparatus used to determine volatile content 55
Figure 3.2.4.2.3: Ash oven - apparatus used to determine ash content 56
Figure 3.2.4.2.5: Bomb calorimeter - apparatus used to determine calorific value 57
Figure 3.2.5: Autopore IV 9500 porosimeter - apparatus used to determine porosity 58
Figure 4.3.1(a): SEM image observation for heating of the WB2 inertinite coal 67
Figure 4.3.1(b): SEM image observation for heating of the WB2 mixture coal 68
Figure 4.3.1(c): SEM image observation for heating of the WB2 mixture coal 69
Figure 4.3.1(d): SEM image observation for heating of the WB2 vitrinite coal 70
Figure 4.3.1(e): SEM image observation for heating of the WB2 vitrinite coal 71
Figure 4.3.1(f): SEM image observation for heating of the WB2 vitrinite coal 72
Figure 4.3.2(a): SEM image observation for heating of the WB4 inertinite coal 73
Figure 4.3.2(b): SEM image observation for heating of the WB4 inertinite coal 74
Figure 4.3.2(c): SEM image observation for heating of the WB4 mixture coal 75
Figure 4.3.2(d): SEM image observation for heating of the WB4 mixture coal 76
Figure 4.3.2(e): SEM image observation for heating of the WB4 vitrinite coal 77

Figure 4.3.2(f): SEM image observation for heating of the WB4 vitrinite coal 78
Figure 4.3.3(a): SEM image observation for heating of the TS inertinite coal 78
Figure 4.3.3(b): SEM image observation for heating of the TS inertinite coal 79
Figure 4.3.3(c): SEM image observation for heating of the TS mixture coal 80
Figure 4.3.3(d): SEM image observation for heating of the TS vitrinite coal 81
Figure 4.3.3(e): SEM image observation for heating of the TS vitrinite coal 82
Figure 4.3.4(a): SEM image observation for heating of the GG inertinite coal 83
Figure 4.3.4(b): SEM image observation for heating of the GG inertinite coal 84
Figure 4.3.4(c): SEM image observation for heating of the GG mixture coal 85
Figure 4.3.4(d): SEM image observation for heating of the GG mixture coal 86
Figure 4.3.4(e): SEM image observation for heating of the GG mixture coal 87
Figure 4.3.4(f): SEM image observation for heating of the GG mixture coal 88
Figure 4.3.4(g): SEM image observation for heating of the GG vitrinite coal 88
Figure 4.3.4(h): SEM image observation for heating of the GG vitrinite coal 89
Figure 4.3.4(i): SEM image observation for heating of the GG vitrinite coal 90
Figure 4.3.5(a): SEM image observation for heating of the NV inertinite coal 91
Figure 4.3.5(b): SEM image observation for heating of the NV mixture coal 92
Figure 4.3.5(c): SEM image observation for heating of the NV mixture coal 93
Figure 4.3.5(d): SEM image observation for heating of the NV vitrinite coal 94
Figure 4.3.5(e): SEM image observation for heating of the NV vitrinite coal 95
Figure 5.2: Simplified thermal drying plant flow diagram 118
Figure A.1.1: SEM WB2 inertinite experimental coal sample 126
Figure A.1.2: SEM WB2 mixture experimental coal sample 127
Figure A.1.3: SEM WB2 vitrinite experimental coal sample 127
Figure A.2.1: SEM WB4 inertinite experimental coal sample 128
Figure A.2.2: SEM WB4 mixture experimental coal sample 128
Figure A.2.3: SEM WB4 vitrinite experimental coal sample 129
Figure A.3.1: SEM TS inertinite experimental coal sample 129
Figure A.3.2: SEM TS mixture experimental coal sample 130
Figure A.3.3: SEM TS vitrinite experimental coal sample 130
Figure A.4.1: SEM GG inertinite experimental coal sample 131
Figure A.4.2: SEM GG mixture experimental coal sample 131
Figure A.4.3: SEM GG vitrinite experimental coal sample 132
Figure A.5.1: SEM NV inertinite experimental coal sample 132
Figure A.5.2: SEM NV mixture experimental coal sample 133
Figure A.5.3: SEM NV vitrinite experimental coal sample 133

GRAPHS

Graph 4.2.1: TGA mass loss graph for the WB2 coal 61
Graph 4.2.2: TGA mass loss graph for the WB4 coal 62
Graph 4.2.3: TGA mass loss graph for the TS coal 63
Graph 4.2.4: TGA mass loss graph for the GG coal 64
Graph 4.2.5: TGA mass loss graph for the NV coal 65
Graph 4.4.1(a): Proximate analysis results for the WB2 coal 98
Graph 4.4.1(b): Calorific value results for the WB2 coal 99
Graph 4.4.2(a): Proximate analysis results for the WB4 coal 100
Graph 4.4.2(b): Calorific value results for the WB4 coal 101
Graph 4.4.3(a): Proximate analysis results for the TS coal 102
Graph 4.4.3(b): Calorific value results for the TS coal 103
Graph 4.4.4(a): Proximate analysis results for the GG coal 104
Graph 4.4.4(b): Calorific value results for the GG coal 105
Graph 4.4.5(a): Proximate analysis results for the NV coal 106
Graph 4.4.5(b): Calorific value results for the NV coal 107
Graph 4.5.1: Mercury intrusion results for the WB2 coal 109
Graph 4.5.2: Mercury intrusion results for the WB4 coal 111
Graph 4.5.3: Mercury intrusion results for the NV coal 113
Graph B.1: Proximate analysis moisture content results for the WB2 coal 134
Graph B.2: Proximate analysis moisture content results for the WB4 coal 135
Graph B.3: Proximate analysis moisture content results for the TS coal 135
Graph B.4: Proximate analysis moisture content results for the GG coal 136
Graph B.5: Proximate analysis moisture content results for the NV coal 136

TABLES

Table C.1.1: Proximate analysis results for the WB2 virgin coal sample 138
Table C.1.2: Proximate analysis results for the WB2 vitrinite coal sample 138
Table C.1.3: Proximate analysis results for the WB2 mixture coal sample 138
Table C.1.4: Proximate analysis results for the WB2 inertinite coal sample 139
Table C.2.1: Proximate analysis results for the WB4 virgin coal sample 139
Table C.2.2: Proximate analysis results for the WB4 vitrinite coal sample 139
Table C.2.3: Proximate analysis results for the WB4 mixture coal sample 139
Table C.2.4: Proximate analysis results for the WB4 inertinite coal sample 140
Table C.3.1: Proximate analysis results for the TS virgin coal sample 140
Table C.3.2: Proximate analysis results for the TS vitrinite coal sample..... 140
Table C.3.3: Proximate analysis results for the TS mixture coal sample 140
Table C.3.4: Proximate analysis results for the TS inertinite coal sample 141
Table C.4.1: Proximate analysis results for the GG virgin coal sample 141
Table C.4.2: Proximate analysis results for the GG vitrinite coal sample..... 141
Table C.4.3: Proximate analysis results for the GG mixture coal sample 141
Table C.4.4: Proximate analysis results for the GG inertinite coal sample 142
Table C.5.1: Proximate analysis results for the NV virgin coal sample 142
Table C.5.2: Proximate analysis results for the NV vitrinite coal sample 142
Table C.5.3: Proximate analysis results for the NV mixture coal sample..... 142
Table C.5.4: Proximate analysis results for the NV inertinite coal sample 143
Table D.1.1: Mercury intrusion results for the WB2 vitrinite coal sample 144
Table D.1.2: Mercury intrusion results for the WB2 mixture coal sample..... 144
Table D.1.3: Mercury intrusion results for the WB2 inertinite coal sample..... 144
Table D.2.1: Mercury intrusion results for the WB4 vitrinite coal sample 145
Table D.2.2: Mercury intrusion results for the WB4 mixture coal sample..... 145
Table D.2.3: Mercury intrusion results for the WB4 inertinite coal sample..... 145
Table D.3.1: Mercury intrusion results for the NV vitrinite coal sample..... 145
Table D.3.2: Mercury intrusion results for the NV mixture coal sample 146
Table D.3.3: Mercury intrusion results for the NV inertinite coal sample..... 146
Table D.4: Mercury intrusion standard deviation results for the NV inertinite coal sample 146

Nomenclature

BC: Bomb calorimeter; instrument used to determine the calorific value of an experimental sample.

Devolatilisation: The evolution of volatile components from the complex coal structure as it is heated in an oxygenated environment.

Exinite: Lowest density, high reactivity coal maceral evolving from cuticles, spores, resin bodies and algae accumulating in sub-aquatic conditions.

GC: Gas chromatograph; instrument used to determine the chemical composition of a gas sample.

Inertinite: Highest density, low reactivity coal maceral evolving from woody trunks, branches, stems, stalks, bark, leaf tissue, shoots and detrital organic matter fusinitized in aerobic oxidizing conditions.

Macerals: Organic constituents making up the coal structure which evolves from the different organs or tissues of the original plant. The group macerals are termed vitrinite, exinite and inertinite.

Pyrolysis: Devolatilisation of coal under inert conditions.

SEM: Scanning electron microscope; instrument used to microscopically study experimental samples under extreme magnification.

TGA: Thermogravimetric analyser; instrument used to determine the loss of mass occurring in an experimental sample as it is heated.

Virgin coal sample: Original coal sample before gravity separation is done to separate coal samples into their maceral fractions.

Vitrinite: Medium density, high reactivity coal maceral evolving from woody trunks, branches, stems, stalks, bark, leaf tissue, shoots and detrital organic matter gelified / vitrinized in aquatic reducing conditions.

Proximate analysis: Analysis done to determine the composition of a coal sample in terms of ash, fixed carbon, volatile and moisture content. The calorific value is also determined as part of the proximate analysis using a BC.

Chapter 1 Introduction

This chapter will provide an introduction as well as motivation for the research done in this project. It will focus on the scope of the project and the main objectives will be stated.

1.1. Introduction and motivation

One of the major issues facing the coal industry today is the decline in economically recoverable reserves, especially in the Witbank / Mpumalanga region of South Africa. This necessitates a critical review of alternate coal sources; in this investigation the focus will be previously discarded and currently arising coal fines (defined as -500 μm).

It is well known that great value lies within these fines, but that there is a problem with the high moisture content usually associated with fine coal (Potter & Keogh, 1981:217-227). This leads to thermal inefficiencies, handling problems and increased transport costs (Murray & Evans, 1972:290-296). In a study that was conducted to stress the importance of fine coal dewatering, it was discovered that even 1 percent moisture decrease in three million tons of clean coal may lead to a US $300 000 saving in transport cost (Tao *et al.*, 2000:167-171).

Van der Merwe and Campbell (2002:417-420) found that thermal drying can decrease the moisture content in fine coal without any significant water re-absorption. Re-absorption which did occur was less than that observed in an equivalent air dried sample. The next issue to be addressed is how the coal quality changes during and after thermal drying. There are indications that the micro-porous structure of coal becomes damaged, with subsequent effects on combustion and gasification kinetics. It can also be expected that the loss in volatile matter will have consequences on the ease of combustion. For this reason industry tend to use drying techniques such as vacuum drying or steam drying. In this study the effects which thermal drying may have on the physical and chemical properties of fine coal will be investigated to determine whether thermal drying might be a feasible alternative to currently utilised drying methods.

1.2. Objectives

The following objectives were to be achieved in executing this study:

1. Determine the effect of heating on the physical properties of the dominant coal macerals found in South Africa namely vitrinite and inertinite; these properties include:
   a) Mass loss
   b) Physically observable changes on the coal surface
   c) Changes in the chemical composition and calorific value
   d) Changes in the porosity of the coal

2. Determine an optimum drying temperature considering the following effects:
   a) At what stage (temperature) the water and volatiles evolve from the complex coal structure (maximum water and minimum volatile loss).
   b) The influence of the drying temperature on the calorific value of the coal.
   c) Test the hypothesis that heating causes structural damage and deterioration of the pores.

3. Propose a thermal drying process which can be implemented in industry taking the above results into account and investigate the feasibility of such a process.

To meet these objectives, it was decided to set a scope for the investigation.

1.3. Scope of investigation

The scope of this study will include submitting coal samples collected from five different South African mines to the following experiments to obtain data which will be used to meet the objectives posed in paragraph 1.2:

1. The experimental samples will be crushed and sieved to obtain a particle size distribution of 425 to 600 microns. This size was selected as the average particle in this range is classified as fine coal and this 'larger' fraction tend to handle more easily than smaller fractions.

2. Submit the sieved samples to gravity separation to obtain a vitrinite rich, an inertinite rich and a mixture fraction to study in subsequent experiments. This is done to determine the effect of thermal drying on the individual maceral fractions of the coal samples.

3. The separated samples will be heated under inert conditions from ambient room temperature to 1000°C in a TGA, while mass loss data will be collected.

4. The separated samples will be analysed in a SEM while microphotographs are taken as the samples are heated to 930°C in order to study physically observable changes occurring on the surface of the particles.

5. The separated samples will be heated in a regular furnace (under inert conditions) up to predetermined temperatures where after proximate analysis experiments will be conducted to determine the sample's chemical composition and calorific value.

6. Mercury intrusion experiments will also be conducted on the samples, heated to predetermined temperatures in the furnace, to determine the porosity of the samples at the selected experimental temperatures.

Chapter 2 Literature Survey

A literature survey was conducted in order to investigate coal's importance in the world's energy future to ultimately see if investing in the development of a thermal drying process will still be economically feasible. Different drying techniques will be compared to see if thermal drying might be as feasible as the currently used drying methods. An in depth investigation will be done in the combustion / pyrolysis of coal, since the first part of this process is the drying phase, followed by devolatilisation / pyrolyzation and then combustion / char formation. The reason for the investigation into the later stages of combustion and pyrolyzation is firstly, that there is not much literature available on the drying process itself and secondly, that it is important to know what happens to coal should a thermal dryer's operating temperature overshoot. The changes which occur in the chemical structure of coal as it is heated will also be investigated. Lastly, the possibility of spontaneous combustion after heating will be discussed.

2.1. Introduction

Even with all the technology developed over recent years there are still a lot of unknown areas in the coal industry. One of the most important reasons for this is that the rank and composition of the coal varies from one place to another. One can thus say that each piece of coal is unique, and that a study done on coal in China, would not deliver the same results as a study done on South African coal. For this reason this study will be done to determine how various South African coals will react and change (water and volatiles released) when it is thermally dried.

This study will investigate coal's future as energy source in the world, the properties of coal, previous results obtained in this and nearby fields, the drying mechanisms proposed by others, the different drying methods available and the spontaneous combustion of coal, which might occur in stockpiles after drying.

2.2. The future of coal; renewable energy and the hydrogen economy

The future of coal is overshadowed by various 'clean' technologies, among others renewable energy and the 'hydrogen economy'. This paragraph is dedicated to investigate whether these technologies will be feasible within the foreseeable future and thus leave the coal industry redundant.

2.2.1. Renewable energy

Asif and Muneer (2007:1388-1413) stated that a secure and accessible supply of energy is crucial for the sustainability of modern societies and that the continuation of the use of fossil fuels will face multiple challenges. Their investigations revealed that China, India, the UK and the USA are all importers of fuel to sustain their energy demands and that their local oil reserves will only last 9, 6, 7 and 4 years respectively.

Asif and Muneer (2007:1388-1413) further found that the global energy demand is rapidly increasing with an increase in human population, urbanization and modernization and that almost 80% of the global energy demand is provided by the fossil fuels: oil, gas and coal. They further stated that the cost of energy generation from renewable resources is significantly decreasing while the cost of fossil fuel produced energy is at an increase.

The respective fuel shares for primary energy supply and electricity generation published by the International Energy Agency (2008:6&24) in their Key World Energy Statistics report are shown in Figure 2.2.1(a).

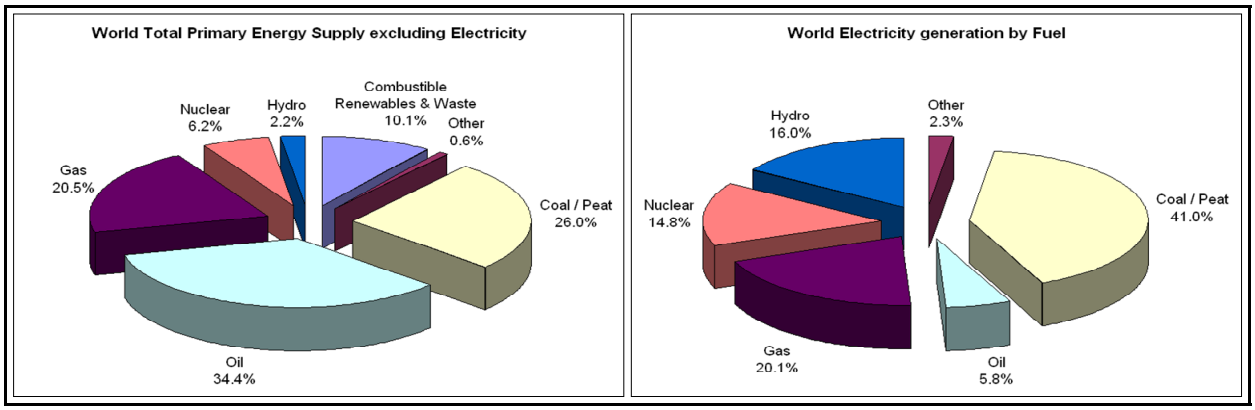

Figure 2.2.1(a): Representation of the world fuel shares for energy consumption in 2006.

As can be seen from Figure 2.2.1(a) coal still accounts for 26% of all primary energy required worldwide, excluding electricity; while 41% of electricity is generated using coal. Figure 2.2.1(b)

represents the potential energy sources compared to the global energy need as found by Asif and Muneer (2007:1388-1413).

As can be seen from Figure 2.2.1(b) gas and oil reserves are very limited compared to the annual world energy consumption, especially if their importance in energy consumption indicated in Figure 2.2.1(a) is considered. With oil and gas reserves depleting fast and experts agreeing that the midpoint of reserve depletion have already been reached (Asif and Muneer, 2007:1388-1413), the importance of coal is expected to play an even bigger role and coal is expected to replace oil and gas in the supply of energy while the world converts to cleaner energy sources. Nuclear energy, the other option, is not expected to play as big a role as coal because of cost (twice as expensive as electricity from gas or wind), radioactive waste, safety and the proliferation of weapons material concerns (Asif and Muneer, 2007:1388-1413).

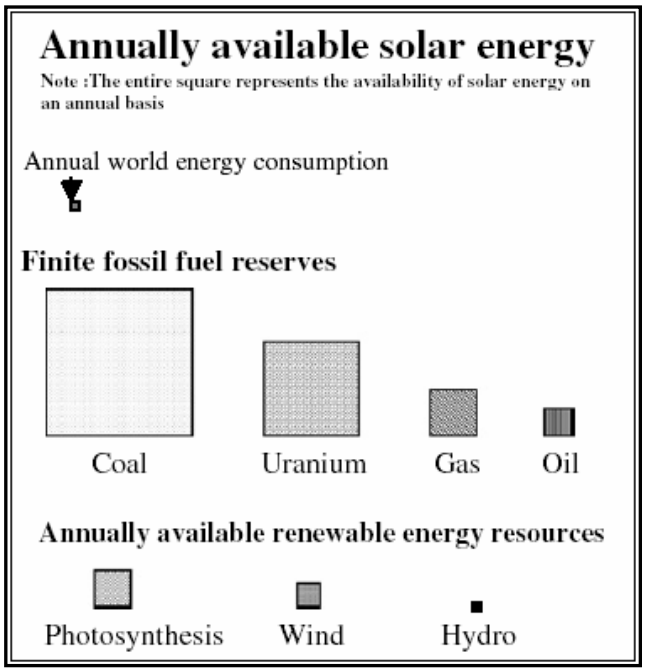

Figure 2.2.1(b): Potential of various energy sources as compared to global energy needs (Asif and Muneer, 2007: 1388-1413).

2.2.2. Hydrogen economy

Penner (2006:33-43) defines the hydrogen economy as the industrial system in which one of the universal energy carriers is hydrogen (the other is electricity) where hydrogen is oxidized to water which may be reused by applying an external energy source for dissociation into hydrogen and oxygen; this is in agreement with the definition offered by Stiegel and Ramezan (2006:173-190). These 'external energy sources' or 'primary energy-supply system classes' are fossil fuels (coal), nuclear reactors and renewable energy sources.

Stiegel and Ramezan (2006:173-190) focused on producing hydrogen from fossil fuels and found that coal in particular is expected to be the primary source for this hydrogen. They however stated that this technology may only be developed on a large scale if carbon sequestration is fully demonstrated and further acknowledged that advanced technologies must still be developed to achieve the level of cost necessary to minimize the impact to the consumer.

Penner (2006:33-43) concluded that the cost of hydrogen energy at the year 2000 was about three times more than the cost of natural gas and differed from Stiegel and Ramezan (2006:173-190) in stating that an important avenue for arriving at the hydrogen economy involves new discoveries or innovations such as the use of waste heat from nuclear fission or breeder reactors.

It can be concluded that the hydrogen economy will not threaten the coal industry within the foreseeable future and that coal might even play a significant role in the development of the hydrogen economy.

2.3. Properties of coal

To evaluate a thermal drying process and compare it with other drying techniques, it is important to understand the properties of the substance being dried. In this case: what is coal, how did it form, what types of water are associated with coal and the reasons this water must be removed from the coal. This will be discussed below.

2.3.1. The nature of coal

What is coal and how did it form? Coal is a complex and heterogeneous (Ndaji *et al.*, 1997:169-177) sedimentary rock that contains more than 50% organic material. It was formed more than 200 million years ago by heaping, thickening and hardening of plant residues in different stages of conservation (Snyman, 1996:595-608).

The debris from these plants accumulated under marshy conditions and was transformed to peat, largely by bacterial action. During the conversion process, the plant matter lost moisture, CO_2 was evolved and humic substances were formed (i.e. it turned into compost). The peat bog was ultimately buried under sedimentary deposits and the later stages of the conversion into coal were brought about mainly by the pressure and heat caused by the overlying strata. Roughly speaking, the mass ratio of wood, transformed to coal, is of the order of 20:1. Repetition of the above processes resulted in the formation of different layers or seams, each having its own particular properties (Van der Walt, 1984:1-22).

Macroscopically, coal consists of different units known as lithotypes. Microscopical studies showed that the different lithotypes are made up of one or more homogenic entities of organic materials, known as macerals, as well as small amounts of minerals. These macerals are not crystalline, and their properties and chemical composition are dependent on the rank of the coal. The macerals are also divided into three groups, known as vitrinite, exinite and inertinite, each giving a unique property to the coal (Snyman, 1996:595-608).

2.3.2. Types of water associated with coal

It is useful to collate the terminology in use to be able to describe the forms of water in coal. The definitions developed by Wakeman (1984:53–63) will be used, which states that water exists within coal in three forms, namely:

1 *Surface water* which lies on the surface of coal particles; this includes moisture held between particles in a coal mass or heap (60% of total moisture in brown coals (Allardice & Evans, 1971b:236-253)).

2 *Capillary, inherent, or structural water* which is absorbed into the capillary structure of individual coal particles (30% of total moisture in brown coals (Allardice & Evans, 1971b:236-253)).

3 *Chemical water*, which is held in chemical combination, usually associated with certain minerals in coal (10% of total moisture in brown coals (Allardice & Evans, 1971b:236-253)).

Mechanical dewatering is only associated with the removal of the first class of moisture, i.e. surface water, which is relatively free to move under imposed pressure gradients.

Removing the inherent moisture requires a thermal dewatering method such as the one investigated in this study.

Chemically bound moisture is not usually considered to be part of the total moisture content of coal and can only be removed by altering the structure of the coal, e.g. by burning it.

2.3.3. Reasons for dewatering fine coal

Many studies of the effect of dewatering fine coal have been conducted, highlighting the following reasons why dewatering is considered important (Wakeman, 1984:53-63).

1. Wet coal incurs higher transportation and handling charges. A study done by Tao *et al.* (2000:163-171) showed that even a 1% reduction in the moisture level of the three million tons coal produced annually in the USA, can lead to a saving of US $ 300,000.

2. Wet coal might freeze and cause handling and utilization problems in cold weather.

3. Moisture reduces the calorific value of the fuel in combustion processes. It was estimated that a 1% decrease in moisture would give a 1.4% increase in calorific value.

4. Excessive moisture in coke plant charges:
   a) increase coking time
   b) makes oven temperature regulation more difficult
   c) contributes to damage of coke oven refractories
   d) increases loads on tar and chemical recovery systems

5. Wet refuse requires additional energy for handling.

6. Refuse ponds occupy land, which may be used more profitably.

7. Refuse decantation ponds are unsightly.

8. Pond impoundments can be unstable and constitute a safety hazard.

9. Refuse pond overflows may be of poor clarity, preventing recycling or discharging into streams.

10. Refuse pond sediments may not consolidate enough to make the land usable at a later date.

2.4. Other research and results

It is important to investigate previous research done and currently employed experimental methods in a study of this nature. In the past a wide variety of experimental methods were used in order to determine different coal properties. These methods include:

1. **Drop tube furnace:** These experiments are done by passing a coal particle through an excess air flame at high temperatures (up to 1750°C), and are used to monitor the reactivity and fragmentation behaviour of the coal particle. Björkman (2001:155-166) compared a drop tube furnace to a very reliable reactor in Sandia, and found the drop tube furnace not to be very reliable.

2. **TGA and GC studies:** The TGA (thermogravimetric analyser) is used to determine the mass loss by a coal particle as it is heated (normally from ambient room temperature to 1000°C but some experiments were done up to 1200°C at a heating rate of 10°C/min; this may vary). In order to determine the composition of the gas which evolves at a certain temperature the TGA is normally used in combination with a GC (gas chromatograph).

3. **Solvent swelling experiments:** This is done by filling a constant diameter tube, with a solvent. A sample within this tube is then heated; the change in the solvent height can be

measured which will be in direct relation to the variance caused by the swelling of the coal sample.

4. **Mass spectrometry:** This experimental method is used to determine the atomic mass of a specific gas in a mixture of gasses, as well as the amount of that gas evolved. When the atomic mass is known, one can identify the component which corresponds to that mass.

5. **SEM:** The SEM (scanning electron microscope) is used to investigate the surface of a coal particle at very high magnification.

Results obtained using these experiments will be discussed below.

2.4.1. Fragmentation behaviour during heating

In a study done on coal combustion Spalding (1951:121-130) found that combustion depends upon particle size, shape, structural and chemical composition; he found that it may involve the conversion of carbon, fragmentation and the formation of fly ash. He also reported that fragmentation could enhance combustion as it results in smaller particles. This was confirmed by Dacombe *et al.* (1999:1847-1857) in their study on UK anthracites and bituminous coals.

Dacombe *et al.* (1999:1847-1857) concluded that the extent of fragmentation increases with an increase in particle size and temperature. Card and Jones (1995:539-547) found that small particles burned away but were replaced by larger ones decreasing in size during their study on both high and low ash content coals. Later Björkman (2001:155-166) concluded that the burn off rate increased as the coal's rank decreased in high and low ash content imported coals.

Gavalas (1981:197-210) stated that fragmentation arises in porous coal because most of the chemical reactions take place on the large internal surface area. The consequence of this is that the diameter remains essentially constant while the carbon is burned away, and an increasingly thick ash layer grows. This is called the shrinking core model (Sotirchos & Yu, 1985:2039-2052). Meanwhile the density decreases due to the increasing porosity. As the pores grow the particle is weakened until, ultimately, it fragments (Sahimi & Tsotsis, 1988:113-121; Helble & Sarofim, 1989:183-196).

Baxter (1992:174-184) suggested that fragmentation preferentially produces particles of diameters 15μm and 2μm.

Chern and Hayhurst (2004:208-221) conducted experiments on near-spherical particles with a diameter of about 14mm heated under conditions of pyrolysis in a fluidized bed. These

conditions will be closer to the conditions of thermal drying than the other studies discussed above.

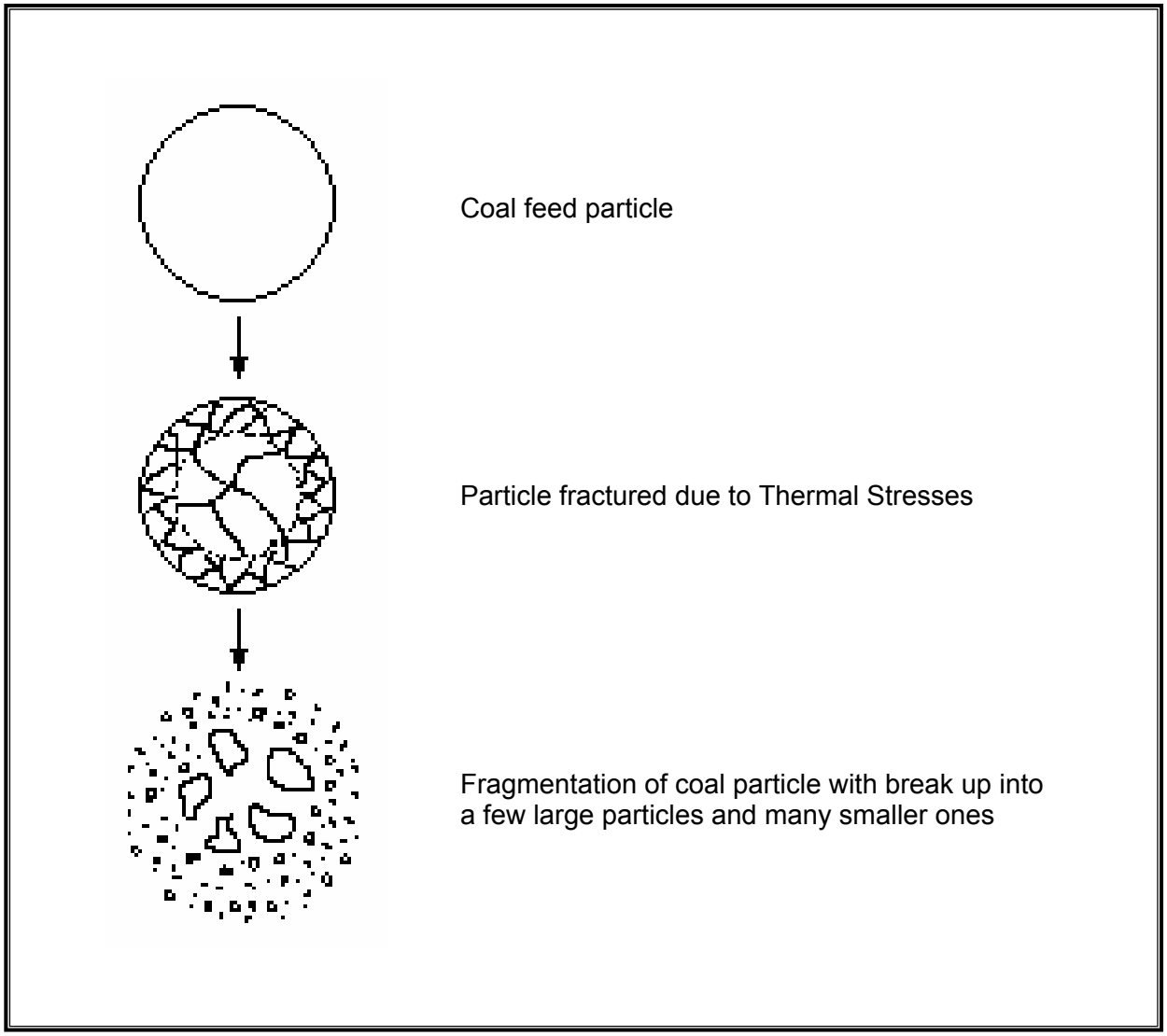

Figure 2.4.1: Graphical representation of the fragmentation model proposed by Dacombe *et al.* (1999:1847-1857).

Chern and Hayhurst (2004:208-221) found that anthracite shattered into pieces soon after entering the hot bed but that a bituminous coal fractured into small lumps of char just after devolatilisation had finished. The explanation they offered for this is that the anthracite fractured because of thermal shock while bituminous coals experience a plastic stage when the reaction zone is a sticky fluid acting as an adhesive, binding the outer bits of cracked char to the core of unreacted coal. Bituminous particles withdrawn from the bed, before fragmentation occurred, showed that a central core of virgin coal was still present with a sharp boundary layer crossing over to the surrounding char, indicating a shrinking core. This model will be further discussed in paragraph 2.5.

2.4.2. Thermal behaviour during heating

During their study on the heating of high quality Bangladeshi bituminous coals, Podder *et al.* (1995:221-226) found that three thermal regions can be observed, namely: (1) 80 to 110°C due to loss of water, (2) 420°C due to primary devolatilisation (coal melts under the reaction heat) and (3) 530°C due to secondary devolatilisation (coal resolidifies).

DTA traces usually show the same trend in behaviour, having three endothermic peaks followed by an exothermic peak. The first small endothermic peak around 100°C is expected to be due to elimination of water molecules. The second endothermic peak appearing in the temperature range 400 to 435°C is related to primary devolatilisation, during which compounds containing carbon, hydrogen and oxygen are released (Serageldin & Pan, 1984:145-160). The third endothermic peak in the temperature range 525 to 550°C is caused by secondary devolatilisation, during which mainly hydrogen is removed. The last exotherm is expected to be caused by the greater degree of orientation of carbon hexagonal planes.

Some investigations on Northern Greece lignites, however, revealed as much as four exothermal and three endothermal peaks (Iordanidis *et al.*, 2001:137-141), which shows how the properties of coal change as the type and rank vary, and again emphasize the need for this study. It could be assumed that pyrogenic water (Rustschev, 1976:254) is the major product that is released in the temperature interval 100 to 200°C. This thermal effect is followed by an endothermic effect in the temperature range 330 to 360°C that is probably due to primary gas release. A small surface area characterized the exothermal effect registered at 420 to 490°C. It may probably be attributed to processes accompanying the semi-coke formation, i.e. pyrolysis products interaction. It is assumed that this exothermic effect might be related to the processes of splitting of the phenol groups, cleavage of C-C bonds and partial transition of the coal matter into a plastic state (Butuzova & Kucher, 1979:46). A flattened exothermic effect were seen at 550 to 590°C, which is assumed to be related to high temperature pyrolysis accompanied by polycondensation reactions (Kasatochkin & Larina, 1975:159). The next endothermic effect in the temperature range 650 to 700°C was probably caused by secondary high temperature gas release (Saranchuk *et al.*, 1993:222). The clearly manifested exothermal effect found at 760 to 840°C is attributed to high temperature poly-condensation processes. Lastly an endothermal effect is observed in the temperature range 800 to 920°C.

2.4.3. Mass loss during heating

Podder *et al.* (1995:221-226) observed two temperature ranges from the TGA weight loss curves during their study on Bangladeshi high quality bituminous coals. The one is between 80 to 110°C, where water loss is expected. The other is in the region between 300 to 600°C, where maximum loss of volatile materials due to primary and secondary devolatilisation occurs.

Podder *et al.* (1995:221-226) was in agreement with Ma *et al.* (1989:1985-1996) who found that weight loss in Victorian brown coals is due to removal of moisture below 150°C, and due to the devolatilisation and combustion of volatile matter and char above 150°C.

In a study done on two Northbohemian low rank brown coal samples, using TGA and mass spectrometry, Balek *et al.* (1995:141-157), in agreement with Podder *et al.* (1995:221-226), concluded that two temperature regions exist where mass loss takes place, namely: 20 to 100°C where the release of physically bound water takes place and the range 300 to 450°C where the pyrolysis of the coal takes place, accompanied by the release of volatile products. The release of water takes place in two steps: in the temperature range up to 100°C (corresponding to the release of physically adsorbed water) and in the temperature interval 400 to 500°C (corresponding to the release of chemically bound water).

Li *et al.* (2003:393-406) differed from Podder *et al.* (1995:221-226), Ma *et al.* (1989:1985-1996) and Balek *et al.* (1995:141-157). They studied the combustion procedure of thirteen Chinese coals of different ranks, ranging from Anthracite to Lignite, in a 20% oxygen / 80% nitrogen atmosphere, and found that four weight loss phases occurred, and that the maximum weight loss rate shifted to lower temperatures as the coal rank decreased. This also differed from van Krevelen (1993:979) who stated that maximum rate of weight loss decreased as the rank (%C) increased. The first phase proposed by Li *et al.* (2003:393-406), around 100°C, is due to the release of the absorbed moisture. The weight losses of this phase generally increase following the coal rank decreasing from anthracite through bituminous to lignite. The second weight loss phase is around 200 to 750°C, associated with the primary devolatilisation, oxidation and combustion of coal. The third phase is around 600 to 1000°C, caused by the combustion of carbon. During the fourth phase (900 to 1200°C), the high temperatures decomposed some inorganic compounds in the ash. At 200°C absorption of oxygen was observed from anthracite and non-caking coal, indicated by a slight increase of the weight of coals in the DTG curves; this demonstrates that oxidation of the coal starts from 200°C.

Jung and Stanmore (1980:74-80) indicated that shrinkage of particles during drying and devolatilisation might occur to 20% of the original volume.

2.4.4. Volatile evolution during heating

The evolution process of the volatile products can also be divided into four phases in accordance to the four weight loss phases proposed by Li *et al.* (2003:393-406). The first is at around 100°C while the second and most yielding, occurs between 200 and 700°C. The third is from 600 to 1000°C and the fourth from 1000 to 1200°C. Li *et al.* (2003:393-406) reported that for all coals studied, water was released in the first, second and third phase. The water released in the first phase was from physically absorbed water, while the water in the second and third phase was from chemically combined or chemically formed water.

Das (2001:489-500), who studied Russian coking coals, proposed that the devolatilisation stage could be divided into two stages. These were primary (260 to 550°C) and secondary (550 to 850°C) devolatilisation. Das (2001:489-500) concluded that during primary devolatilisation about 13 to 30% of the gasses evolved. Methane was found to be the main constituent of the gaseous products in this interval. Das (2001:489-500) also concluded that during secondary devolatilisation about 71 to 87% of the gasses evolved. Hydrogen was found to be the main constituent of the gaseous products in this interval.

Boiko (2000:97-104) found that the absorbed moisture of the Beresovsky deposit, Kansk-Achinsk basin brown coal, is removed in a first stage (20 to 160°C) and the chemically bound moisture in a second stage (160 to 280°C).

Van Krevelen (1993:979) found that hydrogen passes through a very characteristic maximum release phase at about 750°C, almost independent of the type of coal. This was interpreted as a combination of numerous overlapping first-order reactions. Das (2001:489-500) agreed with this, and found that the evolution of H_2 started at about 450 to 495°C, reached a maximum at about 700 to 750°C and continued beyond 850°C. Strezov *et al.* (2004:375-392) stated that hydrogen release was the largest reaction in their study on bituminous coals.

Li *et al.* (2003:393-406) found that CH_3^+ (m/z 15) evolved at about 300 to 600°C, while van Krevelen (1993:979) reported a maximum evolution at 500°C. This was confirmed by Das (2001:489-500), who found that the evolution of methane started at about 390 to 445°C, attained a peak at about 490 to 530°C and ended at about 700 to 750°C.

Van Krevelen (1993:979) reported that CO remains an important constituent between 600 and 800°C, which was confirmed by Das (2001:489-500), who found that CO started evolving at about 350 to 500°C, attained a peak at about 640 to 725°C, reduced gradually and at about 800 to 840°C, started increasing again.

Li *et al.* (2003:393-406) reported that the evolution profiles of carbon dioxide (m/z 44) differ between the coals. It can be divided into three groups according to the coal rank. For the high rank group (anthracite, meager and meager lean coals) the emission increases gradually as the temperature increases in the temperature range <700°C. Then from 700 to 1200°C, the emission intensity increases at a relative lower rate. The mid rank group (lean, primary coking, fat, 1/3 primary coking, gas fat, gas and weakly caking coals) exhibited a different emission pattern. During 200 to 450°C, with temperature increasing, the emission of CO_2 increases at a high rate and reaches the first platform (450 to 600°C) at about 450°C. From 600°C, the emission increases again and reaches the second platform (650 to 1200°C) at about 650°C. For the low rank group (non-caking, long flame coal and lignite) the emission of CO_2 increases sharply from 200°C and reaches a platform at 350°C. For all the coals the emission of CO_2 started from 200°C, again suggesting that oxidation of coal starts from 200°C.

Van Krevelen (1993:979) also reported that the release of hydrogen, carbon monoxide and especially nitrogen is not finished at 1000°C, thus indicating that H, O, and N are strongly bound in the coke structure.

Bronshtein *et al.* (1979:55) observed that most of the ammonia and free nitrogen released up to 500°C, in Russian coking coals, arose from the reaction of the free water of pyrolysis with nitrites and five numbered heterocycles, whereas the intensification of ammonia evolution at 700°C was connected with the reaction of heterocyclic nitrogen with hydrogen.

Li *et al.* (2003:393-406) found that the aliphatic fragments m/z 55, 56 and 57 were detected in the mid rank coals between 200 and 300°C. These fragments were also detected for gas and gas-fat coal between 400 to 500°C. Emission peaks at 200 to 300°C shifted to higher temperatures with coal rank decrease. This emission might come from small organic compounds or functional groups which are physically bound or weakly chemically bound in the pores of the coals. The emission at 400 to 500°C can be considered to be from chemically bound functional groups in the coal structure.

Strezov *et al.* (2004:375-392) found that H_2S and CS_2 had peaks between 500 and 600°C.

Li *et al.* (2003:393-406) reported that sulphur dioxide (m/z 64) and monoxide (m/z 48) were released at high temperatures in the fourth emission period (1000 to 1200°C) for all the samples but anthracite. Sulphur dioxide and monoxide emissions were also detected during the second emission period from 300 to 800°C in the high sulphur coals (with S content 1.42 – 4.00%, meager lean, fat, gas fat, gas and long flame coals). For other mid low rank coals with low sulphur content, small amount of SO_2 and SO were released in this temperature range. No SO_2 and SO were released from 300 to 800°C for low sulphur content high rank coals (anthracite,

meager coal and lean). The emission peaks of sulphur monoxide and –dioxide of the fourth period shifted to lower temperatures with a decrease in the coal rank. Sulphur oxides registered at 300 to 800°C can be attributed to the oxidation of the organic sulphur; elemental sulphur and pyrite sulphur, while these species recorded at 1000 to 1200°C should come from the decomposition of the sulphate in the ash. For the high sulphur-containing coals, the fragment m/z 60 could be detected. This fragment is very much likely to be COS^+ since this fragment was only found in these high sulphur-containing coals.

Li *et al.* (2003:393-406) found that the predominant product release during the third emission period (600 to 1000°C) was carbon dioxide due to the combustion of char, which was the predominant reaction in this period. Water could also be detected in the lower temperatures of this period (< 800°C).

Karcz and Porada (1995:806-809) found that a hydrogen, instead of inert atmosphere causes a roughly fivefold increase in the conversion of carbon to the C_1-C_3 hydrocarbons at a relatively high conversion of almost 40% in their study on an upper Silesian bituminous coal.

2.4.5. Chemical and structural changes during heating

Coal is a heterogeneous material and has a macromolecular structure consisting of chains of aromatic and hydro-aromatic units which are joined by covalent cross-links, hydrogen bonds and van der Waals interactions to form a three-dimensionally cross-linked network (Ndaji & Thomas, 1995:932-937).

The thermal decomposition of coal is a complex phenomenon comprising of chemical and physical changes within the coal structure (Strezov *et al.*, 2004:375-392). The coal molecular bonds are ruptured upon heating where the weaker bonds start to break at lower, and the stronger bonds at higher temperatures (Saxena, 1990:55-94).

Podder *et al.* (1995:221-226) reported that high quality Bangladeshi bituminous coal undergoes physico-chemical changes when heat treated in the temperature range from 350 to 600°C, during which reactive molecules break along the weakest bonds, forming free radicals which subsequently recombine with other radicals or molecules to form more highly condensed species and volatile compounds. Coals are classified in two types: coking and non-coking. Coking coals (bituminous rank) pass through a plastic or softening state due to a greater degree of molecular orientation and consequently a greater tendency towards parallel stacking in the temperature range from 350 to 450°C depending on the rank (Glass, 1955: 253-268). Prime quality coking coals have volatile contents ranging between 20 to 32%.

Nishioka (1994:57-62) reported that a fraction of the moisture associated with high-volatile bituminous coals might be incorporated in the molecular structure and affect the physical changes accompanying drying. In their study on Victorian brown coals, Murray and Evans (1972:290-296) stated that 7 to 11 water molecules were associated with each oxygen atom in a functional group, and emphasizes that any comprehensive mechanism for water retention and rejection must include this relation as one of its main features. In his experiments Nishioka (1994:57-62) ruled out the possibility of a significant effect due to chemical reactions such as oxidation during the drying step (done up to 95°C). Suuberg *et al.* (1988:387) suggested that physical cross-linking (or association) of some kind was promoted by the drying procedure, which is consistent with the findings observed by Nishioka (1994:57-62). Nishioka (1994:57-62) concluded that these changes are caused by molecular mobility, followed by molecular associations even at low temperatures (~100°C).

Das (2001:489-500) and Ndaji *et al.* (1997:169-177) reported that the weakest bonds in the coal structure are methylene (-CH2-), ethylene and ether (-O-). Das (2001:489-500) reported that two types of reactions might occur simultaneously during pyrolysis of Russian coking coals. They are cracking reactions and the reactions of aromatization and condensation. The cracking reaction consists of the rupture of C-C bonds. They produce components of lower molecular weights than coal. Saturation of the two radicals formed by the rupture of the C-C bonds requires hydrogen and this can be supplied by reactions of aromatization and condensation. These reactions consist of the formulation of more extensive aromatic groups by the dehydration of saturated rings and recombination of aromatic groups with one another by the formation of aromatic C-C bonds. These reactions liberate hydrogen.

As mentioned previously, Ndaji *et al.* (1997:169-177) reported that coal is a complex and heterogeneous material. They also stated that it is generally accepted that it consists of a three-dimensional cross-linked macromolecular network, often described as the macromolecular phase, within which are trapped lower-molecular-weight species that constitute a mobile phase. Non-covalent interactions such as hydrogen bonding and π-π interactions are also important. Its cross-link density characterizes the molecular structure of coal. The lower the cross-link density, the more open the structure. Coal conversion processes involve changes in the macromolecular structure during the decomposition process. Solomon *et al.* (1993:587-597) found cross-linking, an important phenomena that controls the pyrolysis of coal.

In their experiments Ndaji *et al.* (1997:169-177) found that the changes in the apparent cross-link density begin at temperatures as low as 150°C. The swelling reaches a maximum at 250°C before decreasing with increasing heat treatment temperature. A heat treatment temperature of 150°C is probably too low to cause major thermal decomposition of the macromolecular

structure of coal. The increase in the solvent swelling at 150°C observed for the lignites is possibly caused by the dissociation of non-covalent interactions such as hydrogen bonding and π-π aromatic interactions which may not have re-formed on cooling of the heat-treated coal. Minimum weight loss other than moisture is observed below the minimum cross-link density. Above this temperature of minimum cross-link density, decomposition of the coal structure increases, as shown by the rapid weight loss.

Das (2001:489-500) concluded that: during primary devolatilisation, softening of coal takes place by the extensive molecular disruption and considerable evolution of volatile matter and during secondary devolatilisation, breakage of cross-links leads to the mobility of some of the decomposition products. Low molecular weight molecules form the gaseous products. Medium molecular weight molecules remain to form semi-coke on solidification by the joining up of adjacent aromatic clusters by free radical condensation reactions. Strezov *et al.* (2004:375-392) found that the largest reaction was the contraction of carbon planes with the evolution of hydrogen.

2.4.6. Swelling and plasticity

Gale *et al.* (1995:94-100) found that the presence of oxygen in the gas atmosphere has no effect on swelling of high volatile bituminous Utah and Pittsburgh coals until char combustion has begun. Street *et al.* (1969:343-365) found that chars prepared in nitrogen had much larger swelling ratios, more open structures, and smaller internal surface areas than chars prepared in air. They also found that bituminous vitrinites developed the greatest plasticity during pyrolysis. The further removed in rank a coal was from bituminous, the less plastic its vitrinite became.

Tsai & Scaroni (1987:200-206) found that a bituminous coal particle initially swells during the early stages of pyrolysis and then shrinks slightly during the later stages of devolatilisation.

Yun and Suuberg (1993:1245-1254) found the first physical transition (relaxation) to occur at 250 to 300°C, without any significant accompanying weight loss. Another relaxation at around 360°C seems to be coinciding with release of 'guest molecules'. They defined the temperature at which amorphous polymers transform in structure from the glassy state to liquid/rubber state as the 'glass transition temperature', T_g. In coal this transformation has been suggested to appear just before thermal degradation begins (Lucht *et al.*, 1987:56; Hall & Larsen, 1991:228).

Under moderate heating rates, coking coals form bubbles within the plastic phase and the pressure generated in the bubbles causes substantial swelling (Strezov *et al.*, 2004:375-392). Yu *et al.* (2003:1977-1987) observed particle shrinking in sub-bituminous and bituminous Australian coals during the plastic stage due to bubble rupture, and concluded that bubble

behaviour is responsible for coal swelling. They also reported that this observation is coupled to density, and that the density, as well as cross-link density (Ndaji & Thomas, 1995:932-937), decreased as the swelling and bubbling increased. Contrary to this behaviour, thermal coals with non-plastic properties maintain consistency of the open pore surface structure throughout the entire heating range, allowing free escape of the volatiles, with insignificant swelling.

Yun and Suuberg (1993:1245-1254) found that the transition temperature shifts up to 30°C with a change in heating rate from 10 to 80°C. In their study, Gale *et al.* (1995:94-100) concluded that at very low heating rates, swelling does not occur even though there may be significant devolatilisation because pressure build-up from the release of volatiles is too small to expand the particle shell (there is significant time for the volatiles to escape through small pores in the surface before pressure can build up).

2.4.7. The pore structure of coal

Chen *et al.* (2000:961-973) reported that the pore system in low-rank sub-bituminous coal from Wyoming shows enormous variation; pore sizes vary from less than 1nm to over 1μm.

Arenillas *et al.* (2004:1345-1350) found that heat treatment opened up some previously inaccessible narrow micro pores, and/or selectively destroyed others. Jiménez *et al.* (1988:197-221) reported that microporosity is related to rank. It decreases with increasing coal rank to a minimum at 85% of carbon content and then increases up to the anthracite coal rank.

From a SEM analysis, Yu *et al.* (2003:1977-1987) determined, that low-density coals have a closed, flowing texture, while high-density coals have open pores and cracks on its surface.

2.4.8. Catalytic effect of impurities

In a TGA experiment done by Wu *et al.* (1998:891-893) the effect of a metal salt, on the ignition temperature of coal, was investigated. It was found that the lower the first ionization energy, the higher the catalytic activity is. The salts of transition metals also made excellent catalysts (chlorides) and lowers the ignition temperature of coal by 70 to 170°C. Water of crystallization associated with the catalyst is associated with a reduction in the ignition temperature of coal, making salts with water of crystallization more effective catalysts. Transition metal salts exhibit excellent catalytic activity. They increase the volume of the volatile matter and strengthen the homogenous combustion of coal.

Although the results represent a change in the ignition temperature of the coal and not the optimum dewatering temperature, it shows that the presence of a metal salt (catalyst) could possibly have an influence on the dewatering process.

2.5. Mechanisms proposed by others

Through the years many mechanisms were proposed to represent the drying, devolatilisation (pyrolysis under inert conditions) and char formation stages in the coal combustion process. These mechanisms are based on coal gasification, coal combustion and coal pyrolysis respectively, where the latter would be similar to the inert conditions of a thermal drying process.

One of the problems with developing a proper mechanism is that the said stages (drying, devolatilisation / pyrolysis and char formation) usually overlap, and a mechanism for each individual stage would not be sufficient. Some authors proposed mechanisms that consider all these stages; these are discussed below.

Jarvinen *et al.* (2002:357-370) proposed that the temperature in thermally large coal particles is non-uniform, which is in agreement with Heidenreich and Zhang (1999:991-994), who used spherical particles with a diameter of 10-11 mm in their study. Heidenreich and Zhang (1999:991-994), found that some of the techniques used to measure the temperature of the coal particle, such as a thermocouple in contact with the atmosphere inside a furnace, do not show a temperature plateau at 100°C in the centre of the particle, as it should (water evaporates), and this technique is grossly overestimating the actual particle temperature.

Jarvinen *et al.* (2002:357-370) stated that the stages of coal combustion (drying, pyrolysis and combustion) may be assumed to overlap because different temperature regimes exist within the particle. At some point the particle's outer surface is fully devolatilised, while the particles interior is still undergoing drying and devolatilisation. In their model on pyrolysis, Agarwal *et al.* (1986:2373-2383) described this as a moving boundary or drying front. As H_2O and CO_2 flow out from the particle they press through the hot surface layers of char. If the temperature is high enough, the char may be gasified. Figure 2.5.1 shows a graphical representation of this mechanism.

Jarvinen *et al.* (2002:357-370) agreed with most of the model proposed by Agarwal *et al.* (1986:2373-2383). Agarwal *et al.* (1986:2373-2383) did however add that mass transfer, both to and through the particle, is the rate-limiting step for drying and devolatilisation, in conjunction with chemical reactions represented by the distributed activation kinetics of overall coal decomposition. They made the assumptions that moisture and volatile species are evenly distributed within the coal matrix, that devolatilisation is thermally neutral and that the spherical coal particles will retain their shape during the process of drying and devolatilisation. They also assumed that no chemical interaction takes place between the moisture and the volatile species escaping from within the particle. They stated that two distinct stages exist; in the first stage,

the particle would dry and devolatilise simultaneously. In the second, after the drying has finished, the particle would still devolatilise until all the volatile species evolved.

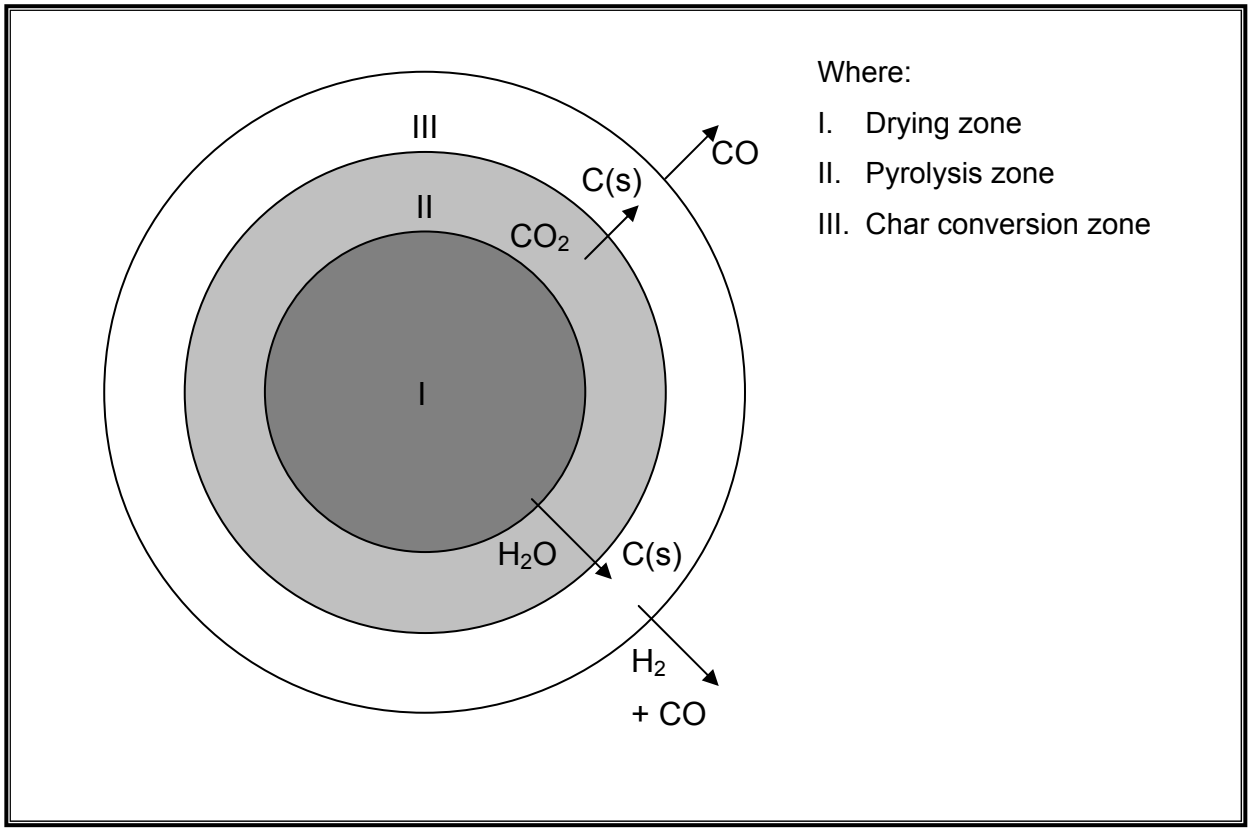

Figure 2.5.1: Graphical representation of the mechanism proposed by Jarvinen *et al.* (2002:357-370).

To model drying and devolatilisation under combustion conditions, Wildegger-Gaissmaier and Agarwal (1990:44-52), as well as Agarwal and Pedler (1986:640-643), divided their analysis into pre-ignition and post-ignition stages. The pre-ignition stages corresponded to drying and devolatilisation under pyrolysis conditions, while post-ignition stages were characterized by the formation of a diffusion flame around the coal particle. The energy feed back from the flame, at a higher temperature than the air, enhances the rate of subsequent drying and devolatilisation. Since thermal drying investigated in this study will not be done at combustion conditions i.e. in the presence of oxygen, these models will not be discussed.

Winter *et al.* (1997:302-314) also proposed a combustion model for a fuel particle burning in a fluidized bed, which describe the drying, devolatilisation, volatile and char combustion, external and internal heat and mass transfer and changing fuel properties. Their model will be discussed because of their unique view on the drying mechanism. They used spherical particles (3 – 20mm) with a bed temperature of 700 to 950°C. If moisture is present in the spherical shell, the drying model calculates the evaporation rates based on the shell's temperature and also the distribution of pores. The water vapour formed is transported (due to the internal pressure gradient) through the particle to the surface, cooling the inner shell of the

particle. The volatiles follow the same mechanism, but burns on the surface of the particle, heating it. After the moisture and volatiles are removed, the char combustion model calculates the carbon oxidation rates.

The drying model developed by Winter *et al.* (1997:302-314) assumes a linear distribution of pores and that the boiling temperature of the moisture within the particle increases with capillary pressure. Calculations predict a boiling temperature from 100 to 200°C. If a single boiling point was used (100°C) the particles temperature would plateau till all drying is complete. The approach used here shows good agreement with their observations but is in contradiction with the temperature gradient through the particles found in experiments conducted by others (Jarvinen *et al.*, 2002:357-370; Heidenreich and Zhang, 1999:991-994; Agarwal *et al.*, 1986:2373-2383; Chern and Hayhurst, 2004:208-221; Chern and Hayhurst, 2006:553-571).

Chern and Hayhurst (2004:208-221; 2006:553-571) focused their work on the pyrolysis (in the absence of oxygen) of coal. In their initial study they indicated that pyrolysis definitely occurs according to the shrinking core model proposed by previous authors (Jarvinen *et al.*, 2002:357-370; Agarwal *et al.*, 1986:2373-2383) where a sharp boundary layer can be seen between the centre core of virgin coal and the surrounding char. The model predicts that apart from the very beginning and end of devolatilisation there is an almost constant velocity observed in the shrinking core of raw coal. They indicated that bituminous coal loses its volatile matter at 550 ± 100°C.

Their model (Chern and Hayhurst, 2004:208-221), based on coal being heated in an inert atmosphere can be presented by the following reaction:

$$\text{Coal} \rightarrow \text{Char} + \text{Volatiles}$$

They (Chern and Hayhurst, 2004:208-221) indicated that water would be one of the first volatile components to be produced at just over 100°C. As the coal is heated further up to 900°C, H_2, CO and CO_2 are produced together with a suit of hydrocarbons ranging from CH_4 up to tars. They also stated that the rate of pyrolysis depends on the size of the particles, its temperature, the rate of heating, the particle's composition, the surroundings, etc.

In their later work, Chern and Hayhurst (2006:553-571) found the production of volatile matter during pyrolysis to be endothermic and not thermo neutral as assumed by others (Agarwal *et al.,* 1986:2373-2383). They also found that the rate at which volatile matter is produced is not controlled by mass transfer as Agarwal *et al.* (1986:2373-2383) proposed but by the heat conduction to the moving reaction front inside the coal particle, providing its diameter exceeds 3mm. They proved this by cementing a thin thermocouple into a coal particle to measure the

temperature midway between its exterior and centre. The temperature was found to be 100°C for about 25 seconds during its pyrolysis indicated that drying requires the latent heat of vaporization. It is also worth noting that their temperature measurement experiments on a coal particle with diameter 7mm indicated that the reaction front took 40 seconds longer to reach a position midway between the particles exterior and centre during devolatilisation than during pyrolysis.

They (Chern and Hayhurst, 2006:553-571) concluded that the initial heating can be roughly separated into two stages according to the temperature at the particles exterior: stage 1 being below 100°C while the second stage will be above 100°C. They agreed with other authors, stating that the thermal decomposition on the particles exterior and drying in the interior may occur simultaneously.

2.6. Different drying methods

Except for the economical aspect of the different drying methods, another very important factor is how the free radical concentration changes when the different drying methods are used on the same coal. This would influence the dried coal's reactivity towards oxidation and later combustion reactions.

Another very important aspect that must be considered is porosity. This will determine the size of the area on which reactions may occur. Favas and Jackson (2003a:53-57) found that milling fractures the coal particles and destroys porosity; this must be kept in mind when porosity changes in coal, caused by dewatering processes are investigated. Favas and Jackson (2003a:53-57) also reported that milling to smaller particle sizes than 35 μm could be counter productive, because the agglomeration of the small particles, which increases the intra-particle porosity, overwhelmed the destruction of porosity caused by milling.

2.6.1. Steam drying

Chen *et al.* (2000:961-973) stated that steam drying of coal is an attractive technology that offers, besides reduction of fire and explosion hazards, improved thermal efficiency. In addition, steam-dried coals appear to be less prone to spontaneous combustion. Baria and Hasan (1986:53-60) agreed with Chen *et al.* (2000:961-973) and concluded that steam dried coal appears to be less liable to spontaneous combustion because of their decreased reactivity to oxygen in the atmosphere.

Early investigations (Wenzel & White, 1951:1829-1837; Chu *et al.*, 1953:1586-1591) intriguingly suggested that the evaporation rate of a liquid in contact with its superheated vapour could

exceed that in air. Subsequent investigations, experimental as well as theoretical- has sought to identify an inversion temperature above which this phenomenon occurs for various flow configurations (Yoshida & Hyõdõ, 1970:207-214). Drying in air is markedly different in that it does not involve the initial condensation period; unless the initial temperature of particles is sufficiently high (≥373 K), drying in steam will inevitably lead to an initial condensation period.

Chen *et al.* (2001:209-223) explained the phenomena (inversion temperature) by a practical example. They assumed that wet coal particles enter the dryer at low temperatures; steam in the gas phase may condense as these particles heat up initially. The condensed water is assumed to lead to the formation of a layer of liquid distributed uniformly on the surface of the particle. During this initial heating period, convective heat transfer from the gas phase and release of latent heat of condensation lead to an increase in the particle temperature. Once the temperature of the particle is greater than the saturation temperature of steam, evaporation takes place.

Chen *et al.* (2001:209-223) concluded that if the objective was to dry the coal to an equilibrium moisture level, steam drying might not be as efficient as air-drying.

Potter and Keogh (1981:217-227) found that steam drying reduced the moisture content to 3 % w/w at a temperature of 170°C and to about 17 % w/w at a temperature of 110°C, while Bongers *et al.* (1998:41-54) reported that steam drying removed sulphur relatively easy.

2.6.2. Vacuum drying

Vacuum drying produces a sudden increase in the free radical concentration, but then stops (Carr *et al.*, 1995:389-394). The absence of any chemical reactivity during vacuum drying at temperatures below 70°C has been reported previously (Allardice & Evans, 1971a:201-210).

Mahidin *et al.* (2003:147-160) emphasized that use of high-pressure equipment in certain pressure drying methods provides crucial economical disadvantages. They also reported that vacuum drying removed the water from the macro pores, but not those from the micro pores, since this is influenced by the surface bonding forces and capillary action, which needs additional energy for further removal.

2.6.3. Hydrothermal dewatering

Hydrothermal dewatering or hot water washing is a non-evaporative, energy efficient drying process for upgrading brown coals with high moisture content. The major advantage of this process is that water is removed as a liquid so that the latent heat of vaporization is saved and much of the water-soluble inorganic material is leached out, decreasing the inorganic content of

the coal (Favas & Jackson, 2003a:53-57). Hydrothermal dewatering is done by heating coal slurry in an autoclave in the absence of air to about 300°C in a block furnace (Ünal *et al.*, 1992:183-192).

Ünal *et al.* (1992:183-192) found that thermal dewatering causes an increase in the free radical concentration of the coal, as confirmed by Favas *et al.* (2003:71-79), thereby enhancing the oxygen reactivity. Ünal *et al.* (1992:183-192) also reported that the hydrophilic properties reduced to that in untreated coal samples. Thermally dewatered coal's elemental analysis differs from that of the untreated coal. The higher carbon content of the sample is due to the greater elimination of oxygen than carbon (mass) in the production of CO_2 during the thermal dewatering (Woon, 1980) as well as the elimination of sulphur and sodium (leached out) (Favas & Jackson, 2003b:59-69).

Drohan (1978) found that thermal dewatering causes collapse of narrow pores in the coal. Favas and Jackson (2003a:53-57) agreed with Drohan's (1978) findings, in that the particle porosity decreased with an increase in temperature.

Favas and Jackson (2003b:59-69) reported that the coal charge recovered as HTD (hydro thermally dewatered) product was measured as 86 $\pm$ 1%. For the range of ranks they surveyed, the benefits of hydrothermal processing tended to increase with decreasing coal rank.

Chen *et al.* (2000:961-973) stated that the cost and complexity of high-pressure equipment required for hydrothermal drying of coal, offsets its advantages.

2.6.4. Air-drying

Air drying of the coal samples is normally done by placing a quantity of ground coal slurry in a breaker and exposing it to temperatures between 15 and 55°C over a period of approximately 6 weeks. Chen *et al.* (2000:961-973) stated that during air drying, the movement of water vapour through the porous dry shell is driven by the concentration gradient; thus assuming pseudo-steady state conditions.

Ünal *et al.* (1992:183-192) found that air-drying reduces the free radical concentration of the coal, which causes a decline in its oxygen reactivity. They also reported that the hydrophilic properties stay the same as in untreated coal samples. Carr *et al.* (1995:389-394) differed from Ünal *et al.* (1992:183-192) and reported that the free radical concentration increased gradually to an ultimately greater concentration than that achieved with vacuum drying.

2.6.5. Gas flow drying

Gas flow drying are normally done by passing a stream of inert gas (nitrogen) over coal in a type of tube furnace at temperatures ranging from 105 to 150°C over a period of 72 hours.

Carr *et al.* (1995:389-394) reported that for gas flow drying (using nitrogen) the free radical concentration increased gradually to an ultimately greater concentration than that achieved with vacuum drying.

2.6.6. Drying by supercritical CO_2 with methanol as entrainer

This is a different approach than those relevant to this study, and will thus only be discussed briefly.

Drying is done by passing supercritical carbon dioxide, with methanol as entrainer, over the coal. Iwai *et al.* (2002:251-255) found that methanol added as entrainer can reduce water content to half of that dried with supercritical CO_2 in thermally dried coal. They also found that substitute adsorption of methanol with water might occur on the coal surface. The methanol adsorbed may enlarge the pores, thus providing easy access for water to the surface.

2.7. Industrial thermal dryers

A wide range of different industrial thermal drying methods exist which vary from laboratory scale drying equipment to high volume industrial equipment. Drytech Engineering specializes in the supply of this type of drying equipment which is briefly described below (http://www.drytecheng.com/Drytech.htm, 2009).

2.7.1. Cabinet dryers

Cabinet dryers (illustrated in Figure 2.7.1) are operated by air which is drawn in through an inlet duct and heated to the required temperature. The air is then distributed from side to side or bottom to top in a circular motion over trays containing the product.

Cabinet dryers are suitable to handle small loads of liquids, slurries, pastes, powders, granules, agglomerates, and solids (objects) up to a maximum of 4000kg and are operated by steam, electricity, thermal oil or gas up to a maximum temperature of 600°C.

Figure 2.7.1: Illustration of a cabinet dryer.

2.7.2. Calciners

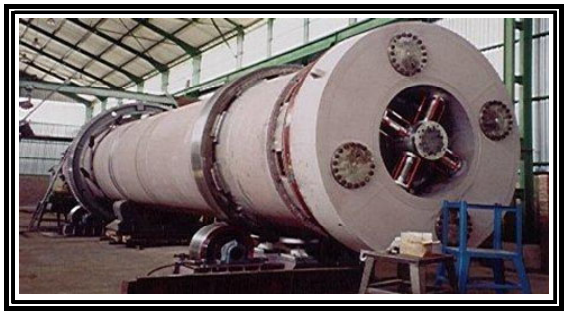

Figure 2.7.2: Illustration of a calciner.

Calciners (illustrated in Figure 2.7.2) transport the feed from the inlet to the discharge of the 'reactor' by the rotation of the drum and the angle of inclination of the drum. The drum tube passes through a furnace which is heated by either electrical elements or gas burners. The energy heats the tube which is in direct contact with the feed internally. Special lifters in the drum promote the exposure of the feed to the heated surfaces by a rolling motion of the material. The product is discharged through a suitable airlock device.

Drying is performed automatically and continuous and the dryer is able to handle powders, granules and non friable agglomerates in both low and high feed rates.

These systems are known to be low dust systems and they are very controllable. Residence time can be altered by varying the speed of rotation and the drum angle. Fills are typically controlled between 7% and 25% of the cross sectional area of the drum.

2.7.3. Conveyor dryers

Conveyor dryers (illustrated in Figure 2.7.3) use a perforated belt to transfer feed materials through the dryer. Heated air is either passed under and through, or over and through the belt and product bed, before being reheated and re-circulated. Units are normally multi zoned and may have differing airflow's in successive zones. Additionally each zone may use a different temperature profile and control. Saturated or close to saturated air is exhausted from the dryer via a central exhaust duct.

Figure 2.7.3: Illustration of conveyor dryers.

Conveyor dryers may be multi pass units, in which the feed is transferred from one belt to another belt below it by gravity. These dryers are usually two or three pass machines.

The dryers can be operated manually, by batch operation or automatically by continuous operation. They can handle large granules, agglomerates, pellets, small solid particles and large solid particles in both low and high feed rates. Conveyor dryers' function with steam, electricity, coal, liquid fuels, or gas as heating source.

2.7.4. Flash dryers

Flash dryers (illustrated in Figure 2.7.4) use a heated gas to pneumatically convey the feed up a flash tube and into a primary air separation device; most commonly a cyclone. Air is induced to the feed area through a hot gas generator where it entrains the feed and flashes off the moisture during the conveying process. The product is fed into the throat of the feed area in a controlled fashion and is introduced into the air stream by means of a venturi or the use of disintegrator technology. The particles attain a velocity in the order of 80% of the conveying velocity. Secondary dust collection such as multiclones, bag houses, scrubbers and electrostatic precipitators are required for fine products.

Flash dryers operate using steam, electricity, coal, liquid fuels or gas with extremely short residence times (seconds).

Figure 2.7.4: Illustration of flash dryers.

Drying is performed automatically and continuously and the dryer can handle both low and high feed rates. These dryers are able to handle slurries, pastes, sludge's, friable filter cakes, powders and granules. The feed must however contain a relatively consistent particle size; very large particles are difficult to handle.

2.7.5. Fluid bed dryers

Fluid bed dryers (illustrated in Figure 2.7.5) use a heated gas to lift and maintain the feed in a fluidized state. Air is introduced into a wind box or plenum using a forced draft fan and is distributed through a distributor plate of solid material by means of a perforated plate, nozzles, ceramic grid or other distribution medium. The bed attains fluid-like properties flowing and mixing. The fluidization provides intimate contact between each material particle and the gas stream creating an extremely efficient transfer medium.

Fluid bed dryers operate using steam, electricity, coal, liquid fuels or gas. Residence times and bed height can be varied by changing the feed and discharge rates.

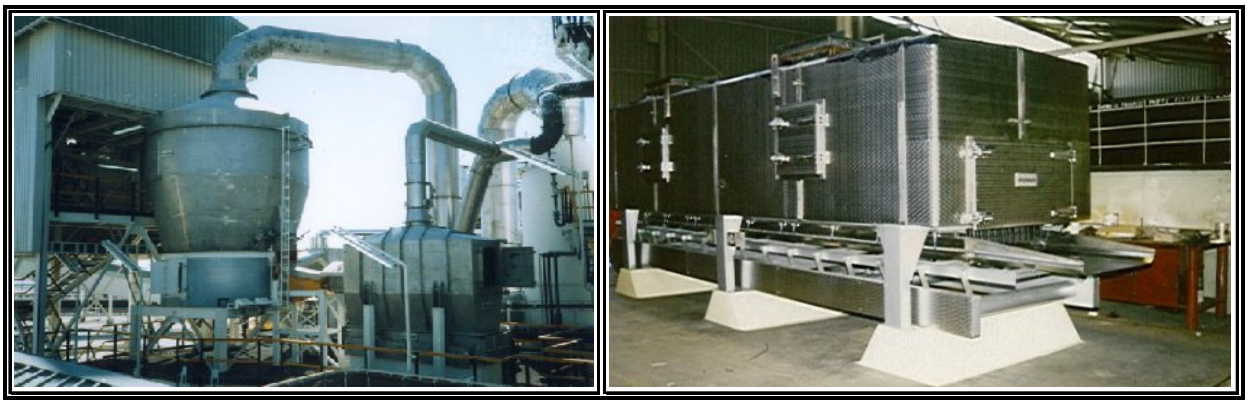

Figure 2.7.5: Illustration of fluid bed dryers.

Drying is performed either manually by batch operation or automatically by continuous operation and the dryer can handle both low and high feed rates. These dryers are able to handle liquids, powders, granules and non friable agglomerates. The feed must however contain a relatively consistent particle size. Very large particles are difficult to handle.

2.7.6. Indirect dryers

Indirect dryers employ similar principles of operation to direct dryers (as described above). The fundamental difference is that the method of heat transfer is predominantly by conduction as opposed to convection. The product contacts the heated surface of the equipment while devices within the unit agitate, mix, scrape, or turn the product exposing new product to the heated surface.

Indirect dryers operate using steam, hot water, thermal oil or gasses. Residence time can be altered by varying the movement of the equipment, speed of rotation or appropriate mechanical aspect.

Drying is performed either manually by batch operation or automatically by continuous operation and the dryer can handle low to medium feed rates. These dryers are able to handle liquids, slurries, pastes, filter cakes, powders, granules and agglomerates.

Indirect dryers include the following:

Tube furnace dryers:

Rotary tube furnace dryers transport the feed from the inlet to the discharge of the dryer by the rotation of the drum and the angle of inclination of the drum. The drum tube passes through a furnace that is heated either by electrical elements or by gas burners. This energy heats the tube which is in direct contact with the feed internally. Special lifters in the drum promote the exposure of the feed to the heated surfaces by a rolling motion of the material. The product is discharged through a suitable airlock device. The evolved moisture is exhausted from the system through an induced draft fan.

Drum dryers:

Drum Dryers (illustrated in Figure 2.7.6.1) consist of a relatively large diameter machined drum that is heated internally. Feed is metered, using different techniques, onto the outer surface of the drum while the drum rotates. The feed dries as the unit rotates, and the product is scraped off the drum surface by means of a 'doctor' blade. The evolved moisture is exhausted from the system through an exhaust hood and an induced draft fan. Machines may have a second drum (double drum dryers) and/or may have the drum installed inside a vacuum chamber for vacuum drying operation.

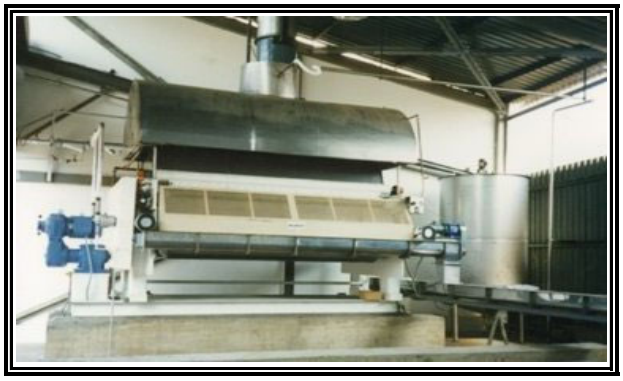

Figure 2.7.6.1: Illustration of a drum dryer.

Pan dryers:

Pan dryers utilize a heated surface upon which the feed is placed. The pan may rotate and the product is discharged off the tray by means of a sweep or blade mechanism. These units may have multiple pans arranged so that the material from one pan discharges onto the next successive pan. The evolved moisture is exhausted from the system through an induced draft fan. The pan may be installed inside a vacuum chamber for vacuum drying operation.

Paddle dryers:

Paddle dryers (illustrated in Figure 2.7.6.2) consist of either a single or twin paddle or screw arrangement (which may or may not be internally heated) running through a trough, which may or may not be jacketed. The feed is introduced at the feed end and is conveyed through the length of the dryer being brought into contact with the heated surfaces. The constant motion and agitation of the screw or paddle exposes new surfaces and intimately mixes the product. Dry product is discharged from the opposite end of the unit. The evolved moisture is exhausted from the system through an induced draft fan. The unit (trough) may be designed for vacuum drying operation.

Figure 2.7.6.2: Illustration of a paddle dryer.

Double cone dryers:

Double cone dryers consist of a double cone mixer that uses an external jacket to heat the internal surface of the unit. As the cone rotates, the material is tumbled and new surfaces are brought into contact with the cone surface. These operations are batch type and are most commonly evacuated for full vacuum operation. Vacuum is pulled by means of liquid ring vacuum pumps. The evolved moisture is exhausted from the system through an induced draft fan or the vacuum pump. Other variations of this technology include single cones with internal scrapers or screws to further agitate the material.

Steam tube dryers:

A steam tube dryer (illustrated in Figure 2.7.6.3) consists of a number of tubes symmetrically arranged, that run the length of the dryer. The tubes are connected to a header into which steam (or other heat transfer fluid) is introduced to provide the energy for the drying process. The feed is introduced into the unit and is brought into contact with the steam tube bundle. In stationary units the motive force is air and will create a fluid bed around the tube bundle. Rotary units will lift the material and cascade it over the steam tubes multiple times while the feed dries. The dry product is discharged from the unit through an airlock device. The evolved moisture is

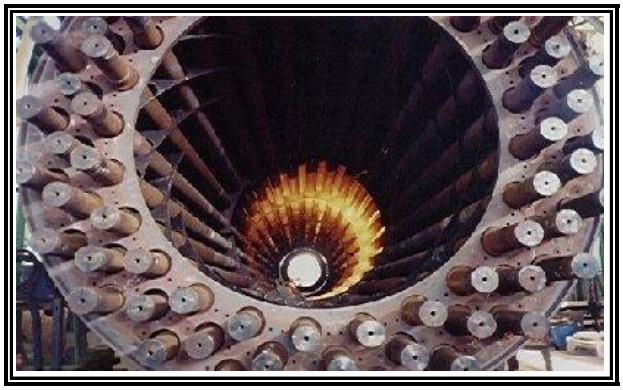
Figure 2.7.6.3: Illustration of a steam tube dryer.

exhausted from the system through an induced draft fan. The unit may be designed for vacuum operation or installed inside a vacuum chamber for vacuum drying operation.

2.7.7. Infrared dryers

Infrared dryers (illustrated in Figure 2.7.7) irradiate the product, transferring energy not only to the surface of the product but to well within the substance of the material. The product however needs to be exposed to the heat source in an effective manner, i.e. in line of sight. Drying is done on high velocity thin flat surfaces. Infrared dryers do not heat the air and thus energy utilization is high.

Figure 2.7.7: Illustration of a infrared dryer.

Infrared dryers operate using electricity or gas. Residence time can be altered by varying transportation and thus exposure times through the dryer.

Drying is performed either manually by batch operation or automatically by continuous operation and the dryer can handle both low and medium feed rates. This extremely efficient method of heat transfer is suitable in industrial processes of drying powders, granules and small solid particles.

2.7.8. Rotary dryers

Rotary cascade dryers (illustrated in Figure 2.7.8) operate by passing the feed material through a rotating cylinder together with a stream of hot gas. Internal lifters or flights elevate the feed and drop it in a curtain from the top to the bottom cascading the feed along the length of the dryer. Flights need to be carefully designed to prevent asymmetry of the curtain. Material moves from one end of the dryer to the other by the motion of the material falling due to the angle of inclination of the drum. Some rotary dryers are double and triple pass units where each drum is nested inside the previous drum.

Rotary louver dryers (illustrated in Figure 2.7.8) operate by supporting and moving the feed material over a set of louvers mounted to an external rotating drum. The hot gas is introduced into a tapered bustle below the feed ring. The air passes through the louvers and then the product before being exhausted from the dryer. The rotation of the drum causes the material to roll and mix providing intimate contact with the drying gas. Material moves from one end of the

dryer to the other by the motion of rolling, some fluidization and due to the angle of inclination of the drum.

Rotary dryers operate using steam, electricity, coal, liquid fuels or gas. Residence time can be altered by varying the speed of rotation and the drum angle. Fills are typically controlled between 7% and 25% of the cross sectional area of the drum.

Figure 2.7.8: Illustration of rotary dryers.

Drying is performed automatically by continuous operation and the dryer can handle low to high feed rates. These dryers are able to handle powders, granules, non friable agglomerates and large solid particles.

2.7.9. Specialized dryers – microwave dryers

The technology behind microwave drying is based on the polarity of the moisture molecule. Water which is a bipolar molecule (and the most common asymmetrically charged molecule) reacts to the microwaves, while non polar molecules do not. Microwaves also penetrate to the centre of the product, being unaffected by shadows or product density. The molecules react by trying to align themselves to the electromagnetic charge. Because the microwaves' electromagnetic field reverses at an extremely high frequency (as much as a couple billion times per second), the bipolar molecules continually change alignment, producing energy that is converted into heat. In effect, the water molecules heat themselves until the product becomes so hot that the water evaporates. Microwave dryers can be incorporated into a number of

standard configurations, such as cabinet, conveyor and tray type systems. The evolved vapours must be able to be extracted from the system; failure to do so might lead to explosions.

2.7.10. Spray dryers

Spray drying (illustrated in Figure 2.7.10) involves the atomization of feed to a spray of droplets which are contacted with hot air in a drying chamber. Sprays are produced by a rotary atomizer or pressure nozzle atomizers. Evaporation of moisture from the droplets and formation of dried particles proceed under controlled temperature and air flow conditions. There are various dryer configurations.

Spray dryers operate using steam, electricity, coal, liquid fuels or gas. Residence times are short but can be altered by varying the drying air velocities somewhat.

Drying is performed automatically by continuous operation and the dryer can handle low to high feed rates. These dryers are able to handle liquid slurries and low viscosity pastes.

Figure 2.7.10: Illustration of spray dryers.

2.8. Spontaneous combustion

The spontaneous ignition of coal (particular lower-rank coals, since they have a greater tendency to spontaneous combustion) poses serious problems in its mining, transportation, storage and treatment. Carras and Young (1994:1-15) reported that drying could increase the natural spontaneous combustion tendency of coals.

It is widely accepted that low-temperature oxidation is the primary source of heat release leading to the spontaneous ignition of stored coal (Nugroho *et al.*, 2000:1951-1961). If the heat generated by oxidation is not dissipated as fast as it is accumulated, then an increase of temperature will occur and a runaway ignition event can ensue.

Nugroho *et al.* (2000:1951-1961) reported that the removal of water brings about the larger opening of pores particularly for a high moisture coal. This leads to a higher accessibility of oxygen to reactive sites. This is in agreement with the above findings by Carras and Young (1994:1-15).

Nugroho *et al.* (2000:1951-1961) concluded that a smaller particle reduces the critical ambient temperature for spontaneous ignition to occur. A typical critical ambient temperature is about 400 K for all coals at an average particle diameter of 0.06 mm. The higher surface areas found in the low rank coals is thought to be one of the influential factors for the decrease in the critical ambient temperature with increasing low rank coal content in a blend. The change of the critical ambient temperature with particle size is almost negligible for porous coals, but significant for hard coals. A coal bed with mixed up sizes is much more vulnerable than one with segregated sizes.

Chapter 3
Methods and Procedures

This chapter covers the selection and preparation of coal samples as well as the different experimental methods and procedures used to obtain the results discussed in chapter 4.

3.1. Introduction

Coal samples from five different South African mines were selected for experimentation. This was done to cover the bulk of the coal spectrum mined in South Africa; the samples selected are:

- Witbank seam 2 coal – referred to as WB2
- Witbank seam 4 coal – referred to as WB4
- Soutpansberg coal – referred to as TS
- Waterberg coal – referred to as GG
- Free State coal – referred to as NV

These samples were crushed to produce fine coal which was subjected to a series of tests to investigate the chemical and physical changes that occur in the samples during the drying process. The procedures and tests used are discussed in more detail in the subsequent paragraphs.

3.2. Experimental procedures and tests

In this paragraph a detailed discussion of all the procedures and tests used to obtain the results discussed in chapter 4 as well as the reason for the selected tests will be done. The topics which will be discussed include the following:

- Crushing and separation techniques
- TGA (thermogravimetric analyser) experiments
- SEM (scanning electron microscope) experiments

- A combination of a nitrogen furnace with proximate analysis
- Mercury intrusion experiments

3.2.1. Crushing and separation techniques

The coal samples mentioned in paragraph 3.1 were crushed, milled and sieved to produce fine coal in the -600 +425 μm particle range.

Figure 3.2.1: Illustration of crushing and separation technique to separate coal samples into their size and maceral fractions.

This 'larger' range was chosen for the purpose of experimental analysis as the bigger coal particles tend to handle much easier than smaller particles (powder) and the average particle size in this range can still be classified as fine coal. The laboratory sieves used to achieve this size separation are illustrated in Figure 3.2.1(a).

The coal samples were further separated in their maceral fractions, vitrinite, inertinite and a mixture of the two by means of gravity separation using a zinc chloride solution prepared at a specific gravity (SG) of 1.3 and 1.4 as can be seen in Figure 3.2.1(b) and 3.2.1(c). It can be assumed that the bulk of the vitrinite, or vitrinite rich fraction, will float at a SG of 1.3, the bulk of the inertinite, or inertinite rich fraction, will sink at a SG of 1.4 and that most of the mixture of the vitrinite and inertinite will sink / float in between (1.3SG < mixture < 1.4SG) (Falcon & Snyman, 1986:25).

After gravity separation the coal samples were washed thoroughly (Figure 3.2.1(d)) and air dried on plastic bags (Figure 3.2.1(f)). The zinc chloride was filtered where after the SG was readjusted (if required) to be reused as shown in Figure 3.2.1(e).

Virgin coal samples were used in parallel with the separated maceral fractions in the experiments described below to investigate and compare the influence of the thermal drying process on both the virgin coal and the separated maceral fractions.

3.2.2. TGA (thermogravimetric analyser) experiments

This experiment was chosen as it produces a graph of mass loss plotted against temperature. The experimental sample is placed in a small pan and heated in a small oven while being weighed to produce the required graph (see Figure 3.2.2). In conjunction with the proximate analysis discussed in paragraph 3.2.4 this data can be used to determine at what temperature as well as in which quantity water and volatile mater is lost.

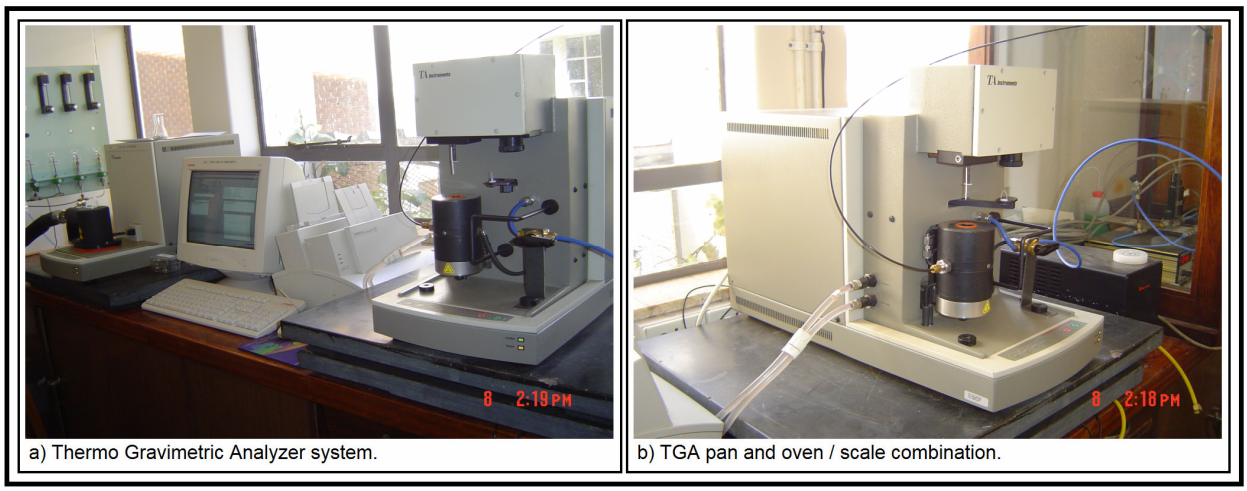

a) Thermo Gravimetric Analyzer system.

b) TGA pan and oven / scale combination.

Figure 3.2.2: Illustration of the thermogravimetric analyser.

The TGA 2050 Thermogravimetric Analyzer by TA Instruments was selected for this experiment. The nitrogen supply valve is opened in order to establish a 10ml/min nitrogen flow through the small oven chamber to prevent the sample from oxidizing during the experiment, simulating an industrial thermal drying method conducted in an inert atmosphere.

The small platinum sample pan is now cleaned by burning any residue left from previous experiments off over a gas flame. The sample pan is then loaded into the TGA to be taired (zeroed) where after a small quantity of coal (approximately 10 to 15mg) is placed on the pan and loaded into the TGA for the experiment.

After a suitable heating program is selected, the experiment is started and run by a computer program. The heating program selected for the purpose of this study is a constant heating rate of 10°C/min from 30 to 1000°C. The TGA heats the coal sample at the selected heating rate and the computer program plots the mass of the sample at the measured temperature as the sample is heated. After the experiment is finished the oven cools down and opens automatically at a safe temperature, ready for the next sample. Repeatability on coal was reported to be within ± 3°C (Saha *et al.*, 2010:369-378; Benfell *et al.*, 1996:67-74).

The reason for the selection of a heating rate of 10°C/min rather than a faster rate (as would be expected in industry) is both to allow the heat to conduct through all particles (heat transfer by means of convection, not conduction) to obtain a more accurate representation of mass loss data to compare with the proximate analysis described in paragraph 3.2.4 and because of equipment limitations.

3.2.3. SEM (scanning electron microscope)

The SEM (Figure 3.2.3(a)) will be used at higher heating rates (50°C/min) than the rates used in the TGA experiments in order to monitor physical changes that occur on the coal surface when it is heated at rates similar to those expected in industry.

The SEM bombard the small sample chamber in the heating stage (Figure 3.2.3(b)) with electrons where after an image is created by the collection of backscatter electrons. The sample chamber is lowered directly into the heating stage making heat transfer conductive and as a result virtually instantaneous with almost no lag on the temperature displayed. This is also the reason higher heating rates can be used during the SEM experiments than the rates used during the TGA experiments.

TIF images are created as the sample is heated from 30 to 930°C at pre-selected time increments resulting in images every 1 to 2°C. These images are then ‘strung’ together to create a short video showing the physical changes which occur while the sample is heated.

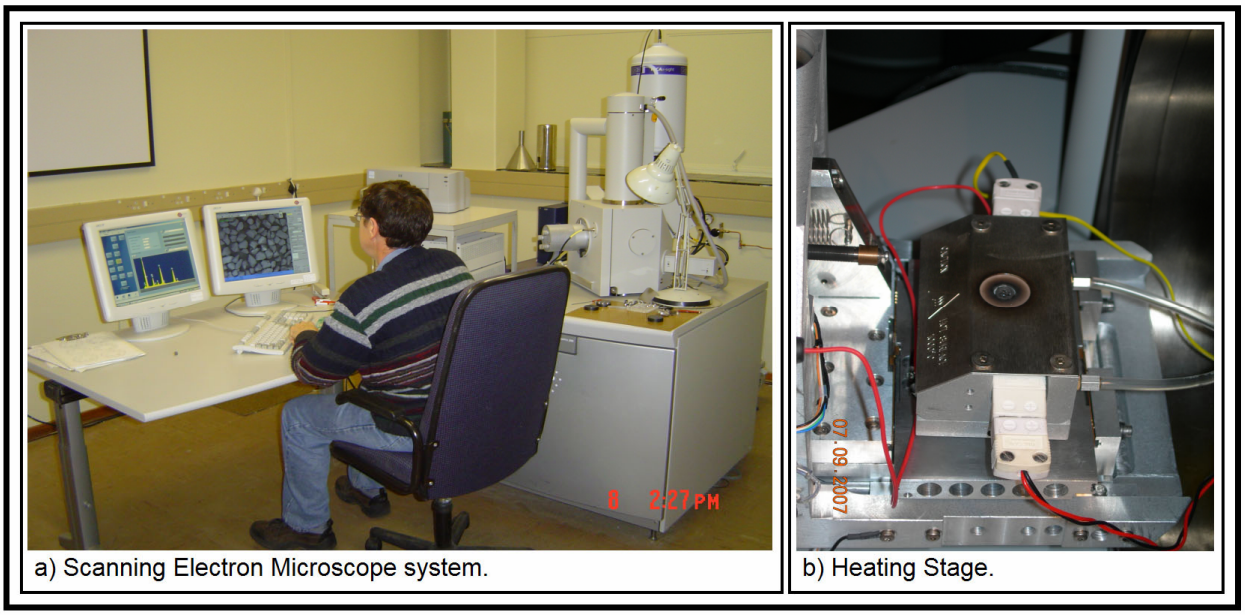

a) Scanning Electron Microscope system.

b) Heating Stage.

Figure 3.2.3: Illustration of the scanning electron microscope.

These videos can then be used in conjunction with the results obtained from the other experiments to better understand the physical changes which occur in coal particles when heated.

3.2.4. Nitrogen furnace with proximate analysis

This procedure will be split into two sections namely:

- Nitrogen furnace and preparation of coal samples
- Proximate analysis on these samples

This is done to focus on the two procedures individually. The reason these procedures are not discussed in two separate paragraphs is that the nitrogen furnace is only used to heat the coal samples to different predetermined temperatures. Proximate analyses will then be conducted on these samples; no results will thus be obtained and reported from the nitrogen furnace experiment only.

3.2.4.1. Nitrogen furnace and preparation of coal samples

A small enclosure was constructed from stainless steel which was connected to a nitrogen supply at the back in order to flush the environment inside the enclosure with nitrogen, thus creating an inert atmosphere as would be employed in industry. A thermocouple was also installed at the top of the enclosure to measure and control the temperature inside the experimental area. The coal samples were loaded inside this enclosure in separate pans, as can be seen in Figure 3.2.4.1(b), to allow simultaneous heating of the samples where after the

enclosure was placed in a regular furnace to control the temperature as specified in paragraph 3.2.4.2 and 3.2.5 below.

As can be seen in Figure 3.2.4.1(b and c) this enclosure was constructed with the nitrogen supply tube coiled on top of the enclosure box to allow ample time for heat transfer through the supply tube to the nitrogen from the environment inside the furnace. This was done to ensure that no 'cold spots' are created inside the enclosure box and that all samples are heated to exactly the same temperature.

The experiment was done by placing the cold samples inside the enclosure, heating the samples to the required temperature at the maximum rate allowed by the furnace (approximately 10°C/min) and 'soaking' the samples at this temperature for approximately 30 minutes to allow all moisture and volatile matter which might evolve ample time to do so.

a) Furnace used for preparation of Proximate Analysis samples.

b) Enclosure constructed to heat samples in a N_2 atmosphere.

c) Enclosure in Furnace, ready for start of experiment.

d) Samples in Climate Room after heating is completed.

Figure 3.2.4.1: Preparation of the proximate analysis samples in the nitrogen furnace.

After the heating cycle was completed the samples were allowed to cool down inside the enclosure within the nitrogen atmosphere. When the temperature reached 40°C the samples were removed and exposed to the conditions in a climate room (Figure 3.2.4.1(d)) to reach steady state with the environment as required by the standards discussed in paragraph 3.2.4.2.

3.2.4.2. Proximate analysis

Proximate analysis were done on all samples heated to pre-selected temperatures in the nitrogen furnace in order to compare them to each other and to aid and better understand the results obtained in the TGA and SEM experiments.

Coal samples were selected as described below:

First the samples were split according to their maceral composition as per paragraph 3.2.1 thus creating four samples per mine, namely a vitrinite rich, mixture, inertinite rich and an original, virgin sample.

The samples were further split by heating them to 105, 130, 160, 190, 220 and 250°C in the nitrogen furnace. An unheated sample referred to as 'ambient' was also analysed as reference sample. It was decided to limit the maximum experimental temperature to 250°C as it can be assumed that it will not be cost effective to heat samples to higher temperatures in an industrial process.

The proximate analysis consist of:

- Determining of **moisture** according to the SABS 924 standard
- Determining of **volatiles** according to the ISO 562 standard
- Determining of **ash** according to the ISO 1171 standard
- Determining of **fixed carbon** by subtracting the above values from 100% composition

In addition, the **calorific value** of all samples was also determined with the use of a bomb calorimeter.

The methods indicated above are briefly described below; for more information please refer to the mentioned standards.

1) Moisture (SABS 924):

a) Place the moisture crucible in the vacuum oven at 6.7kPa(a) and 105 to 110°C in order to remove any moisture which might be present (shown in Figure 3.2.4.2.1(a)). Allow the crucible to cool down for 10 minutes on a metal plate where after it must be placed in a desiccator (Figure 3.2.4.2.1(b)) to prevent any moisture re-absorption while it cools down to the ambient temperature. Weigh the crucible and note the mass as m_1. Place the crucible back in the desiccator; the crucible is now ready for the experiment.

b) Place the sample in the atmosphere for a period of 30 minutes to allow the moisture in the particles to reach equilibrium with the humidity in the environment. Mix the sample

for 1 minute to ensure that no segregated spots are present. Spread approximately 1 gram of the selected sample over the complete surface of the moisture crucible, weigh the sample and note the mass as m_2.

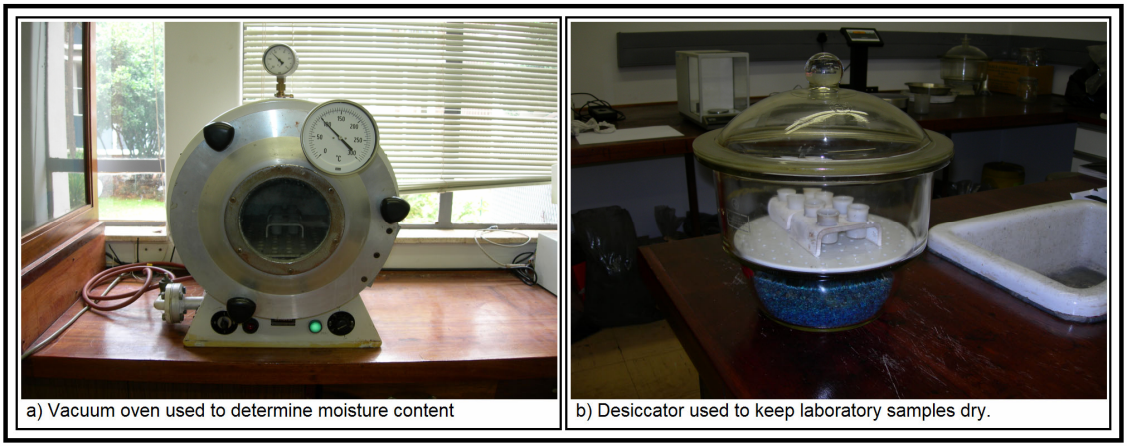

a) Vacuum oven used to determine moisture content

b) Desiccator used to keep laboratory samples dry.

Figure 3.2.4.2.1: Vacuum oven - apparatus used to determine moisture content.

c) Place the lid of the crucible in the desiccator and the crucible in the vacuum oven at 6.7kPa(a) and 105 to 110°C for one hour. Remove the crucible, replace the lid and allow the crucible to cool down on a metal plate for 10 minutes. Place the crucible back in the desiccator and allow another 10 minutes of cooling before weighing it to note m_3.

d) The moisture content can now be determined to the nearest 0.1% by means of the following formula:

$$Moisture = \frac{m_2 - m_3}{m_2 - m_1} \times 100\% \quad \text{where:}$$

m_1 = mass of empty crucible with lid

m_2 = starting mass of crucible, lid and moist sample

m_3 = end mass of crucible, lid and dry sample

2) Volatiles (ISO 562):

a) Place the sample in the atmosphere for a period of 30 minutes to allow the moisture in the particles to reach equilibrium with the humidity in the environment. Mix the sample for 1 minute to ensure that no segregated spots are present.

b) Place the volatile crucibles in the volatile oven shown in Figure 3.2.4.2.2(a and b) at 900 ± 5°C for a period of 7 minutes in order to remove any moisture and other volatile matter which might be present. Remove the crucibles from the oven and allow them to cool down where after they must be placed in a desiccator to avoid any moisture re-absorption. Weigh the empty crucibles and note m_1.

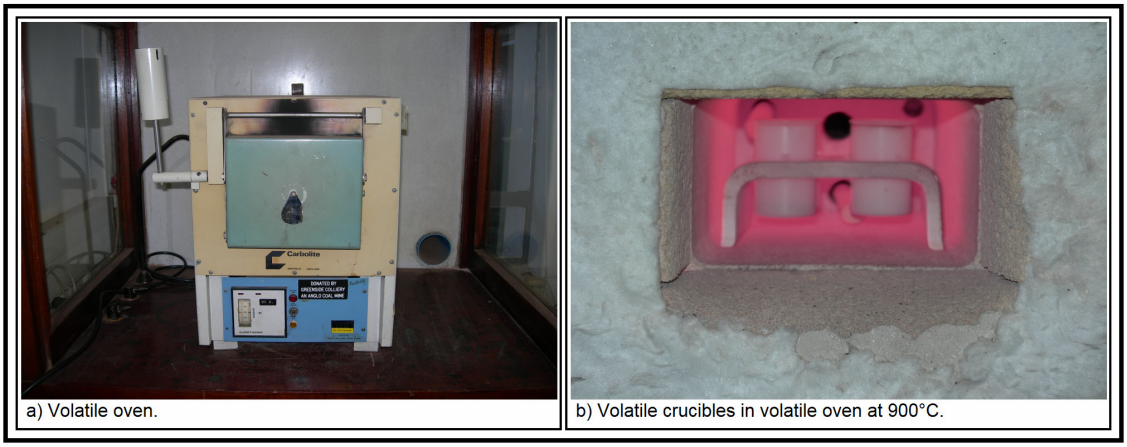

a) Volatile oven. b) Volatile crucibles in volatile oven at 900°C.

Figure 3.2.4.2.2: Volatile oven - apparatus used to determine volatile content.

c) Place approximately 1g (±0.1g) of sample in each crucible and weigh m_2. Place the crucibles in a cold crucible stand.

d) Place the crucibles with the stand in the volatile oven at 900 ± 5°C for a period of 7 minutes ± 5 seconds (as shown in Figure 3.2.4.2.2(b)). Remove the stand with crucibles from the volatile oven and allow sufficient time to cool down before placing it in a desiccator, preventing moisture re-absorption. Weigh the crucibles to determine m_3.

e) The volatile content can now be determined to the nearest 0.1% by means of the following formula:

$$Volatiles = \frac{100\% \cdot (m_2 - m_3)}{m_2 - m_1} - Moisture$$ where:

m_1 = mass of empty crucible with lid

m_2 = starting mass of crucible, lid and original (moist) sample

m_3 = end mass of crucible, lid and devolatilised sample

Repeatability should be within 3% of the mean result while reproducibility should be within 0.5% of the absolute result or 4% of the mean result; whichever is greater.

Care must also be taken to report any small deviations from the normal procedure or any odd observations made.

3) Ash (ISO 1171):

a) Place the sample in the atmosphere for a period of 30 minutes to allow the moisture in the particles to reach equilibrium with the humidity in the environment. Mix the sample for 1 minute to ensure that no segregated spots are present.

b) Place the ash crucibles in the oven shown in Figure 3.2.4.2.3(a and b) at 815 ± 10°C for a period of 15 minutes in order to remove any volatile and igniting matter which might be present. Remove the crucibles from the oven and allow them to cool down

where after they must be placed in a desiccator to avoid any moisture re-absorption. Weigh the empty crucibles and note m_1.

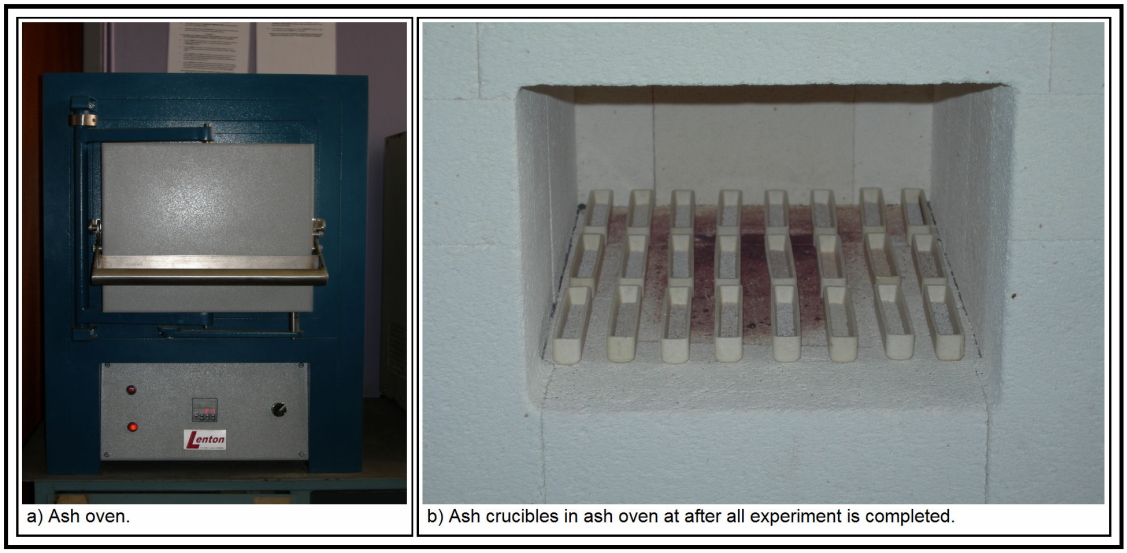

a) Ash oven.

b) Ash crucibles in ash oven at after all experiment is completed.

Figure 3.2.4.2.3: Ash oven - apparatus used to determine ash content.

c) Place between 1 and 2 grams of sample into each crucible and weigh m_2.

d) Place the crucibles into the ash oven and set a program to heat the samples to 500°C over a period of 30 minutes. The samples must be heated from 500 to 815°C over a period of 30 to 60 minutes where after all samples must be 'soaked' at 815 ± 10°C for a period of 60 minutes. Remove the samples and allow sufficient time to cool down in a desiccator preventing moisture re-absorption. Weigh the crucibles with the remaining ash and note m_3.

e) The ash content can now be determined to the nearest 0.1% by means of the following formula:

$$Ash = \frac{m_3 - m_1}{m_2 - m_1} \times 100\% \qquad \text{where:}$$

m_1 = mass of empty crucible

m_2 = starting mass of crucible and original (moist) sample

m_3 = end mass of crucible and remaining ash

Repeatability should be within 2.0% of the mean result for an ash percentage smaller than 10% and within 0.2% of the absolute result for an ash percentage larger than 10%.

Care must also be taken to report any small deviations from the normal procedure or any odd observations made.

4) Fixed carbon:

The fixed carbon content can now be determined by means of the following formula:

$$F.Carbon = 100\% - (Moisture\% + Volatile\% + Ash\%)$$

5) Calorific value:

The calorific value of each sample is determined using a bomb calorimeter (BC). The experiment is done by weighing approximately 0.5 to 1 gram of each sample into a small metal (for conductive purposes) crucible. The sample is placed in the BC where after the BC chamber is sealed and pressurized with pure oxygen. The instrument determines the calorific value of each sample by measuring the increase in temperature of a certain amount of water when the predetermined weight of sample is burned in the pressurized oxygen atmosphere. From this increase in temperature the total energy release for each sample can be determined. This value in conjunction with the mass of the sample burned can now be used to calculate the calorific value of each sample. The calorific value is reported in MJ/kg by the BC. An illustration of the bomb calorimeter can be seen in Figure 3.2.4.2.5.

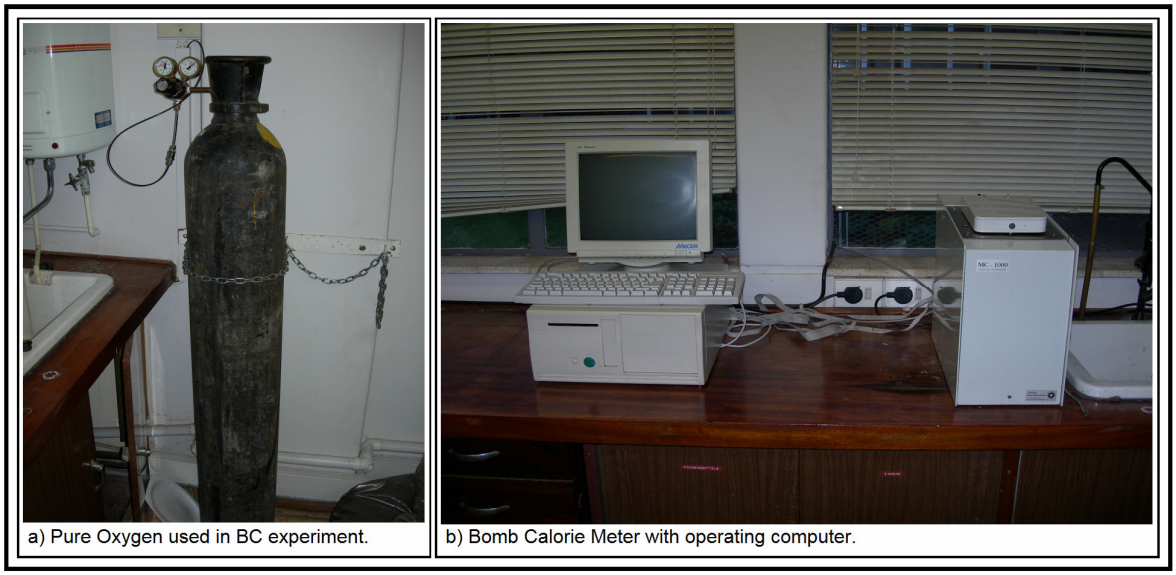

a) Pure Oxygen used in BC experiment.

b) Bomb Calorie Meter with operating computer.

Figure 3.2.4.2.5: Bomb calorimeter - apparatus used to determine calorific value.

3.2.5. Mercury intrusion

This experiment was chosen in order to gather additional data to complement the other results obtained in this study as it produces information on the porosity, total pore area, median pore diameter and average pore diameter of the experimental sample. This data can then be used in conjunction with the other results to analyse and better understand what physically happens to the fine coal when exposed to thermal drying.

It was decided to select only three of the five coal samples to conduct this experiment on because of restrictions on time and availability of the apparatus. The selected samples were the Witbank seam 2 coal, the Witbank seam 4 coal and the Free State coal.

Samples were prepared according to paragraphs 3.2.1 and 3.2.4.1. The sample test temperatures included the ambient sample as well as 105, 190, 250, 300, 350 and 400°C.

An Autopore IV 9500 porosimeter, which can be seen in Figure 3.2.5(a), was used to produce the required data. The instrument determines the porosity of a sample by applying various levels of pressure to a sample immerged in mercury. The pressure required to intrude mercury into the sample's pores is inversely proportional to the size of the pores.

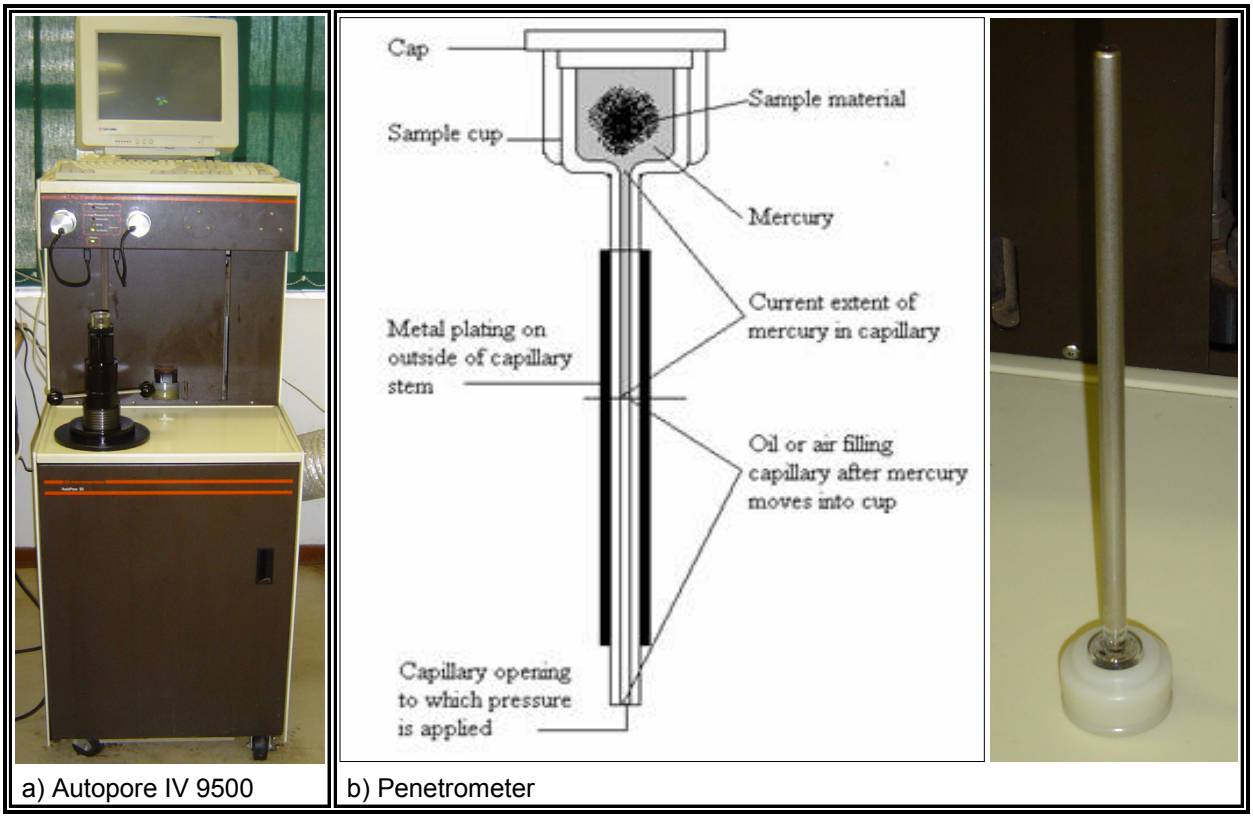

a) Autopore IV 9500 b) Penetrometer

Figure 3.2.5: Autopore IV 9500 porosimeter - apparatus used to determine porosity.

The Autopore IV 9500 porosimeter consist of both a low-pressure and high-pressure port for increased sample throughput. The penetrometer, used to contain and transfer the sample throughout the experiment, can be seen in Figure 3.2.5(b). A sample of about 1g is weighed into the penetrometer where after it is sealed with high-pressure grease and weighed again. The low-pressure port is used to apply a vacuum of 35µm Hg over the sample contained inside the penetrometer. This is done to remove all air and moisture from the sample. Once the required vacuum is achieved the penetrometer is filled with mercury and pressurized to 206kPa. The penetrometer is now weighed again to obtain the assembly weight before it is moved to the

high pressure port where mercury is forced into the sample and all its pores up to a maximum pressure of 206MPa.

With the measured weights, the Autopore IV 9500 software calculates the data mentioned above. It is important to understand exactly what the supplied data represents and indicates; this is briefly described below:

- **Porosity:** This property is a measure of the void spaces in the coal.
- **Total pore area:** The total area of all pores intruded by mercury.
- **Median pore diameter:** The diameter of the pore for which 50% off all pores have a larger diameter and 50% off all pores have a smaller diameter.
- **Average pore diameter:** This is the pore diameter off all pores summed together and divided by the total number of pores.

The data obtained is presented in the form of four graphs plotted against the sample test temperature; these graphs are analysed and discussed when compared to one other.

Chapter 4
Results and Discussion

In this chapter the results obtained from all experiments described in chapter 3 will be displayed and discussed.

4.1. Introduction

Certain experiments were selected producing the results indicated below to aid in understanding the changes which occur when coal particles are exposed to thermal drying conditions. The equipment used as well as the experimental procedures followed were discussed in chapter 3.

It was decided to present the experimental results below in the same order in which the experimental procedures were discussed in chapter 3. For convenience purposes the order is shown below.

Order in which experimental results are presented:

- TGA (thermogravimetric analyser) experiments
- SEM (scanning electron microscope) experiments
- A combination of a nitrogen furnace with proximate analysis
- Mercury intrusion experiments

Coal sample order as a subsection to the experimental results:

- Witbank seam 2 coal – referred to as WB2
- Witbank seam 4 coal – referred to as WB4
- Soutpansberg coal – referred to as TS
- Waterberg coal – referred to as GG
- Free State coal – referred to as NV

4.2. TGA results

The TGA results represent the percentage of the original sample's mass remaining as each coal sample is heated from 30 to 1000°C at 10°C/min in a nitrogen (inert) atmosphere; this is done at atmospheric pressure.

To ensure all results are comparable all data was processed with the 100% mass taken at 30°C.

4.2.1. TGA results for the WB2 coal

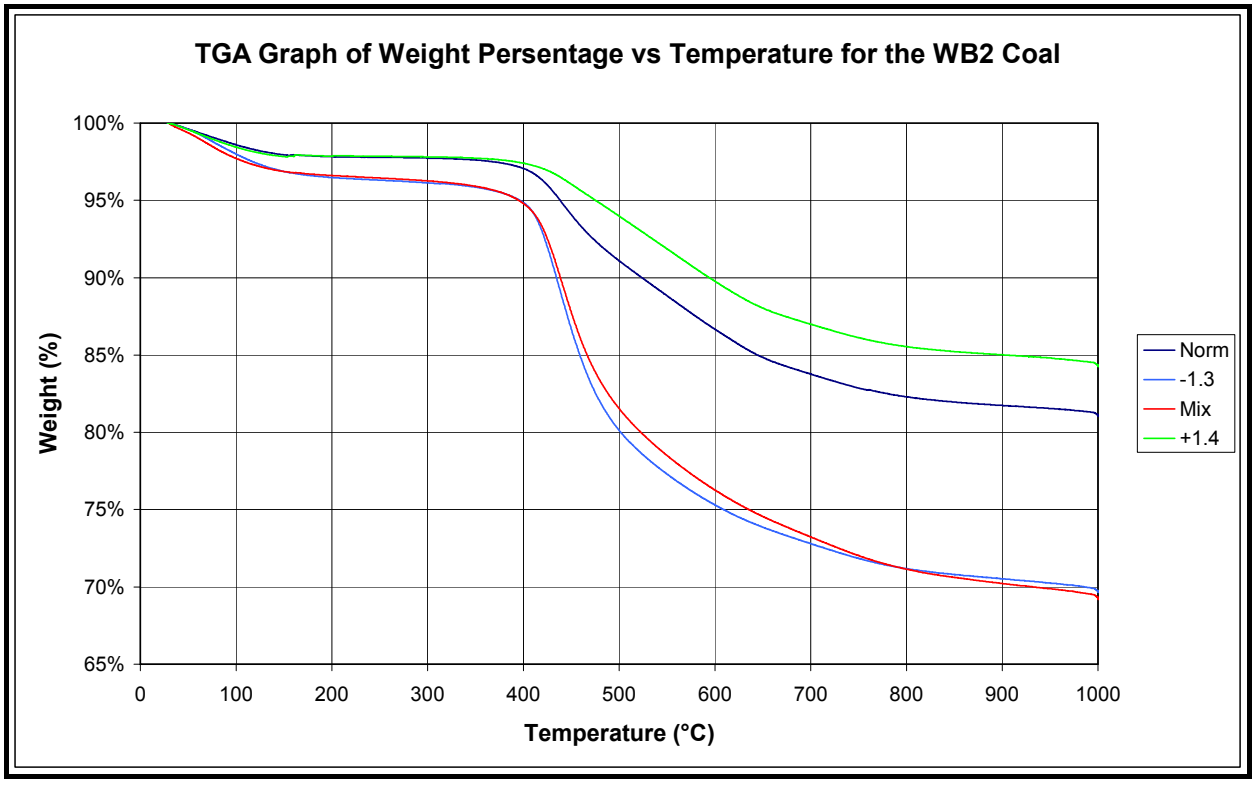

Graph 4.2.1: TGA mass loss graph for the WB2 coal.

As can be seen from Graph 4.2.1, mass loss in the heavier inertinite fraction was the least over the total heating range which can be attributed to the fact that this is the least reactive maceral fraction of the coal and that most of the ash containing particles processed with the coal will sink with the inertinite fraction during the initial density separation process. The mixture and vitrinite fractions show almost the same mass loss, indicating that they contain similar amounts of volatile matter. As expected, the virgin coal sample (before separation) represents an average of the three separated samples.

If the first part of the mass loss curve is considered, it is observed that all samples loose mass at a fairly constant rate up to 150°C where after the rate of mass loss decreases up to about

200°C. Between 200 and 350°C almost no mass loss can be observed where after primary devolatilisation initiates starting between 350 and 450°C. It is also observed that the mixture fraction shows the largest initial mass loss which might be attributed to the interfaces between the vitrinite and inertinite fractions which create planes causing a hydrophilic environment in which water can accumulate.

4.2.2. TGA results for the WB4 coal

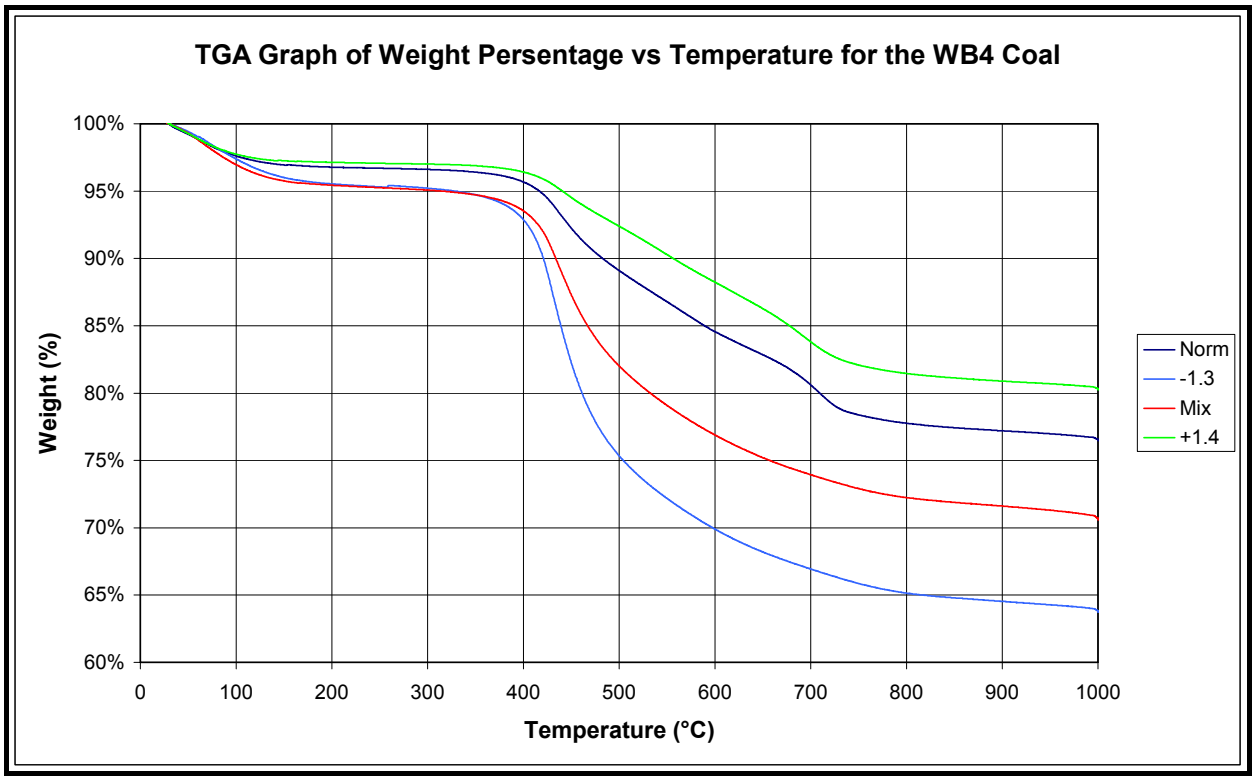

Graph 4.2.2: TGA mass loss graph for the WB4 coal.

As can be seen from Graph 4.2.2, mass loss in the heavier inertinite fraction was the least over the total heating range which correspond to the trend seen in the WB2 coal above. The mixture fraction again shows the largest initial mass loss which can be attributed to the interfaces between the vitrinite and inertinite fractions. Above 350°C the mass loss for the vitrinite fraction increases substantially when compared to the mixture fraction indicating a high volatile content associated with the vitrinite fraction as confirmed by the proximate analysis indicated in Graph 4.4.2(a). As expected, the virgin coal sample again represents an average of the three separated samples.

4.2.3. TGA results for the TS coal

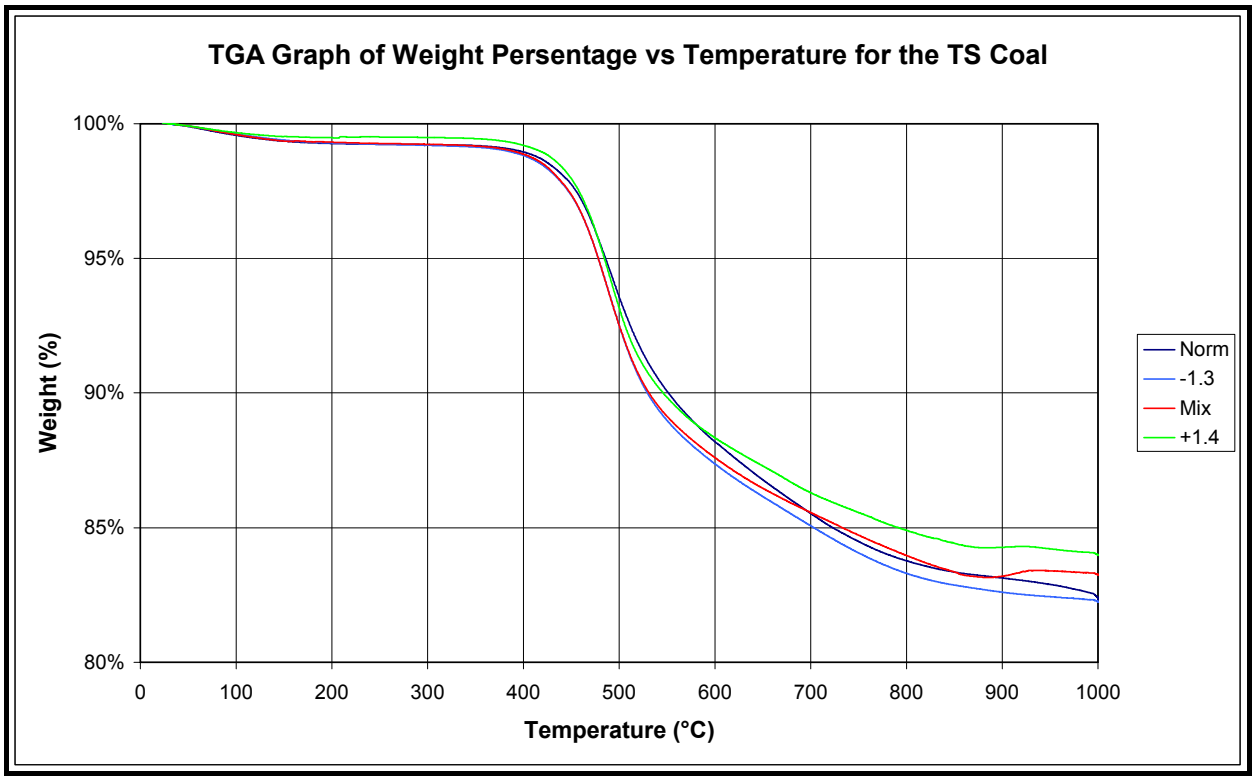

Graph 4.2.3: TGA mass loss graph for the TS coal.

As can be seen from Graph 4.2.3, mass loss in the heavier inertinite fraction was again the least over the total heating range which can be attributed to the same reasons given for the WB2 coal above. This coal is the highest ranked coal in South Africa which can be seen from the results as very little difference in the separated samples is observed with the inertinite showing similar properties to the vitrinite. Less than 20% mass loss occurs up to 1000°C which correspond to the low volatile, high carbon content normally associated with this coal. The virgin sample's mass loss deviates slightly from what may be expected if the separated sample's curves are considered. This deviation does not raise concern as it is very small and can be attributed to a very small experimental sample loaded into the TGA pan (in this experiment 15.358mg) which does not represent as good an average as a 1g sample would.

If the first part of the mass loss curve is considered, it is observed that mass loss follows the same trend as described for the WB2 and WB4 coals. In the case of the TS coal, the mass loss between the mixture and other fractions is however almost unnoticeable which can be attributed to the high vitrinite purity of the coal resulting in a low quantity of interface planes in which water can collect.

4.2.4. TGA results for the GG coal

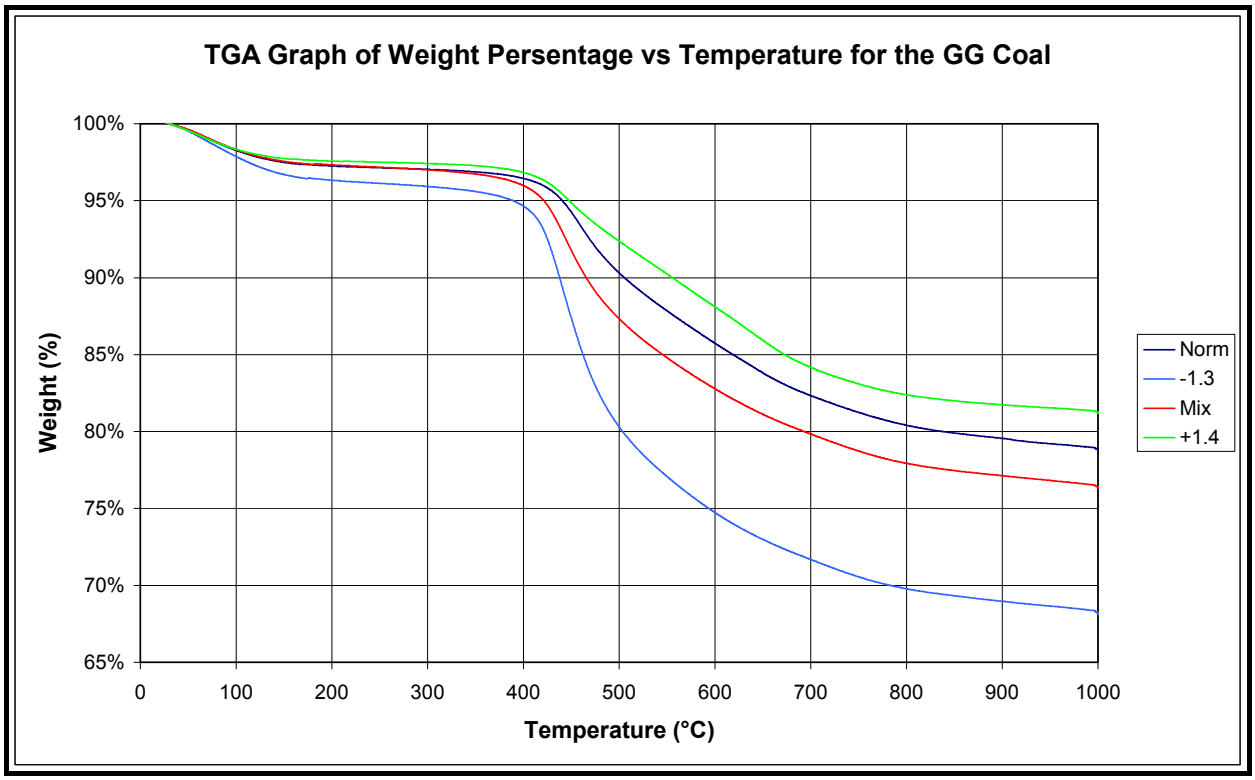

Graph 4.2.4: TGA mass loss graph for the GG coal.

As can be seen from Graph 4.2.4, mass loss in the heavier inertinite fraction was again the least over the total heating range which can be attributed to the same reasons given for the WB2 coal above. The mass loss in the initial stages of the mixture and vitrinite fractions however differ substantially form the trend observed in the other coals as the vitrinite fraction shows a larger mass loss during the 'drying' stage opposed to greater mass loss observed in the mixture fraction of the other coals. This can be explained by the fact that the vitrinite fraction has a higher moisture content that the other fractions (refer to Graph B.4 in appendix B) indicating that the vitrinite fraction must be more hydrophilic than the other fractions. Upon heating Graph B.4 concurs with the findings indicated above as the vitrinite sample loses its moisture rapidly compared to the other fractions. A possible explanation to this phenomena is that the Waterberg coal naturally occurs in a 'bar-coded' form in stead of coal 'seams' normally associated with coal, where very thin layers of coal is interfaced with thin soil layers. The GG coal was thus formed as a result of 'abnormal' conditions which could have resulted in the higher moisture content and hydrophilic properties associated with the vitrinite fraction. Above 350°C the mass loss for the vitrinite fraction correspond to the trend observed in the WB4 coal where the mass loss increase even more when compared to the mixture fraction indicating a high volatile content associated with the vitrinite fraction. This can again be confirmed by the

proximate analysis indicated in Graph 4.4.4(a). As expected, the virgin coal sample represents an average of the three separated samples.

4.2.5. TGA results for the NV coal

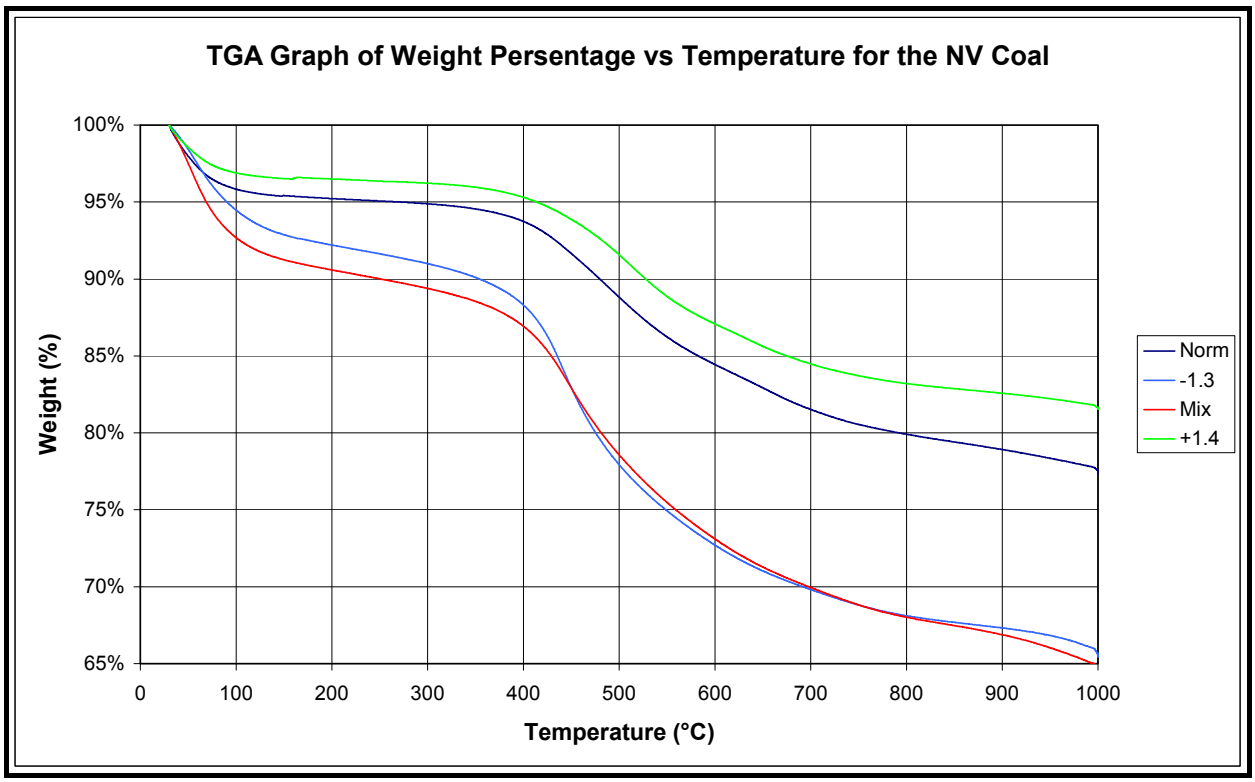

Graph 4.2.5: TGA mass loss graph for the NV coal.

As can be seen from Graph 4.2.5 mass loss in the heavier inertinite fraction was again the least over the total heating range which can be attributed to the same reasons given for the WB2 coal above. The mixture and vitrinite fractions differ in mass loss over the initial heating period where after the two curves join up to the end of the heating range indicating a larger volatile content in the vitrinite fraction as can be seen in Graph 4.4.5(a). As expected, the virgin coal sample represents an average of the three separated samples.

4.2.6. Discussion of TGA results

As can be seen from the TGA results described in paragraph 4.2 above, deviations occur in the mass loss data after primary devolatilisation initiates but for all samples tested the trend up to when this start remains fairly constant.

The first part (drying) of the mass loss curve indicates that all samples lose mass at a fairly constant rate up to 150°C where after the rate of mass loss decreases up to about 200°C. Between 200 and 350°C almost no mass loss can be observed where after primary

devolatilisation initiates starting between 350 and 450°C. This corresponds to the findings by others as described in paragraph 2.4.2.

When the TGA results are considered it is suggested that thermal drying must not be utilized above 150°C and certainly not above 200°C as water evaporation decreases after this temperature and the use of additional energy to heat the coal to higher temperatures will not be cost effective. Ejecting the coal from the dryer at higher temperatures will also make the coal more prone to oxidation, spontaneous combustion and dust explosions.

4.3. SEM results

The SEM results are represented in the form of videos which can be viewed on the accompanying DVD disc. For the purpose of this dissertation it was decided to capture images from the videos reflecting significant changes which occur as the samples are heated. These video images will also be accompanied by a short discussion of observations made as the coal particles are heated.

Photos taken after the experimental samples were removed from the SEM are shown and discussed in appendix A.

The videos depict one or more coal particles as they are heated from 30 to 930°C at a rate of 50°C/min and an absolute pressure of 410Pa. Unfortunately the SEM can only operate under vacuum which differs from the atmospheric pressure expected in industry but this effectively provides an oxygen poor environment which corresponds to an industrial drying method.

4.3.1. SEM results for the WB2 coal

WB2 inertinite sample:

The Witbank 2 seam inertinite particles remain stagnant when it is heated from 30°C. From 477°C slight movement in the particle to the top left hand corner is observed with a sudden shift in position at 492°C. From 492 to about 517°C the centre particle starts to move as well. At 517°C a crack starts to form in the centre particle and movement stops. At 656°C the particle to the top jumps to an unknown location. From 724°C the bottom particle starts to move in position where after all particles demonstrate a simmering movement which stops at about 778°C. No further movement is observed up to 901°C where after heating is suspended. Good separation of the sample is observed as no ‘plastic’ or ‘melting’ behaviour can be seen; these particles represent the harder inertinite fraction.

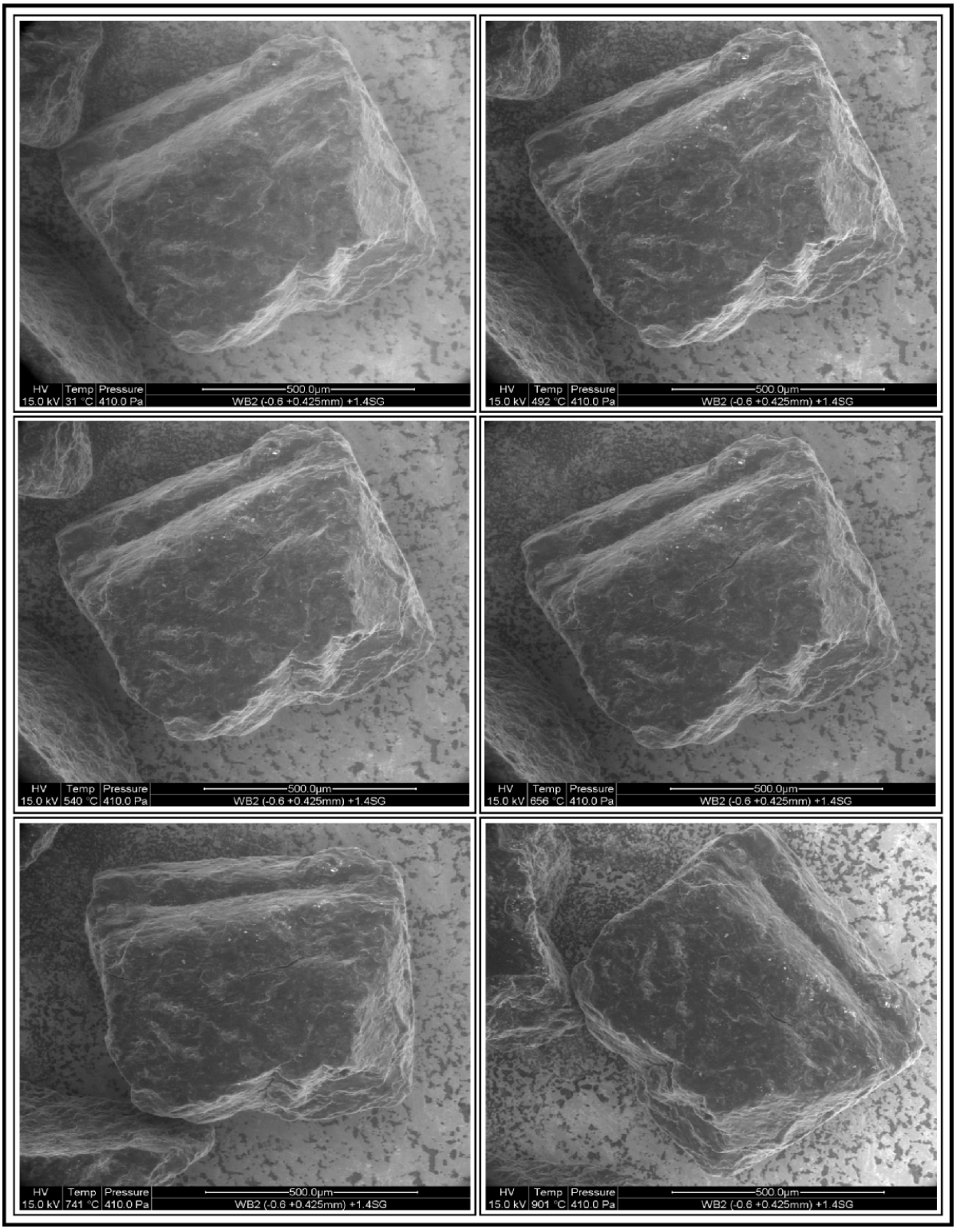

Figure 4.3.1(a): SEM image observation for heating of the WB2 inertinite coal.

WB2 mixture sample:

The Witbank 2 seam mixture particles remain stagnant when it is heated from 30°C. At 389 and 413°C very little movement is observed. At a temperature of 424°C a crack starts to appear in

the particle to the top right of the current view. From a temperature of 447°C minor movement is observed again with small bubbles appearing from below the particle at 454°C. At a temperature of 463°C the particle jumps to a different location; cracks and melted plastic areas can be seen on the particle's surface.

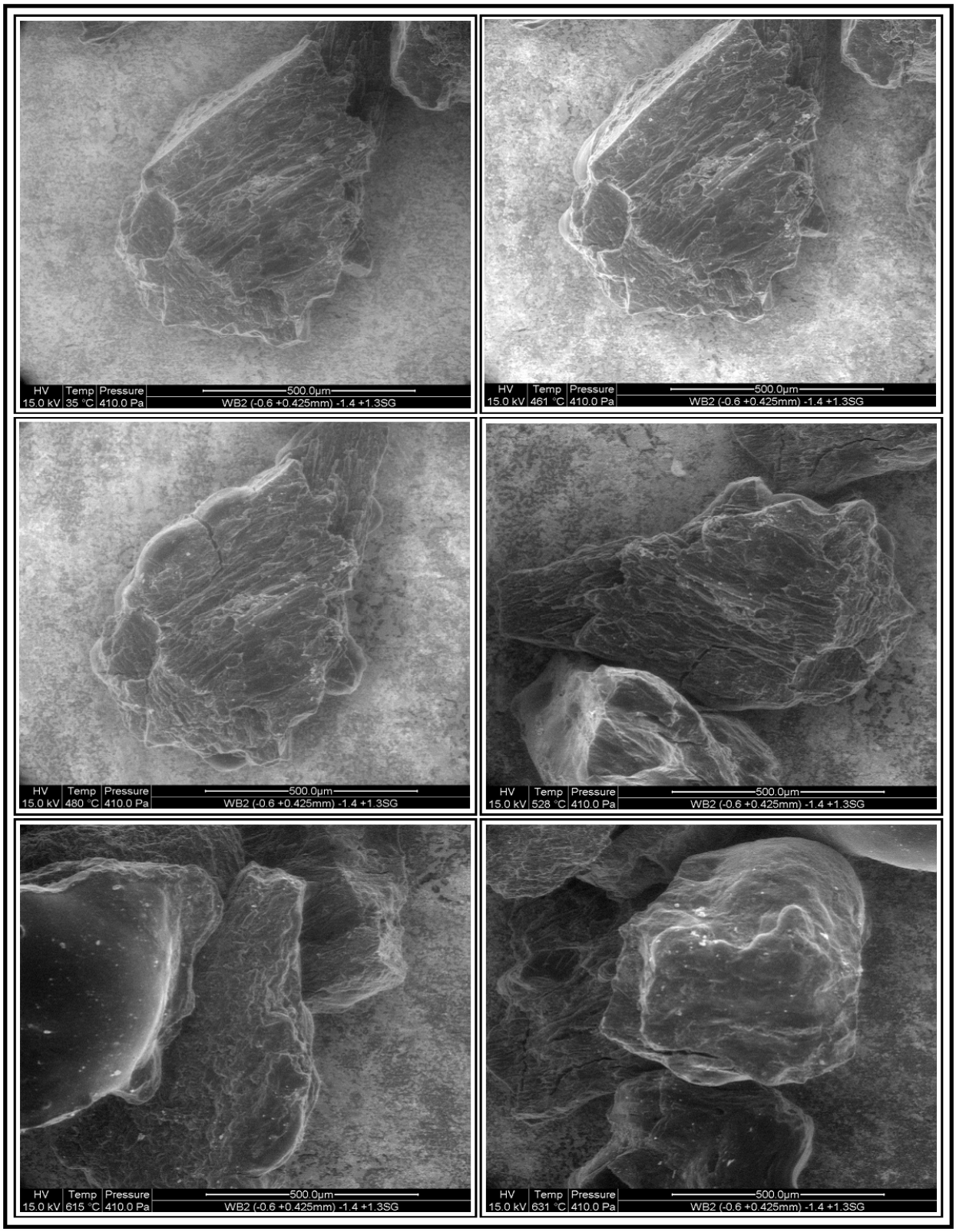

Figure 4.3.1(b): SEM image observation for heating of the WB2 mixture coal.

The crack opens up as the melted bubble expands at a temperature of 480°C. From 500 to 523°C a period of rapid movement and jumping takes place which calms down to slight movement up to a temperature of 601°C. From this temperature the particles shift into periods of rapid jumping movement. At a temperature of 620°C the particle in centre view jumps to an unknown location. These spells of rapid jumping stabilizes at a temperature of 644°C. Very little movement is observed up to 730°C when rapid jumping movement takes over again and continues up to 746°C where after small shifts in position takes place up to 758°C. Minor to no movement continues up to 881°C when a last period of simmering takes place up to 886°C. No further movement can be seen up to 901°C when heating is suspended. Good separation of this fraction is observed as both the harder inertinite fraction which forms cracks as well as the more plastic vitrinite fraction which forms plastic bubbles can be seen.

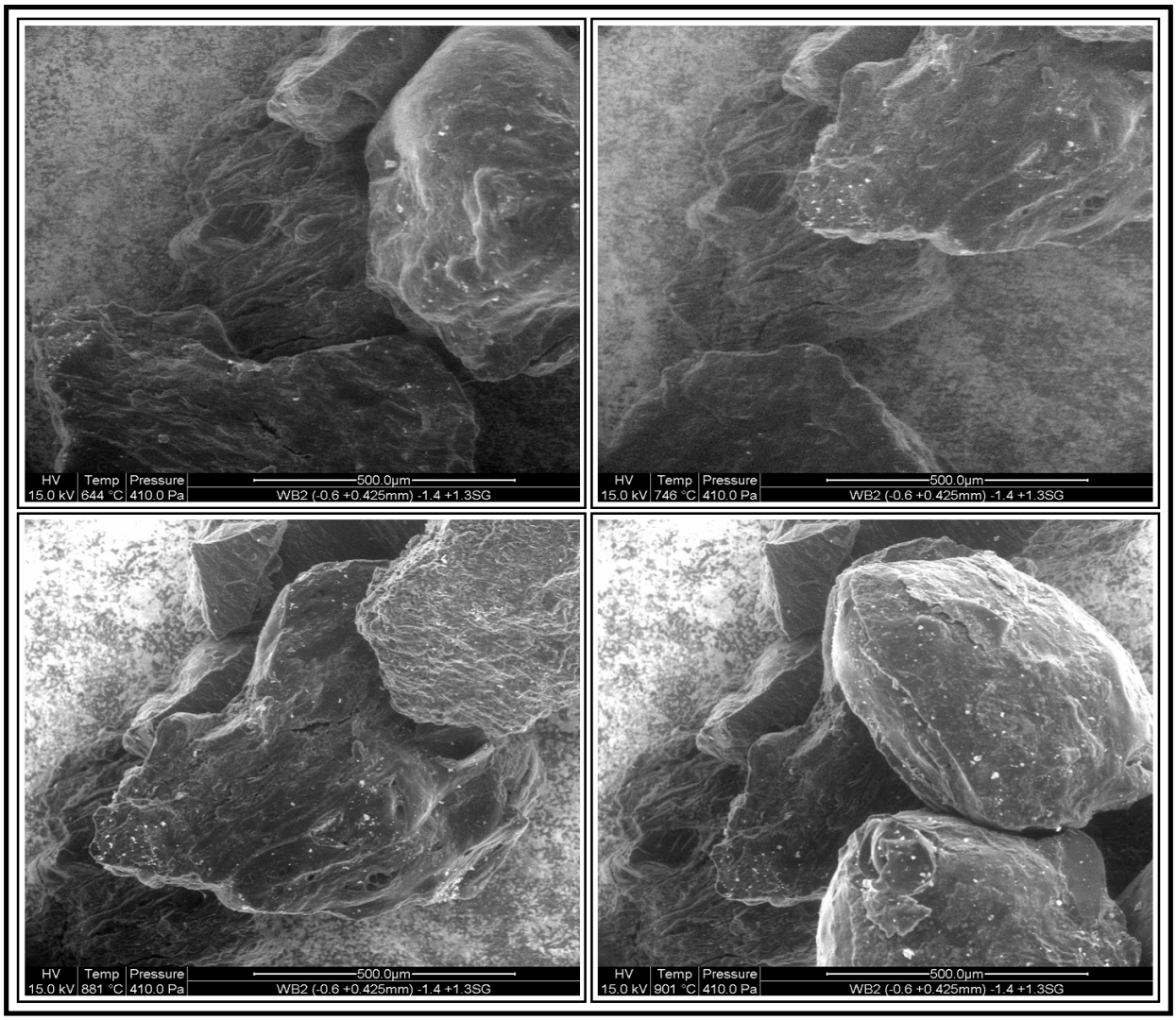

Figure 4.3.1(c): SEM image observation for heating of the WB2 mixture coal.

WB2 vitrinite sample:

The Witbank 2 seam vitrinite particles remain stagnant when it is heated from 30°C. Very little movement is observed in increments from a temperature of 267°C with the first real visible movement at a temperature of 357°C when the centre particle shifts slightly. More shifting movement is observed in the centre particle at 378 and 384°C. Between 406 and 408°C the centre particle shows slight simmering movement where after all particles start to move. The centre particle starts to turn on its side and enters a plastic state at 434°C. All particles continue to shift around and the centre particle swells up to a maximum size at 446°C. The centre particle enters a stage with extreme swelling at the bottom end which reaches a maximum at 477°C. In this period all other particles enters a plastic state as well. Blow down in the centre particle starts slowly with little overall movement and continues up to a temperature of 530°C when the particle to the left shows a sudden jerk at 531°C.

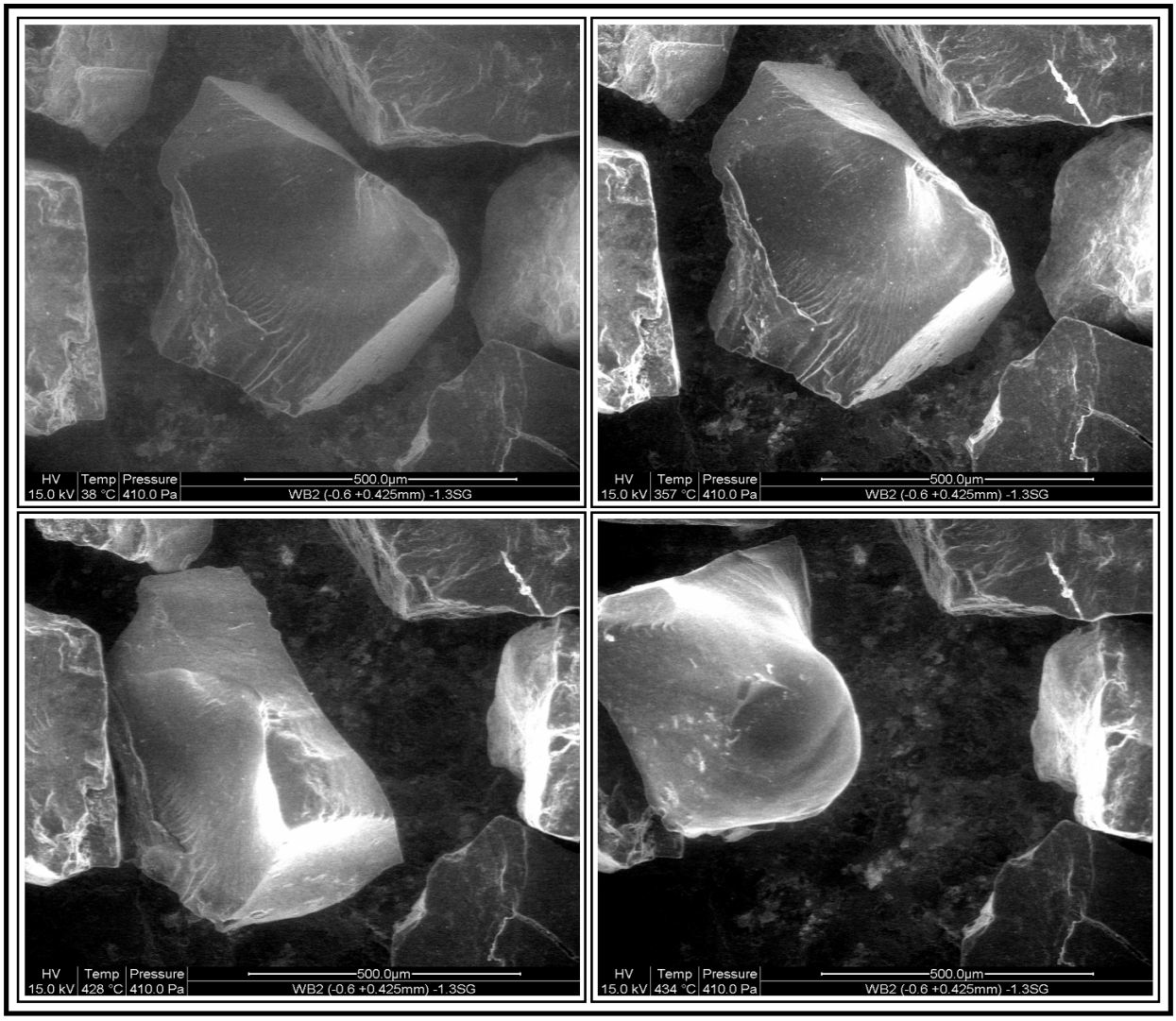

Figure 4.3.1(d): SEM image observation for heating of the WB2 vitrinite coal.

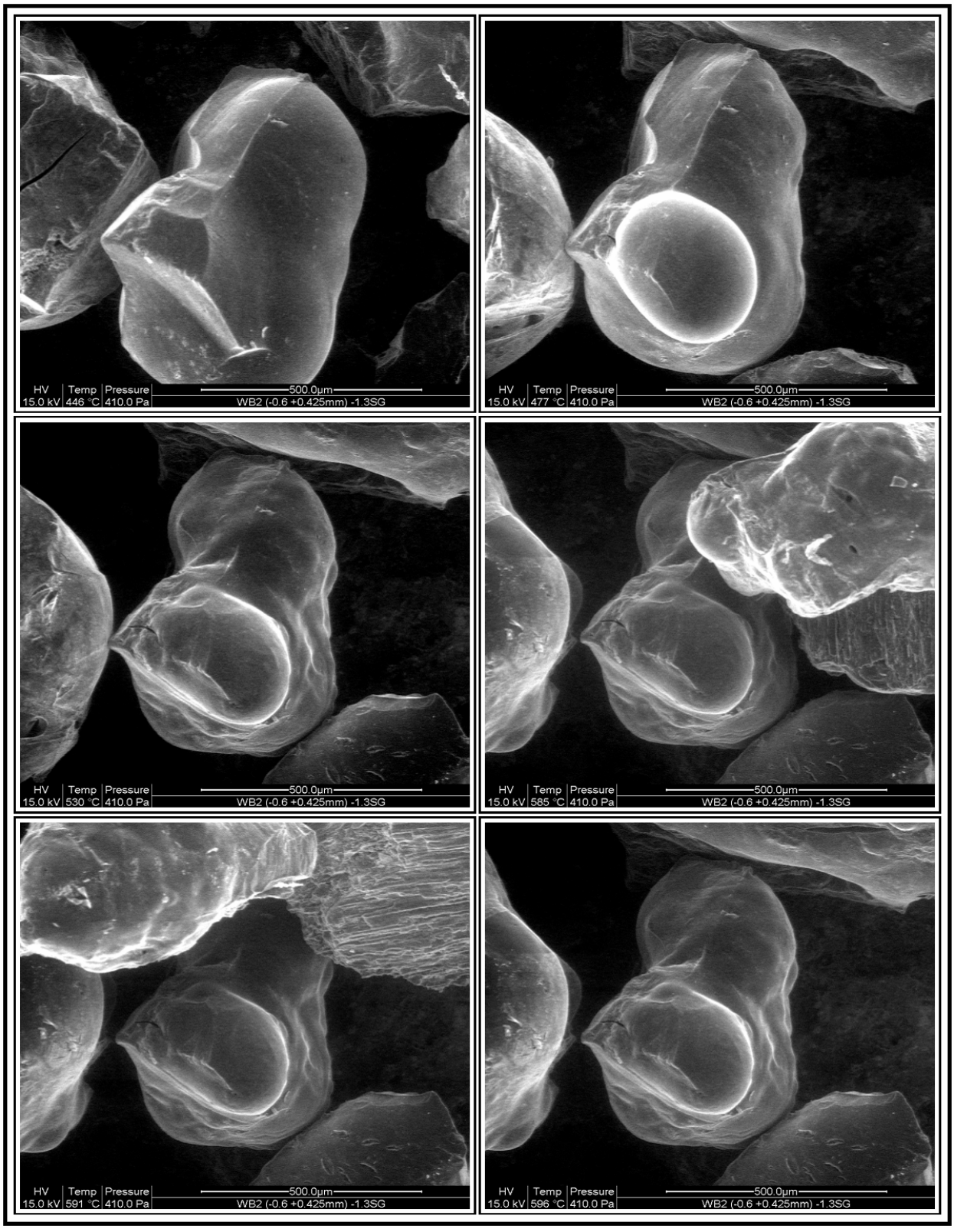

Figure 4.3.1(e): SEM image observation for heating of the WB2 vitrinite coal.

From this temperature no movement is observed up to a temperature of 583°C from which different particles jump into and out of view. These sudden jumps are observed at 588, 594, 597 and 599°C. These jumping movements continue in periods between 612 to 695 and 733 to 750°C. The movement slows down dramatically from this temperature and only small shifts can

be observed at temperatures of 760, 783 and 788°C where after almost nothing can be seen up to 869°C. From 869 up to 900°C intervals where some particles show rapid jumping movement can be observed. Good separation of this fraction is observed as most particles were converted into a complete plastic state.

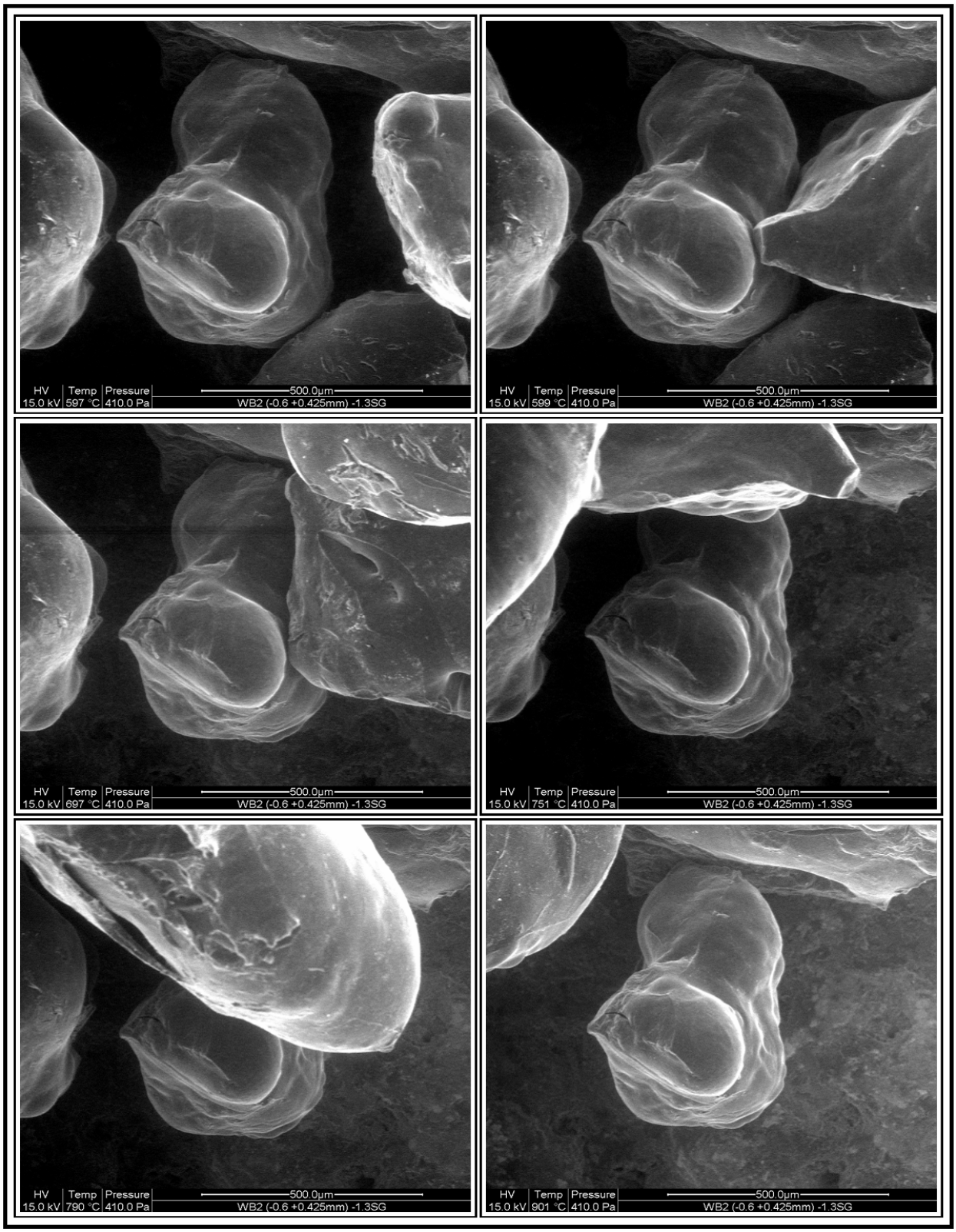

Figure 4.3.1(f): SEM image observation for heating of the WB2 vitrinite coal.

4.3.2. SEM results for the WB4 coal

WB4 inertinite sample:

The Witbank 4 seam inertinite particles remain stagnant when it is heated from 30°C. At a temperature of 363°C a barely noticeable shift can be observed in the centre particle. This is repeated at a temperature of 420°C. Barely noticeable shifting and rotating movement can also be observed in this particle between temperatures of 447 and 491°C. A small jerk is seen in the bottom left particle at a temperature of 523°C. Between temperatures of 553 and 579°C small movements is observed in the bottom left particle. Barely noticeable movement can be seen in the bottom and centre particles at a temperature of 591°C. Small movements are observed in the top left particle between temperatures of 606 and 624°C when a sudden jerk cause a dramatic shift in all particle positions. Cracks can also be seen after this shift occurred. Continuous movement is observed in intervals from this temperature up to 768°C.

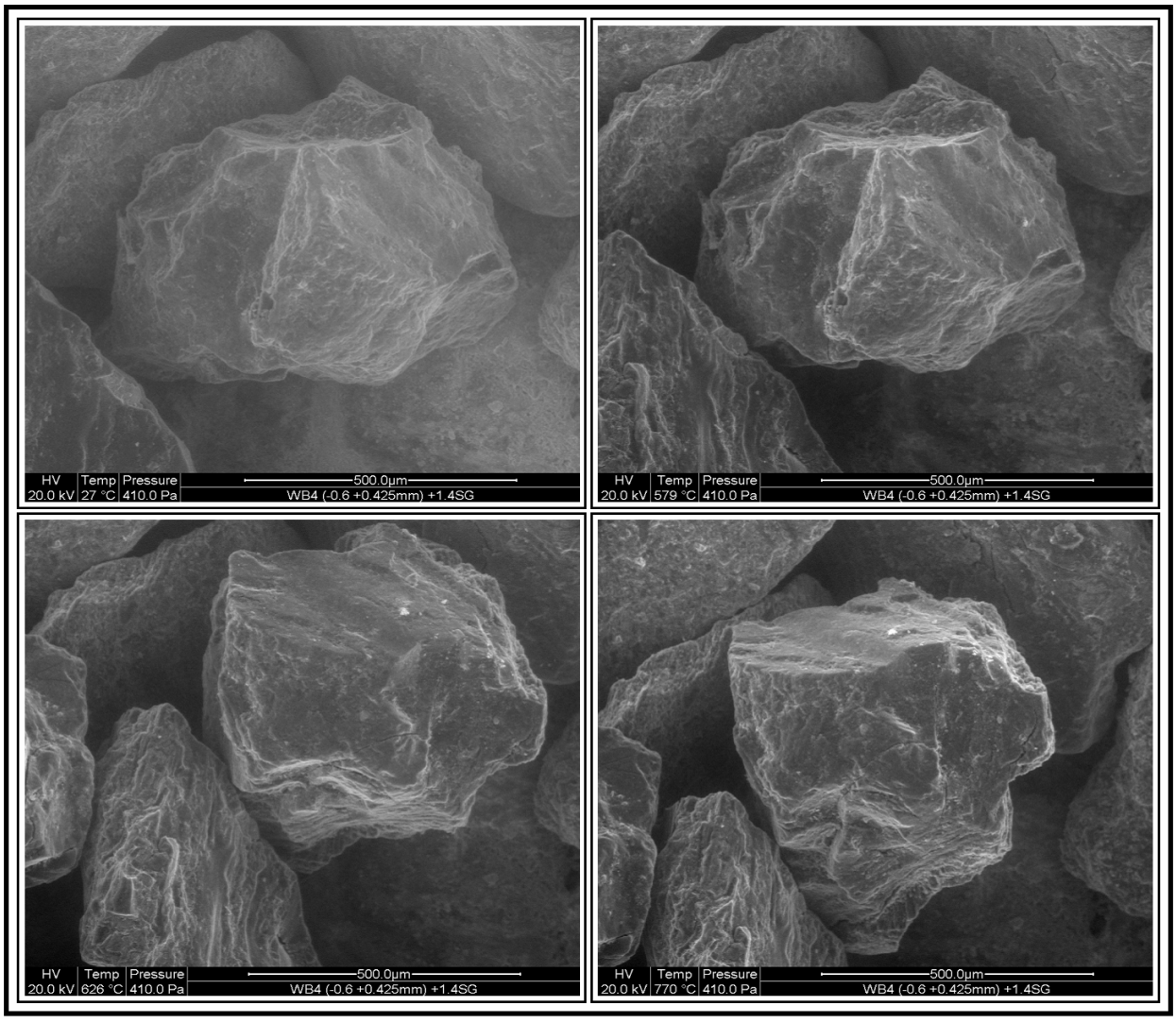

Figure 4.3.2(a): SEM image observation for heating of the WB4 inertinite coal.

At a temperature of 787°C a major jerk shifts all particles out of position again. More cracks are observed in this new view. Continuous movement dominates with another small jerk at 861°C. Except for a final jerk at 918°C, very little movement is observed from this temperature up to 930°C when heating stops. Good separation of the sample is observed as no 'plastic' or 'melting' behaviour can be seen; these particles represent the harder inertinite fraction.

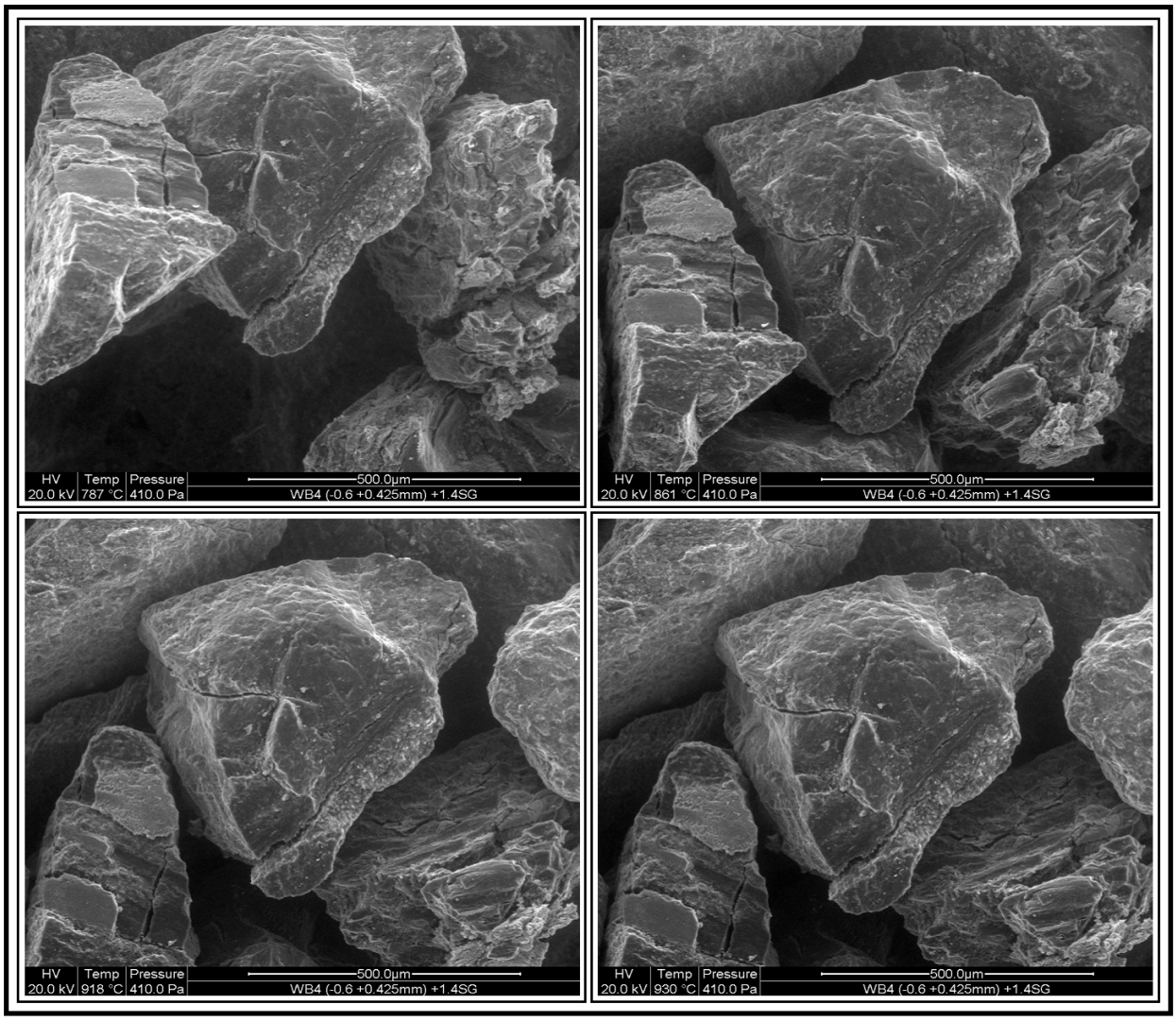

Figure 4.3.2(b): SEM image observation for heating of the WB4 inertinite coal.

WB4 mixture sample:

The Witbank 4 seam mixture particles remain stagnant when it is heated from 30°C. Barely noticeable shifts are observed at 298 and 384°C with the first small jerk being observed at 423°C. From this temperature slight simmering movement can be seen up to 447°C when cracks start to form rapidly as the particles show slight swelling and plastic behaviour. Simmering movements continues during this period. From a temperature of 497°C up to 531°C the simmering movement cools down and the centre particle shows a slight shrinking effect. At a temperature of 531°C sudden jerks causes the left particle to move out of frame while the

bottom particle shows a few major movements which decrease at 535°C. Major jerks at 543, 557, 570 and 575°C shifts the centre particle upwards. The movement of the centre particle is followed leaving the bottom particle out of view.

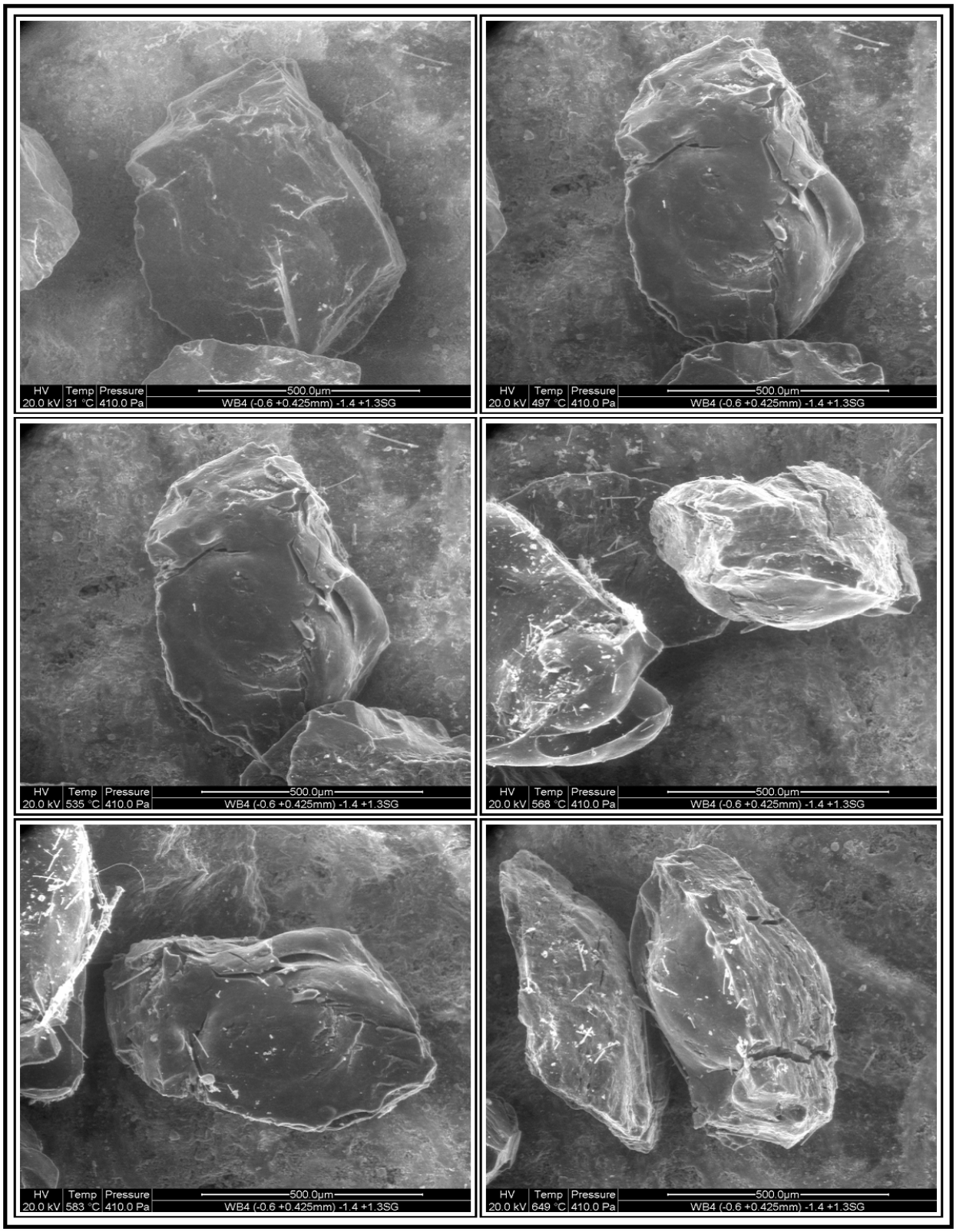

Figure 4.3.2(c): SEM image observation for heating of the WB4 mixture coal.

From 575°C up to 613°C almost no movement is observed. From a temperature of 613 up to 622°C a period of rapid jumping is entered where after fewer jerks are observed. This movement decrease to only slight movement from a temperature of 642°C. From 671 up to 688°C another period of rapid jumping is entered followed by a few jerks at 700°C. From this point it seems as if the plastic fraction causes the particles in view to stick or melt together as the particles move as a unit. The group of particles remains fairly motionless up to 741°C when particles from the bottom show rapid movement causing the particles in view to shift from position.

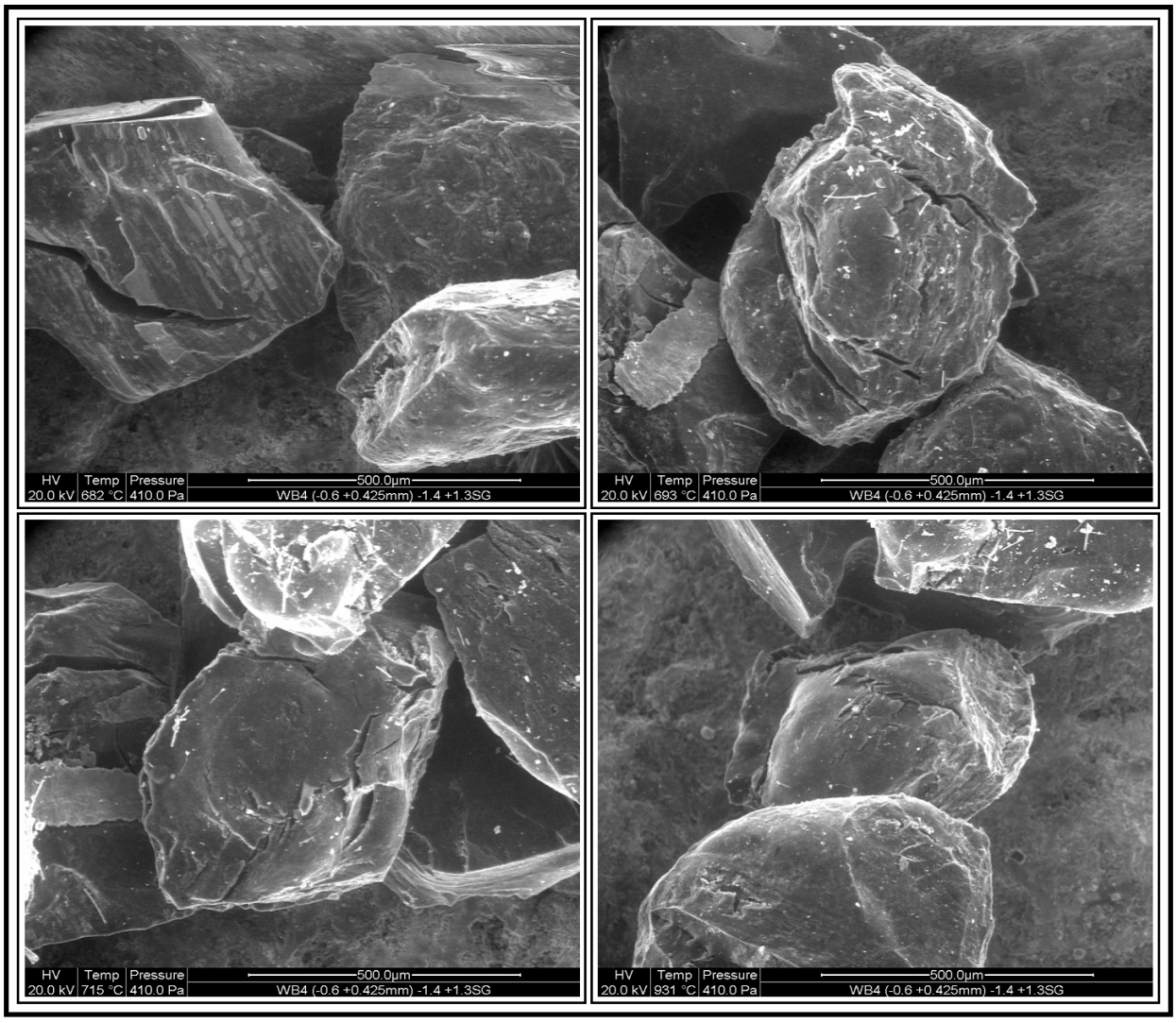

Figure 4.3.2(d): SEM image observation for heating of the WB4 mixture coal.

Slight simmering movements dominate from this point up to a temperature of 802°C when a major shift moves the particles from position once more. From this temperature dominant simmering is observed in the top particles with the centre and bottom particles remaining fairly motionless. This simmering behaviour in the top particles decreases and stops at 829°C. Very little simmering shifts are observed from this temperature up to when heating is suspended at a

temperature of 931°C. The particles in view represent a clear mixture of vitrinite and inertinite where the particles in view shows a few cracks but also swelling and plastic behaviour from a temperature of around 450°C.

WB4 vitrinite sample:

The Witbank 4 seam vitrinite particles remain stagnant when it is heated from 30°C. Barely noticeable shifts in some particle positions are observed from a temperature of 363°C. A crack starts to from in the top particle from 406°C which opens up fast from 421°C. Rapid shifting movements are observed from 432°C with simmering and swelling from 439°C. This behaviour continues up to a temperature of 456°C when extreme simmering and jumping movements dominate up to 785°C where almost no observations can be made as a result of the very fast movements. After the rapid jumping stops the particles in view shows extreme swelling (plastic) and cracking behaviour.

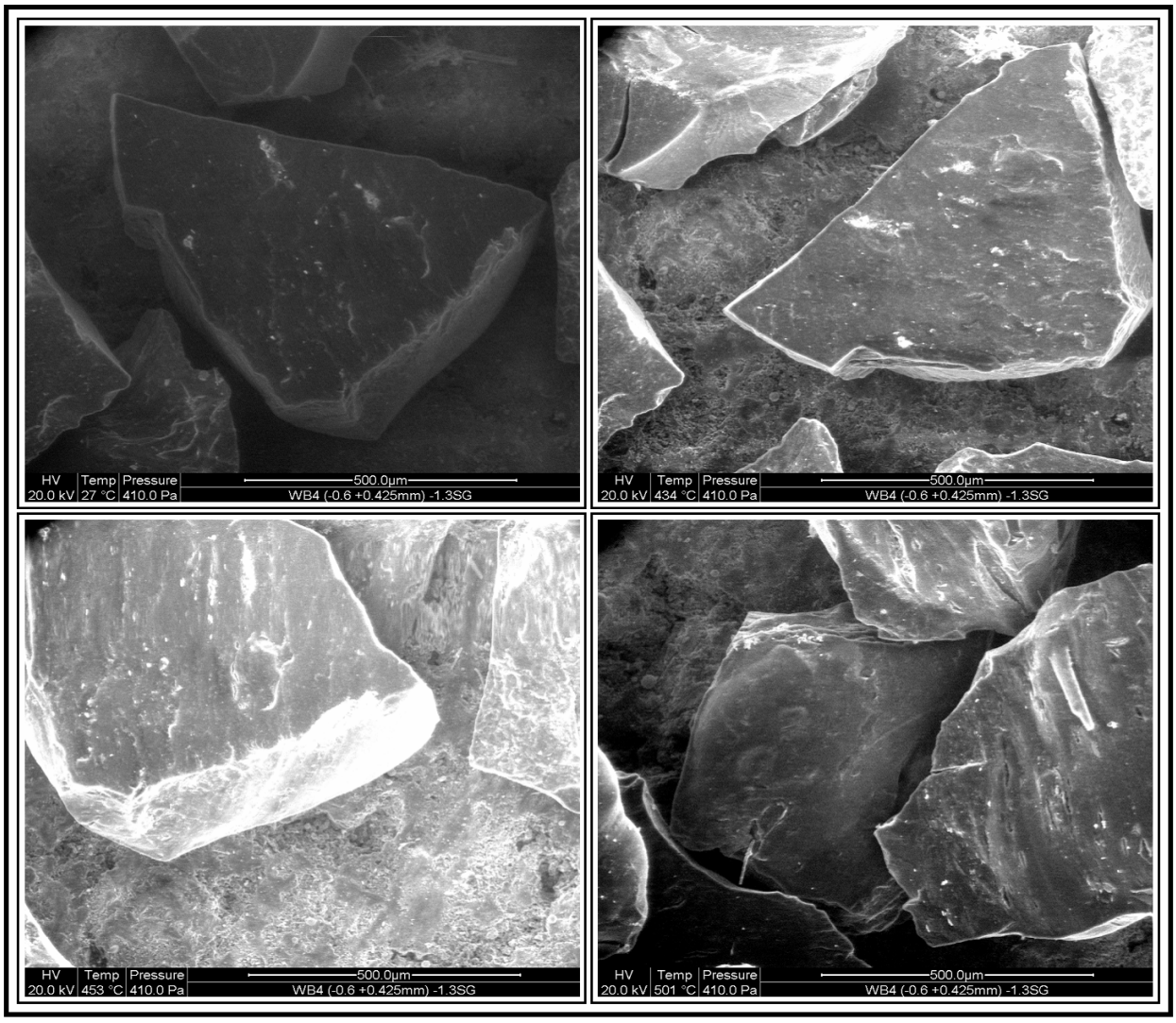

Figure 4.3.2(e): SEM image observation for heating of the WB4 vitrinite coal.

Slight movement continues from this temperature up to 863°C when simmering movements take over once again. Rapid jumping starts from 894°C up 917°C where after only small jerks are observed up to 931°C when heating is suspended. Good separation of this maceral fraction is observed as most particles were deformed because of this fraction's plastic properties.

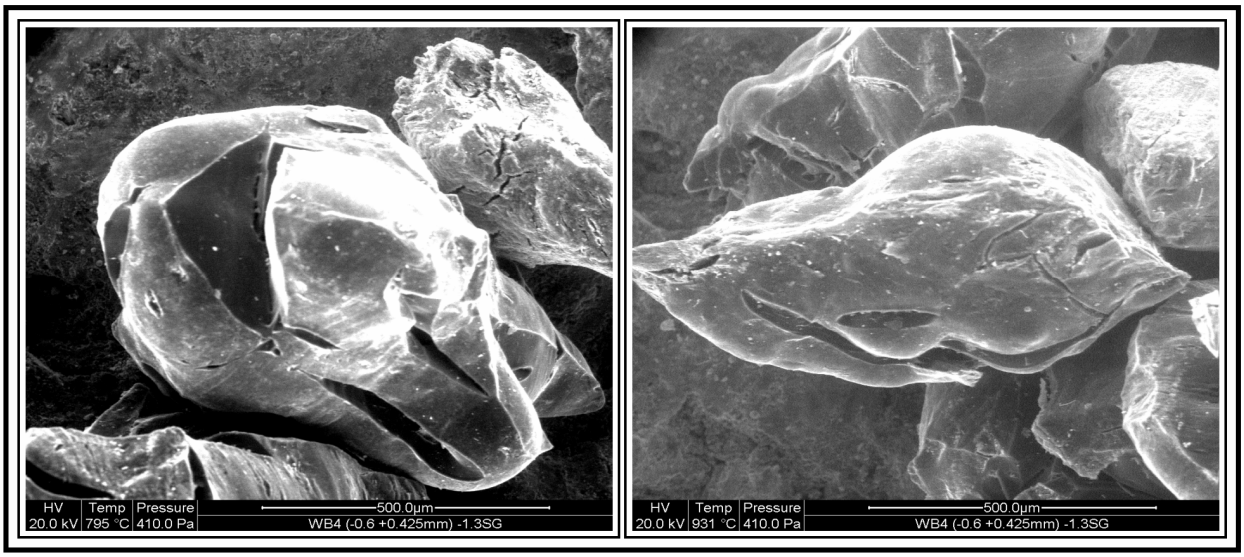

Figure 4.3.2(f): SEM image observation for heating of the WB4 vitrinite coal.

4.3.3. SEM results for the TS coal

TS inertinite sample:

The Soutpansberg inertinite particles remain stagnant when it is heated from 30°C. From 460°C slight movement in the particle to the top left hand corner is observed.

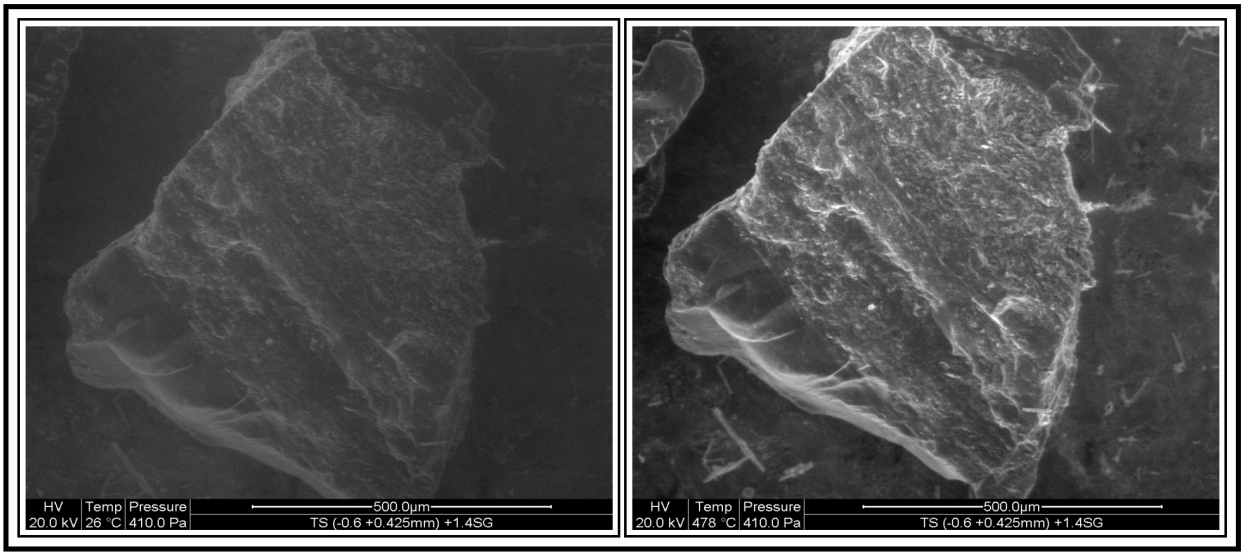

Figure 4.3.3(a): SEM image observation for heating of the TS inertinite coal.

A slight simmering motion continues up to 518°C when a small section of this particle starts to form a 'plastic bubble'. The simmering motion continues as the 'plastic bubble' swells further up to 540°C where it starts to 'blow down'. At this point the plastic part of the top particle also melted into the particle in main view. The simmering motion continues up to a temperature of 597°C where major evolution of gas causes the 'plastic bubble' to show major boiling motions. From 607°C very little motion can be observed up to 636°C where after movement stops up to 931°C when heating is suspended. Good separation of this inertinite fraction can be seen as almost no plastic state is reached during heating.

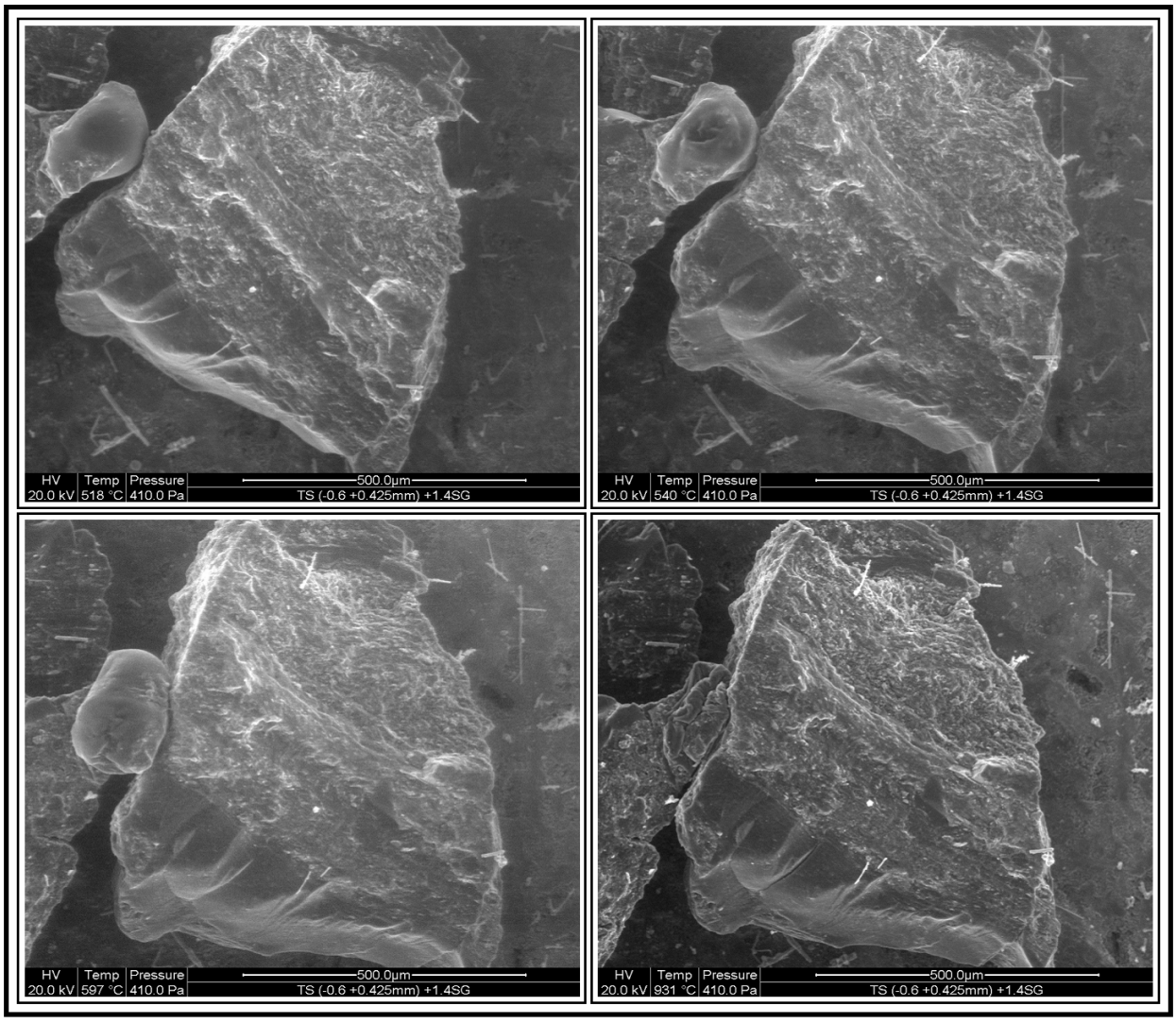

Figure 4.3.3(b): SEM image observation for heating of the TS inertinite coal.

TS mixture sample:

The Soutpansberg mixture particles remain stagnant when it is heated from 30°C. From a temperature of 405°C slight movement is observed as cracks starts to form on the centre particle's surface. These cracks start to open up fast from 433°C as the whole coal particle swells into a large plastic state. This swelling and movement continues to between 510 and

533°C when blow-down starts and continues up to 632°C. During this blow-down stage rapid, continuous swelling, boiling and evolution of gas can be seen. After this temperature is reached movement stops until heating is suspended at a temperature of 930°C.

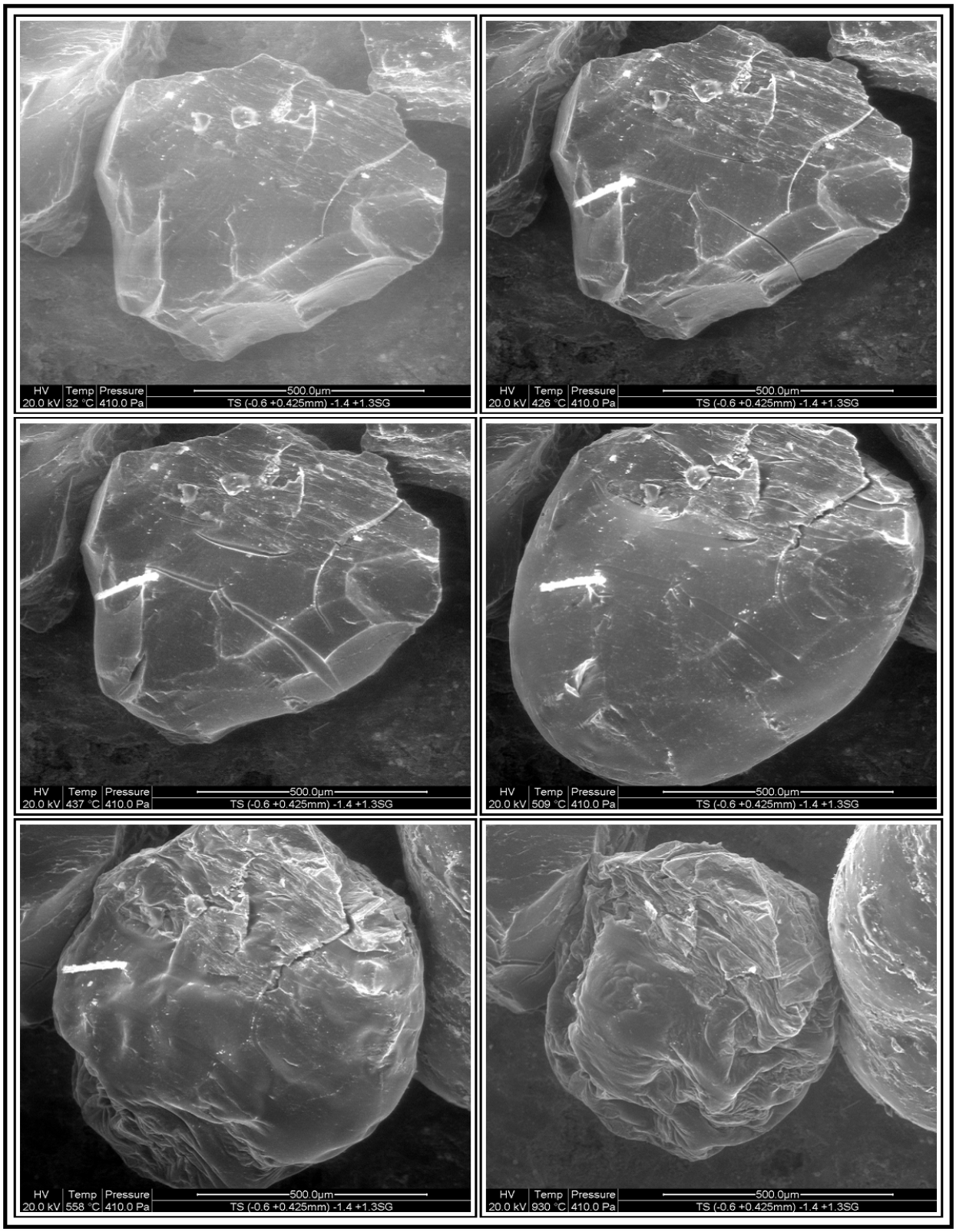

Figure 4.3.3(c): SEM image observation for heating of the TS mixture coal.

The particles in view represent a clear mixture of vitrinite and inertinite where the particle to the left cracked a bit but remained solid (inertinite), the particle to the right turned into a complete plastic bubble (vitrinite) and the centre particle consists of both the maceral fractions; to the top, inertinite and to the bottom, vitrinite. These particles also formed a few cracks, representing the plastic vitrinite as well as the harder inertinite.

TS vitrinite sample:

The Soutpansberg vitrinite particles remain stagnant when it is heated from 30°C. Slight movement can be observed from 421°C. Swelling starts from 449°C and reaches its peak in the centre particle at 479°C. Slight blow-down can be seen from 538°C. At 583°C all the particles in view are swollen to their full extents. The particles remain like this up to 755°C when an interval of rapid moving and jumping is entered up to 786°C. The particles remain in these positions up to a temperature of 854°C where a second rapidly moving period starts up to 863°C.

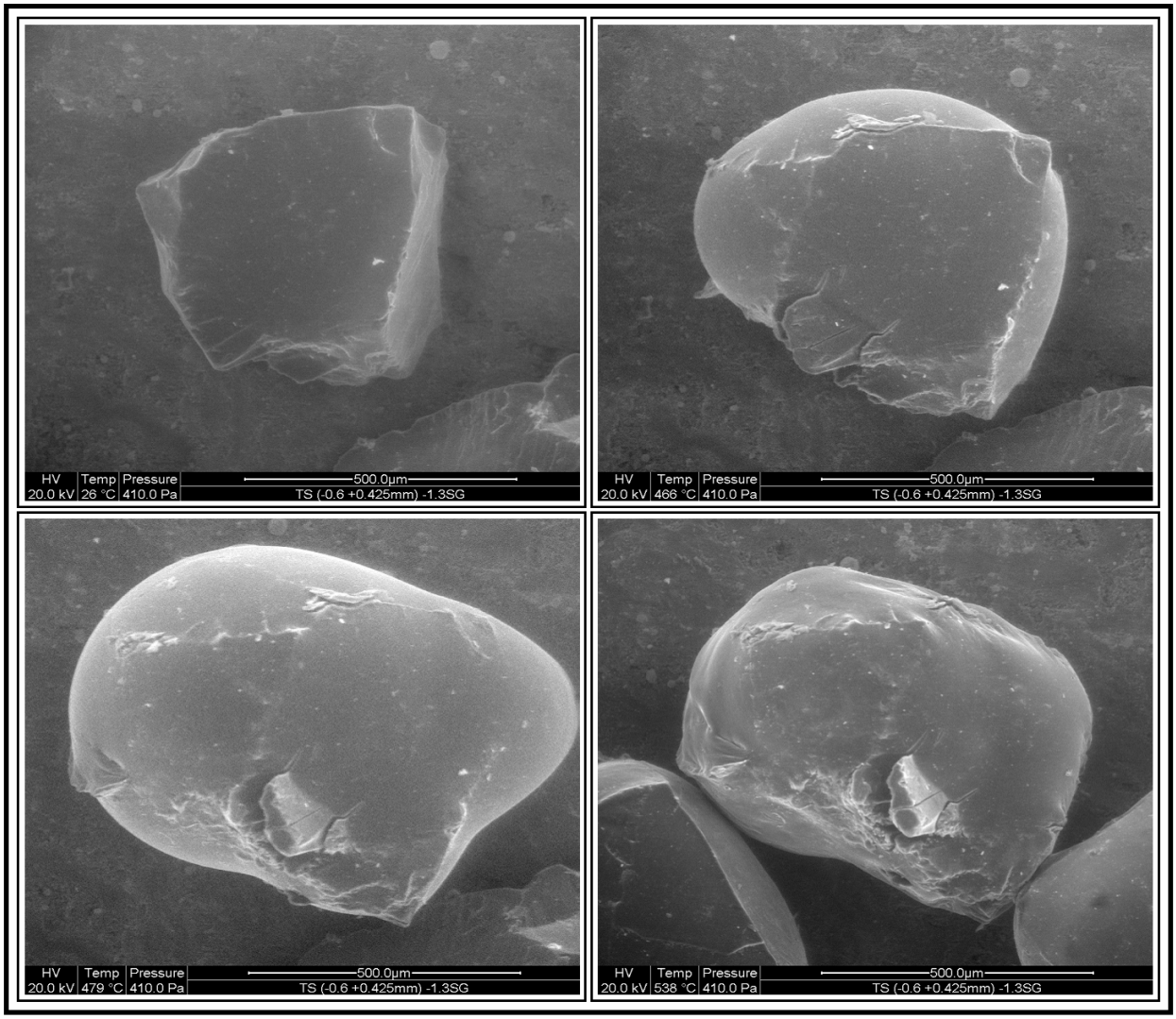

Figure 4.3.3(d): SEM image observation for heating of the TS vitrinite coal.

After this second interval all particles remains in their positions up to 931°C when heating is suspended. Again good separation can be seen as all particles turned into large plastic bubbles with no cracks which represent the more 'plastic' vitrinite.

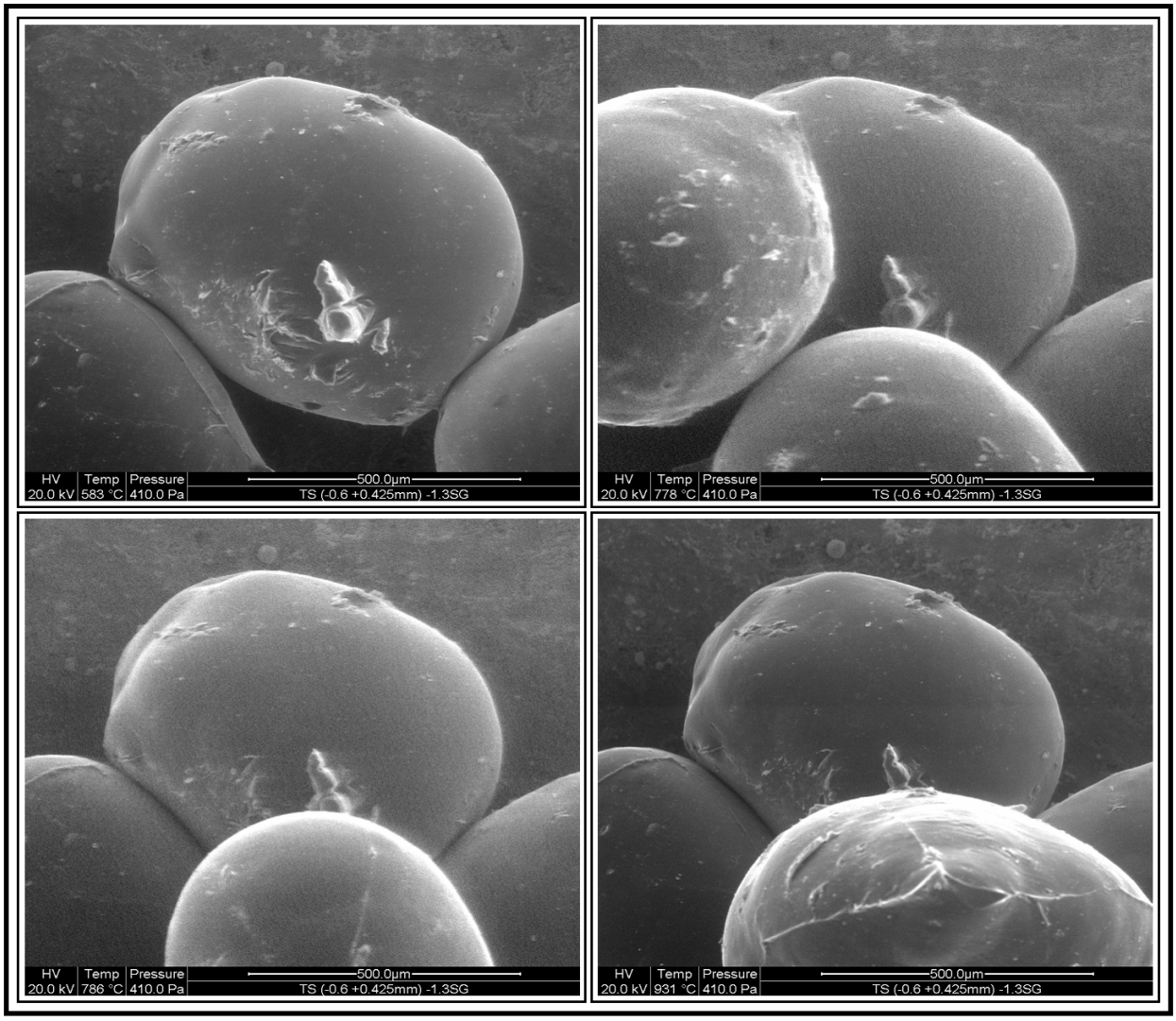

Figure 4.3.3(e): SEM image observation for heating of the TS vitrinite coal.

4.3.4. SEM results for the GG coal

GG inertinite sample:

The Waterberg inertinite particles remain stagnant when it is heated from 30°C. From 494°C minor movement start and the particle in view shifts slightly to its one side. This movement can also be seen at 502, 507 and 523°C. A crack starts to form at the top of the particle from a temperature of 500°C which is clearly visible at 540°C. At 556 and 574 to 588°C minor movement can be seen again. From 597 to 600°C major movement are observed. Between 644 and 649°C the particle twists slightly and 'jumps' to a different location at 652°C. From 652 to 691°C a slight simmering movement is observed. Between 692 and 698°C major movement

can be seen again. From 698 to 762°C slight simmering movement is observed again where after movement stops to 787°C. At 789°C the particle shifts slightly. At 809°C major movement 'shoots' the particle to an unknown location.

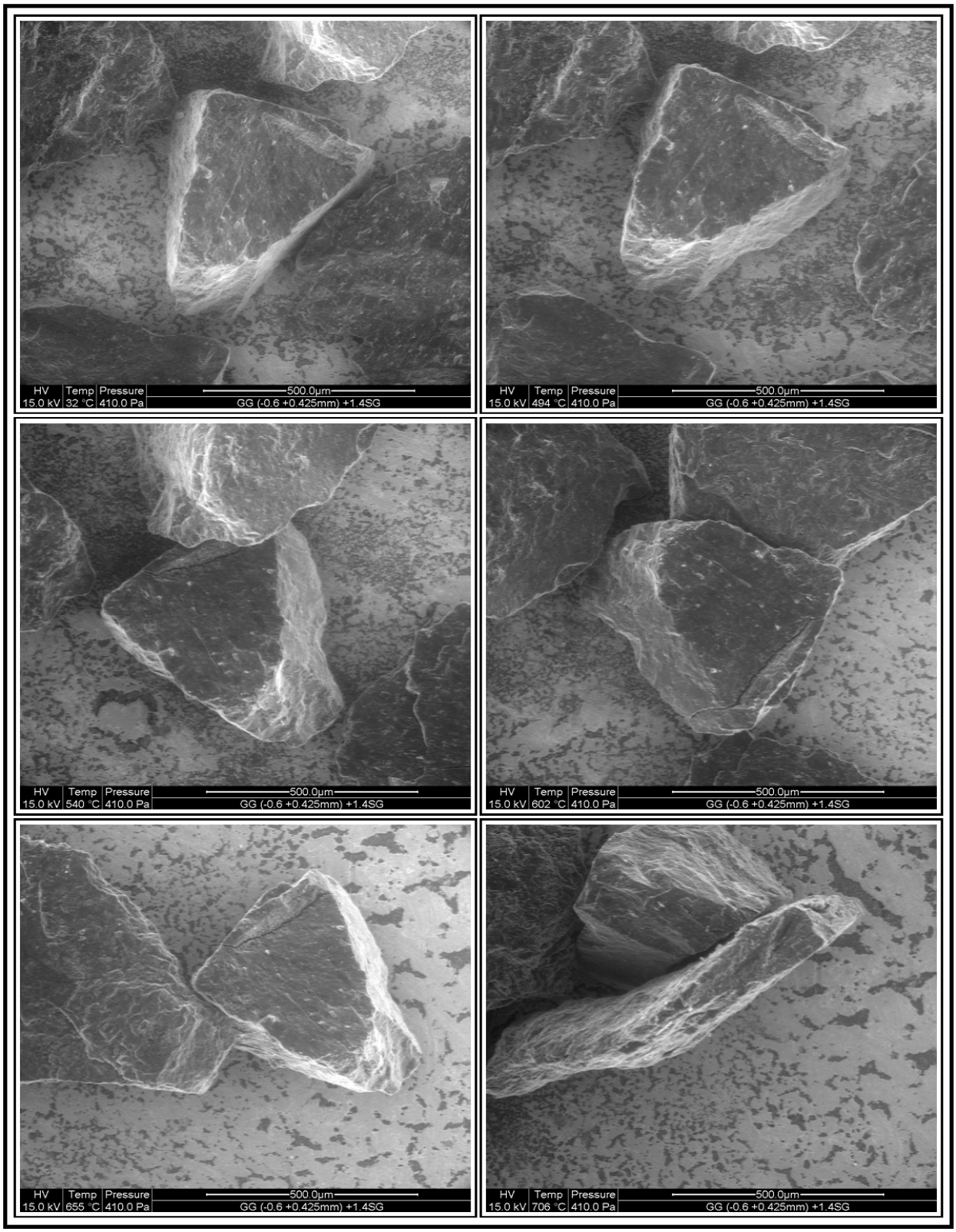

Figure 4.3.4(a): SEM image observation for heating of the GG inertinite coal.

A different particle is viewed which remains fairly motionless up to a temperature of 858°C. From 860 to 863°C minor movement is observed again. Between 863 and 905°C the particle again remains fairly motionless where after it 'shoots' to a unknown location and different particles are viewed.

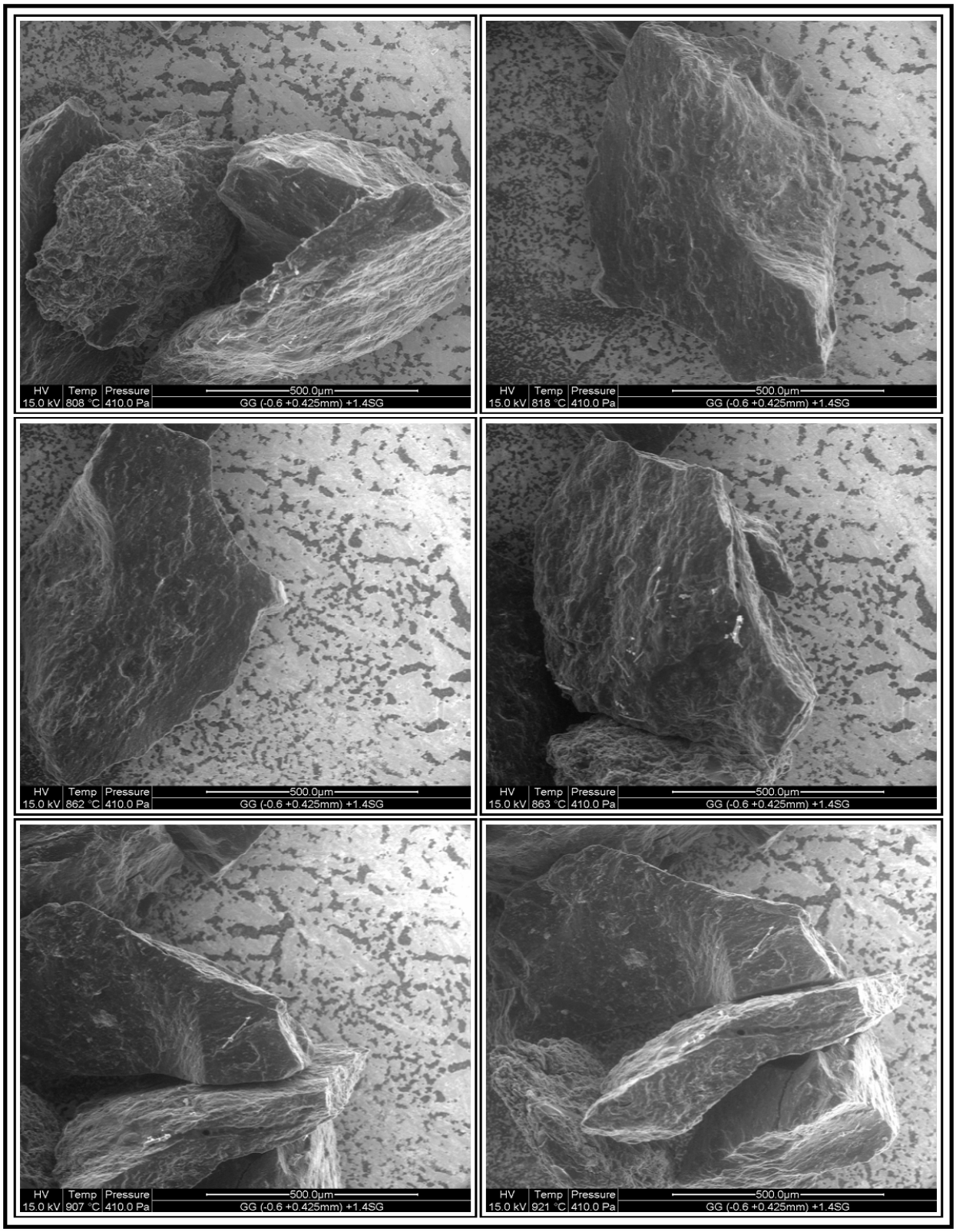

Figure 4.3.4(b): SEM image observation for heating of the GG inertinite coal.

These particles show simmering movements up to a temperature of 921°C where after heating is suspended. Good separation of the sample is observed as no 'plastic' or 'melting' behaviour can be seen; these particles represent the harder inertinite fraction.

GG mixture sample:

The Waterberg mixture particles remain stagnant when it is heated from 30°C. A small pointy shape appears at the bottom of the particle in view at a temperature of 260°C. At 472°C the particle to the left shifts slightly more into view. From 400°C a crack starts to form from the bottom of the particle which is clearly visible at a temperature of 480°C. From 480 to 533°C slight simmering movement can be seen while certain areas on the particle turn to expanding plastic segments. The previously mentioned crack also widens in this range. From 535 to 544°C major movement is observed. Between 544 and 571°C the particle remains fairly motionless.

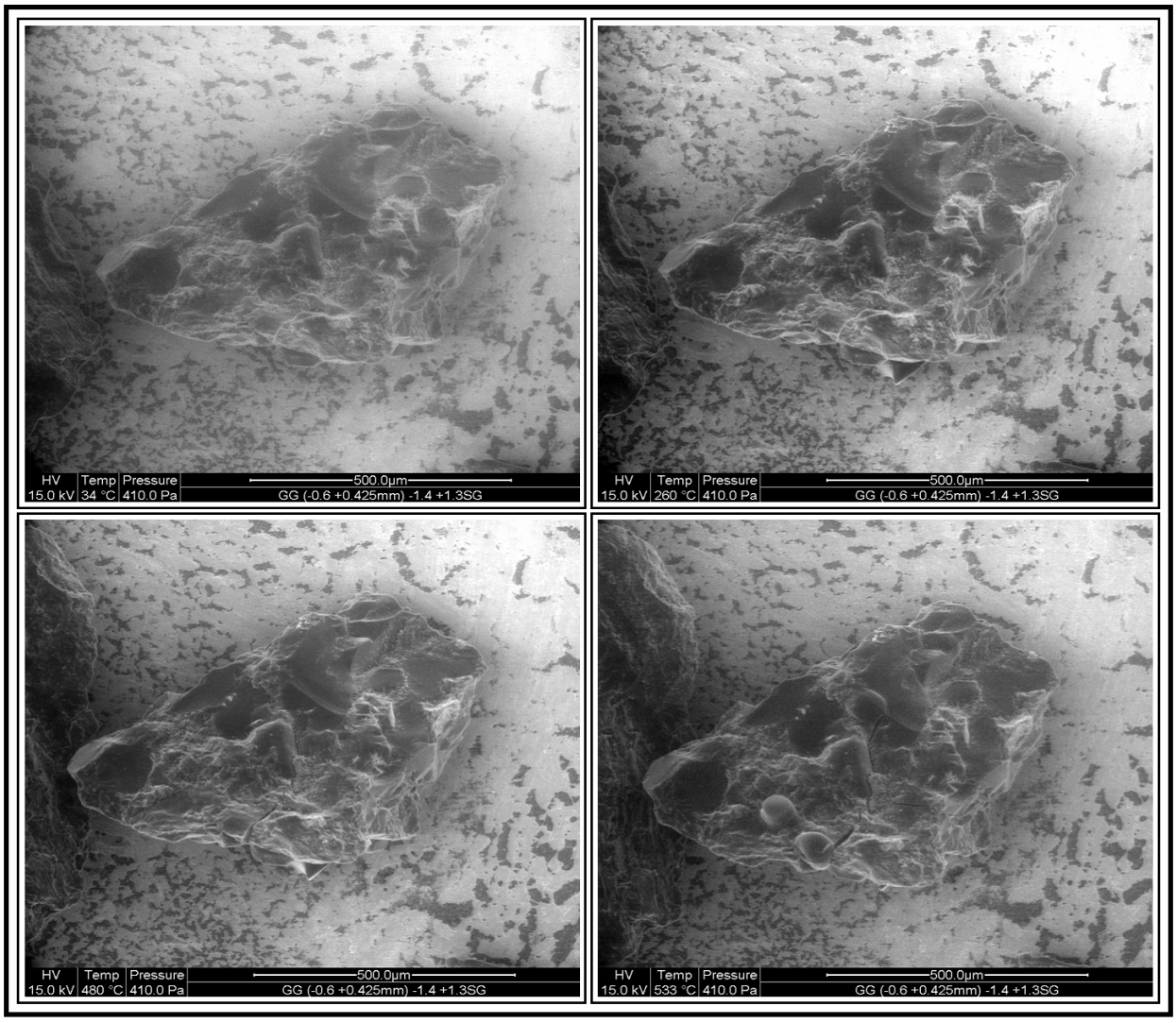

Figure 4.3.4(c): SEM image observation for heating of the GG mixture coal.

At 574°C the particle to the top (which turned to a complete plastic state) shift and stick on top of the monitored particle. From this temperature to 603°C slight simmering movements are observed where after major movement between 605 and 610°C moves the plastic particle from the previously monitored particle's top.

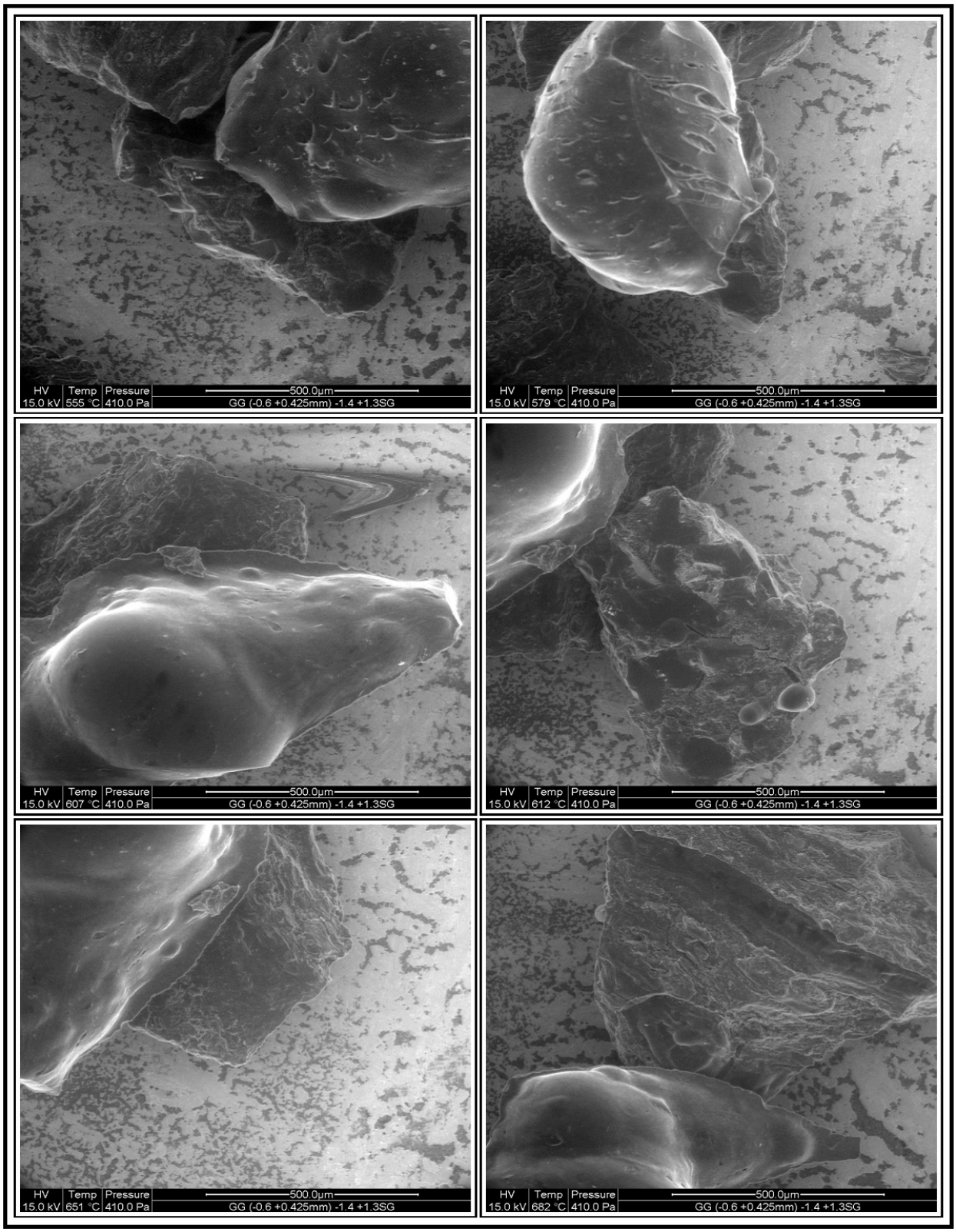

Figure 4.3.4(d): SEM image observation for heating of the GG mixture coal.

The particle remains fairly motionless up to a temperature of 646°C when it 'shoots' to an unknown location. Between 646 and 682°C intervals with simmering movement in the particles viewed can be observed. From 682°C the movement stabilize and very little is observed up to a temperature of 723°C.

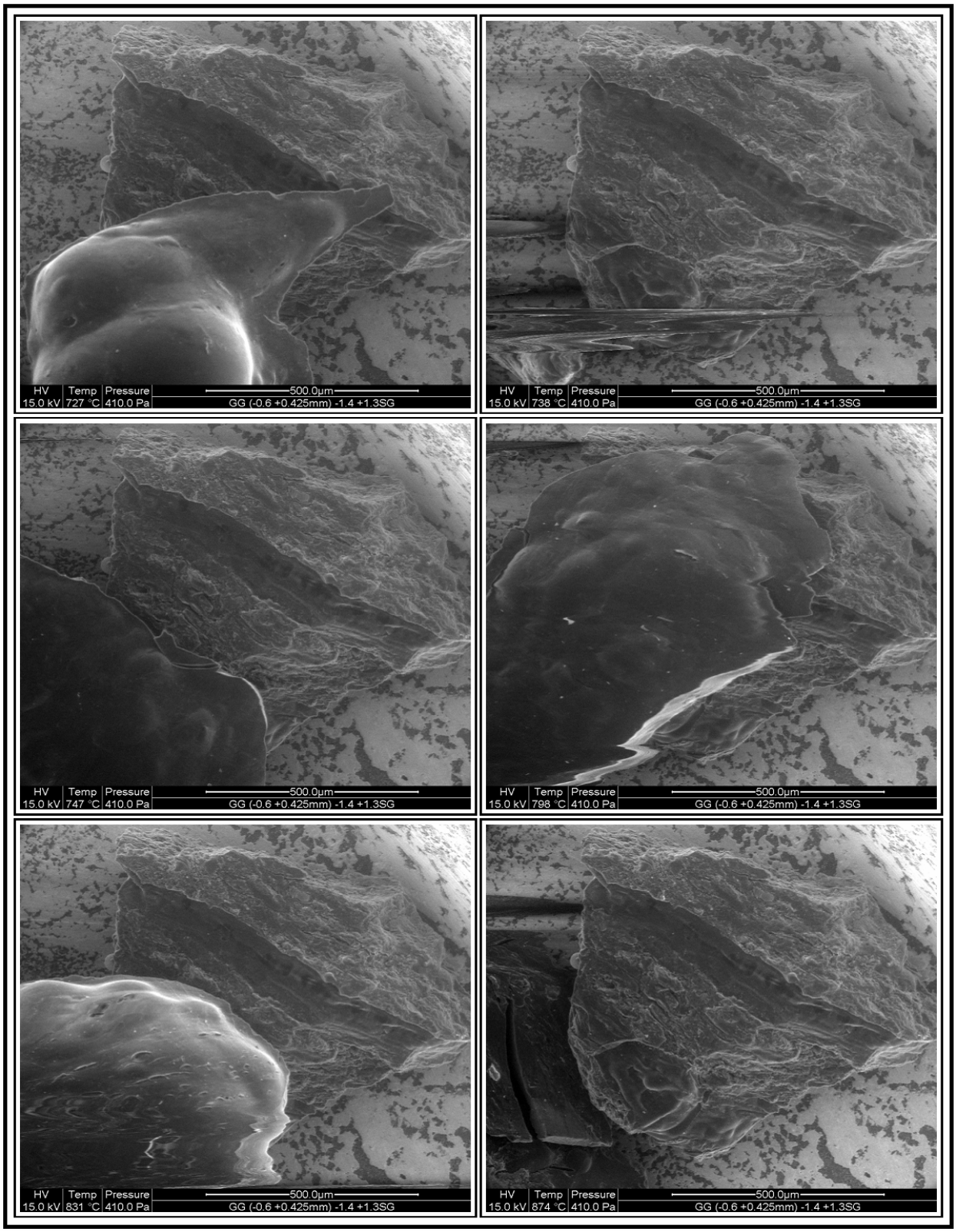

Figure 4.3.4(e): SEM image observation for heating of the GG mixture coal.

Now the particle to the bottom shifts on top of the particle in main view. From 738 to 903°C major jumping movement in most particles occur while the particle in main view remains 'stuck' to the side of the crucible. From 903 to 921°C no further movements can be observed. The particles in view represent a clear mixture of vitrinite and inertinite where the particles show the plastic vitrinite as well as the harder inertinite.

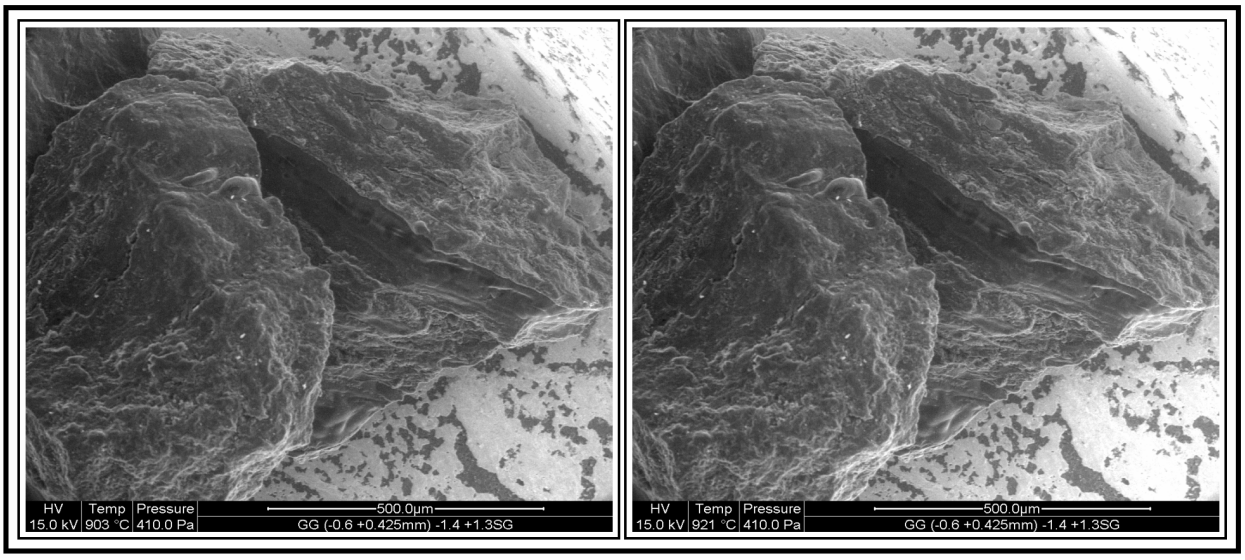

Figure 4.3.4(f): SEM image observation for heating of the GG mixture coal.

GG vitrinite sample:

The Waterberg vitrinite particles remain stagnant when it is heated from 30°C. Slight movement of the particle in view is observed from a temperature of 390°C with slight shifts in position at 430, 441 and 447°C.

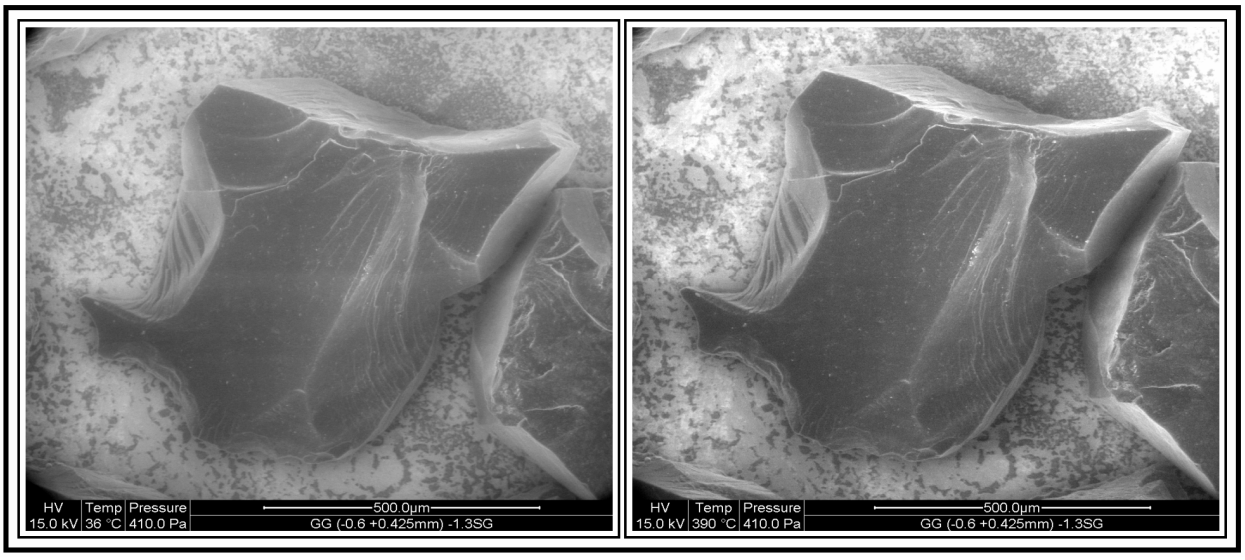

Figure 4.3.4(g): SEM image observation for heating of the GG vitrinite coal.

From a temperature of 441°C a crack becomes visible which opens up fast and causes continues movement up to a temperature of 467°C where after the particle shows considerable swelling when it enters a plastic, rapidly simmering state up to a temperature of 485°C with some pores starting to show.

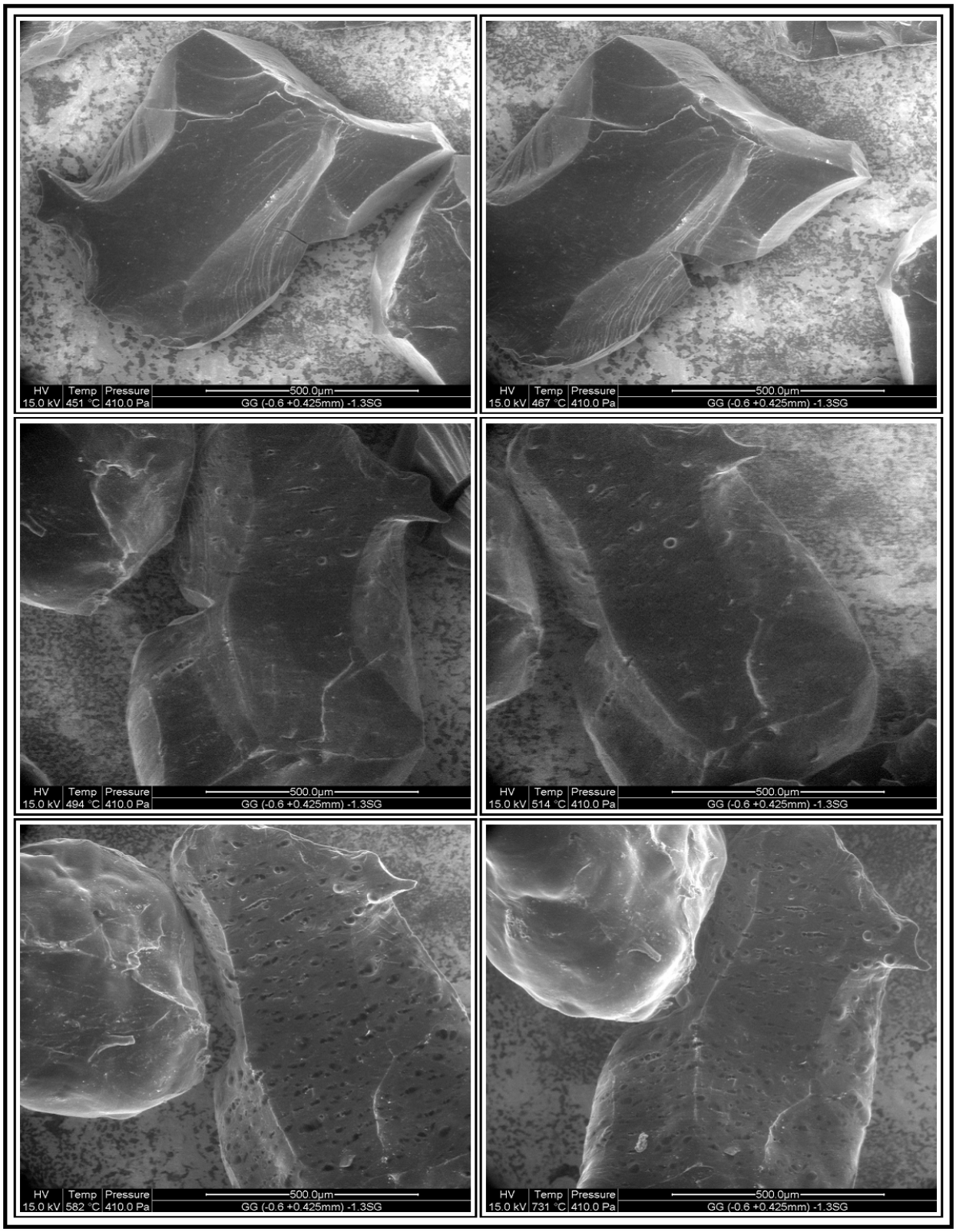

Figure 4.3.4(h): SEM image observation for heating of the GG vitrinite coal.

Minor movement continues from this temperature up to 503°C when rapid movement takes over up to 511°C. From 511°C up to 711°C very little movement can be seen with pores opening up some more; the particles in view shift around slightly. Between 713 and 731°C more aggressive jolts can be seen where after only slight movement is observed up to a temperature of 903°C. From 905 to 910°C major 'jumping' movement in all particles 'shoots' the monitored particle to an unknown location. From 910 to 920°C almost no movement can be seen where after heating is suspended.

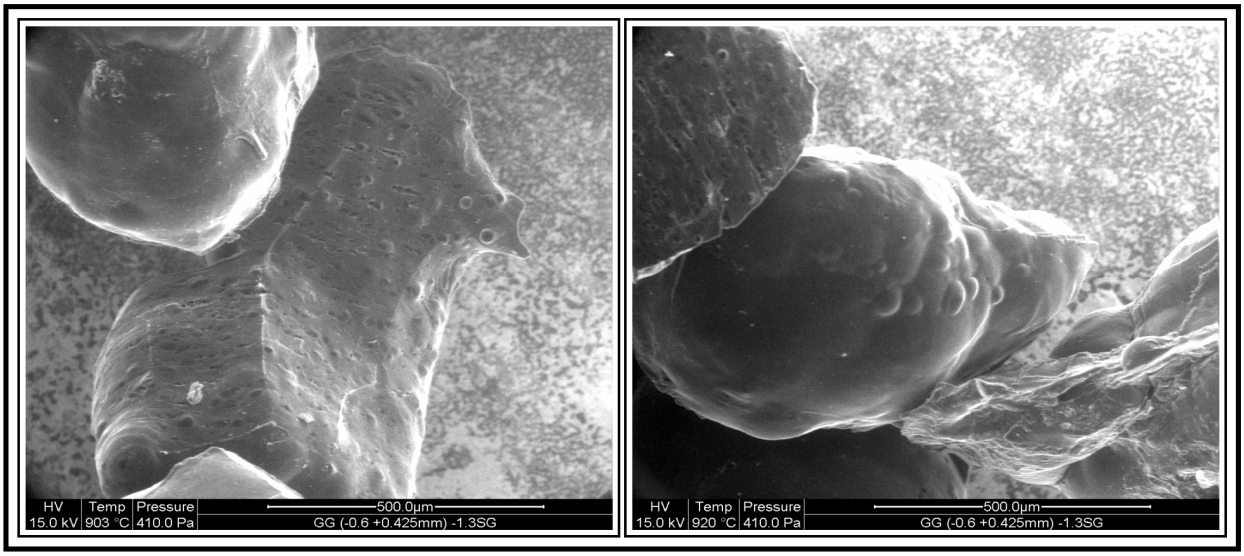

Figure 4.3.4(i): SEM image observation for heating of the GG vitrinite coal.

4.3.5. SEM results for the NV coal

NV inertinite sample:

The Free State inertinite particles remain stagnant when it is heated from 30°C. The top left particle shifts in position at a temperature of 446°C followed by barely noticeable shifts by the bottom particle at temperatures of 605 and 639°C. The top particle shifts almost unnoticeably at a temperature of 651°C which is followed by a major shift at 660°C. The bottom particle shows a major shift at 666°C followed by a very small shift at 716°C. The top particle shows a major shift in position at 724°C with another small shift at 745°C where after the bottom particle shifts out of view at 748°C. The top particle shifts slightly at 760°C and enters a simmering phase from 779°C through to 931°C. During this simmering phase a major shift in particle positions occur at a temperature of 829°C as the centre and left particles shifts in position and a particle enters the viewing field from the bottom. This is followed by small shifts in the left particle at temperatures of 850 and 877°C. The centre particle shows a small shift at 887°C where after the bottom particle shifts from view at 923°C. No further movement is observed except for the simmering of the top particle up to 931°C when heating is suspended. Good separation of the

sample is observed as no ‘plastic’ or ‘melting’ behaviour can be observed; these particles represent the harder inertinite fraction.

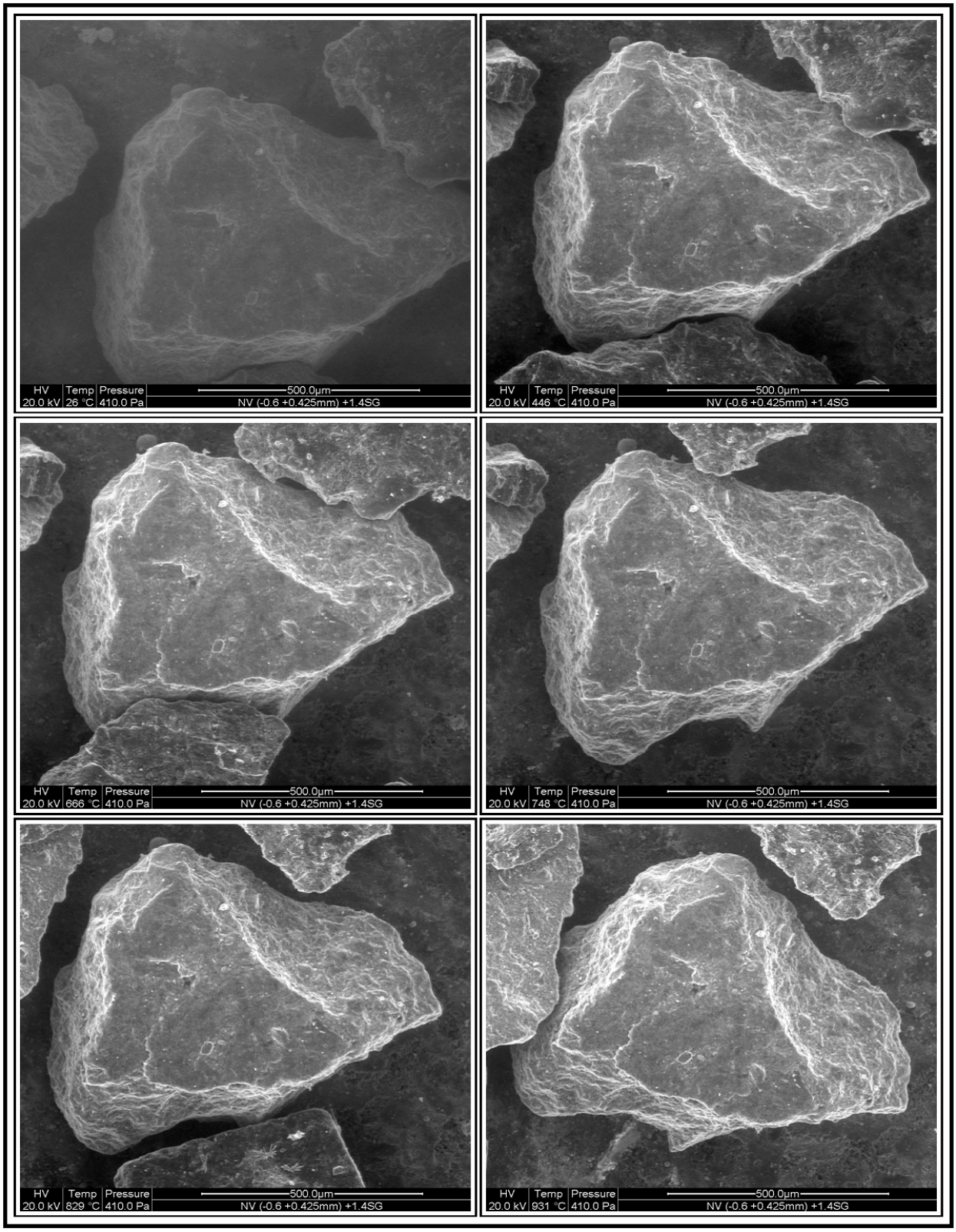

Figure 4.3.5(a): SEM image observation for heating of the NV inertinite coal.

NV mixture sample:

The Free State mixture particles remain stagnant when it is heated from 30°C. Barely noticeable simmering in the centre particle is observed at temperatures of 161 and 187°C. Small cracks also start to become visible from this point. The first shift in particle positions is observed in the centre particle at a temperature of 383°C. Barely noticeable simmering starts from 398°C which builds up into larger movements and finally a shift in all particle positions at 495°C. The simmering effect continues with major shifts at temperatures of 547, 597, 604 and 651°C. This is followed by a small shift at 666°C where after the small cracks formed when heating started, opens up. From 707 to 709°C extreme simmering causes a major shift in particle positions. Simmering continues and intensifies with major shifts in particle positions between 745 and 746°C. Slight simmering continues with cracks being observed in most particles. The bottom particle shifts out of view as a result of the simmering at a temperature of 828°C with motion stopping at 849°C.

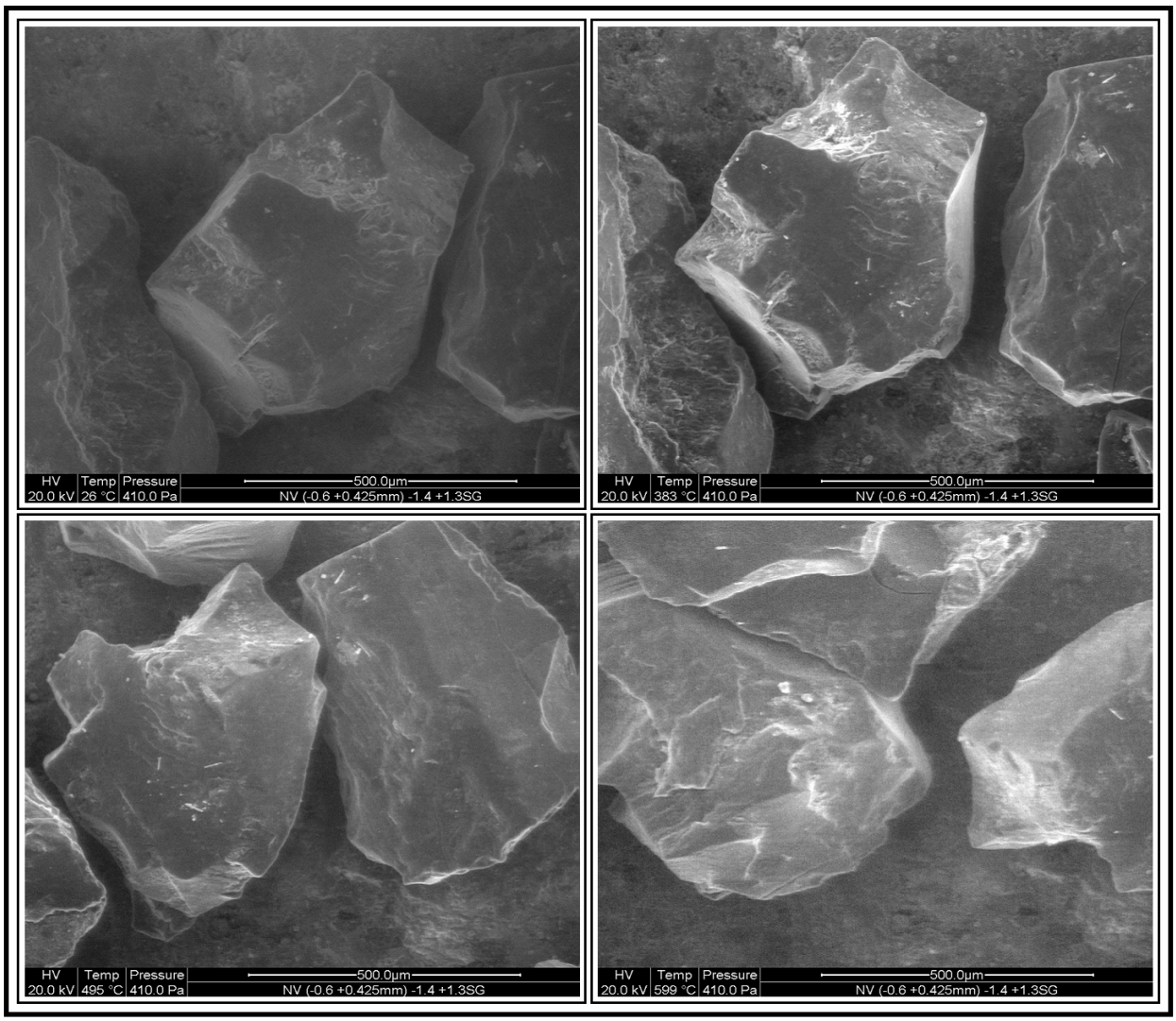

Figure 4.3.5(b): SEM image observation for heating of the NV mixture coal.

No further movement is observed from this temperature up to 931°C when heating is suspended. The particles represent a mixture of vitrinite and inertinite where the particles show a few cracks when heated. No plastic behaviour is however observed which can be attributed to the fact that this coal (Free State) contains almost no vitrinite and the small fraction present is of very low quality.

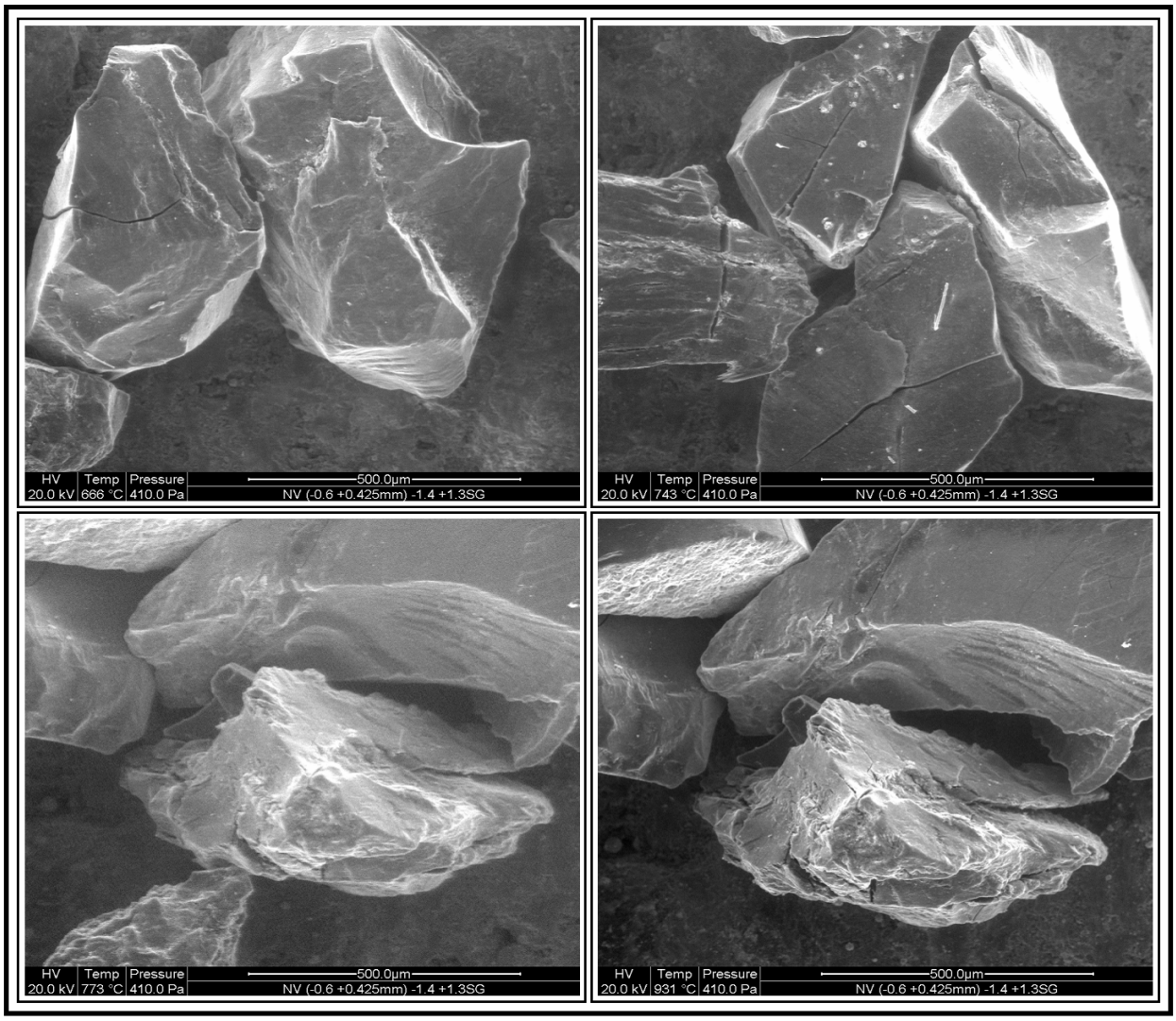

Figure 4.3.5(c): SEM image observation for heating of the NV mixture coal.

NV vitrinite sample:

The Free State vitrinite particles remain stagnant when it is heated from 30°C. Barely noticeable shifts are observed in the centre and top right particles at 170 and 176°C. A slight jerk is also observed in the top right particle at 250°C which is followed by a slight simmering motion in this particle between temperatures of 264 and 279°C. This simmering motion is repeated between 294 and 297°C. Continuous movement in all particles except the left particle starts at a temperature of 429°C with cracks opening up in the left particle. The centre particle shifts slightly on its left side at 491°C with two more shifts at 535 and 541°C. Cracks can also

be seen on other particles from 541°C. At 544°C simmering movements in the centre particle starts with movement in all particles toning down after 624°C. The centre particle shows a major shift to its side at 668°C where after periodic continuous movement in all particles sets in again.

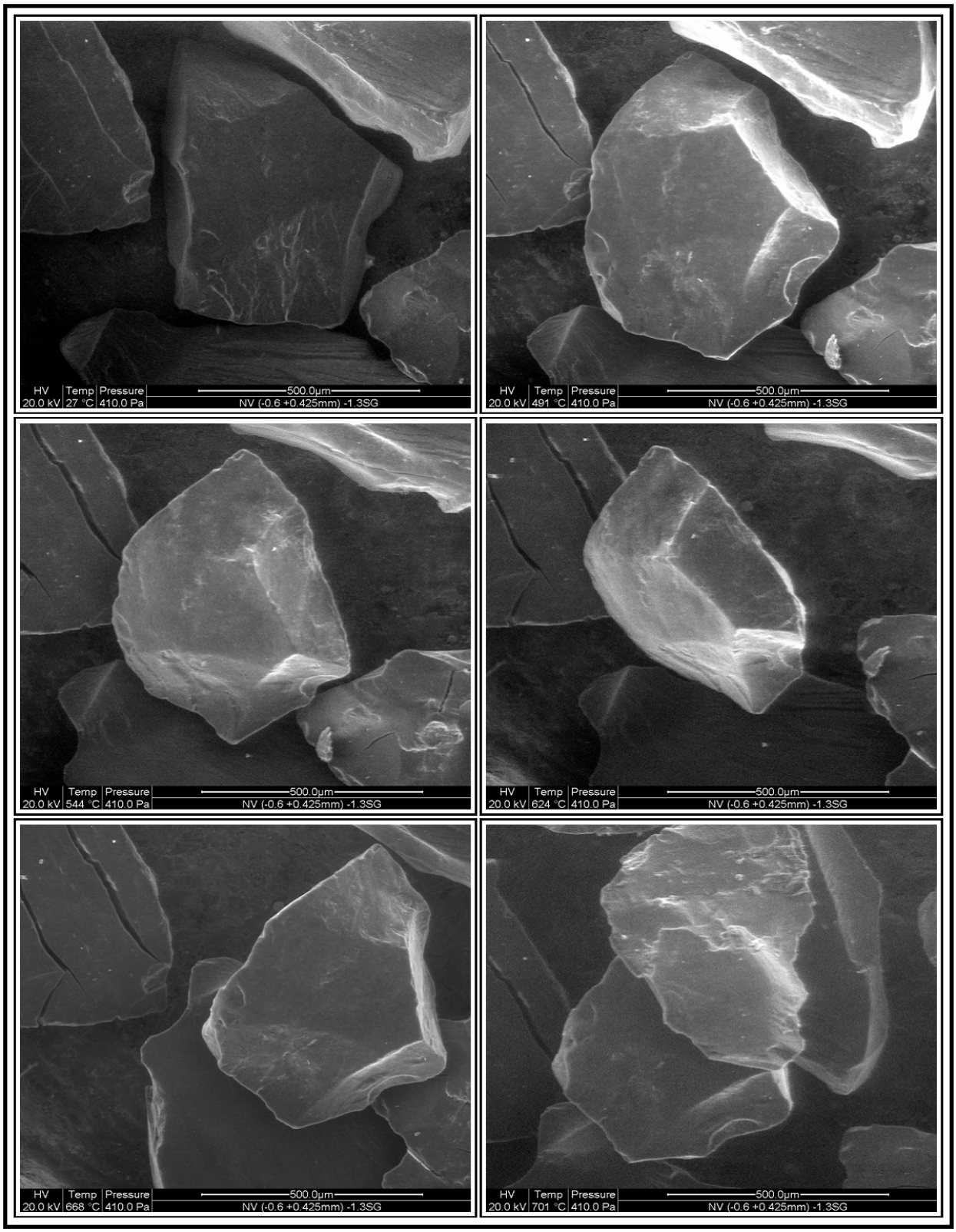

Figure 4.3.5(d): SEM image observation for heating of the NV vitrinite coal.

At 691°C a particle jumps on top of the centre particle from a location out of view and rotates by 180° at a temperature of 706°C. Periodic movement continues with this top particle rotating slightly at 726°C. At 807°C a major shift in all particle positions occur followed by continuous major shifts between 814 and 830°C.

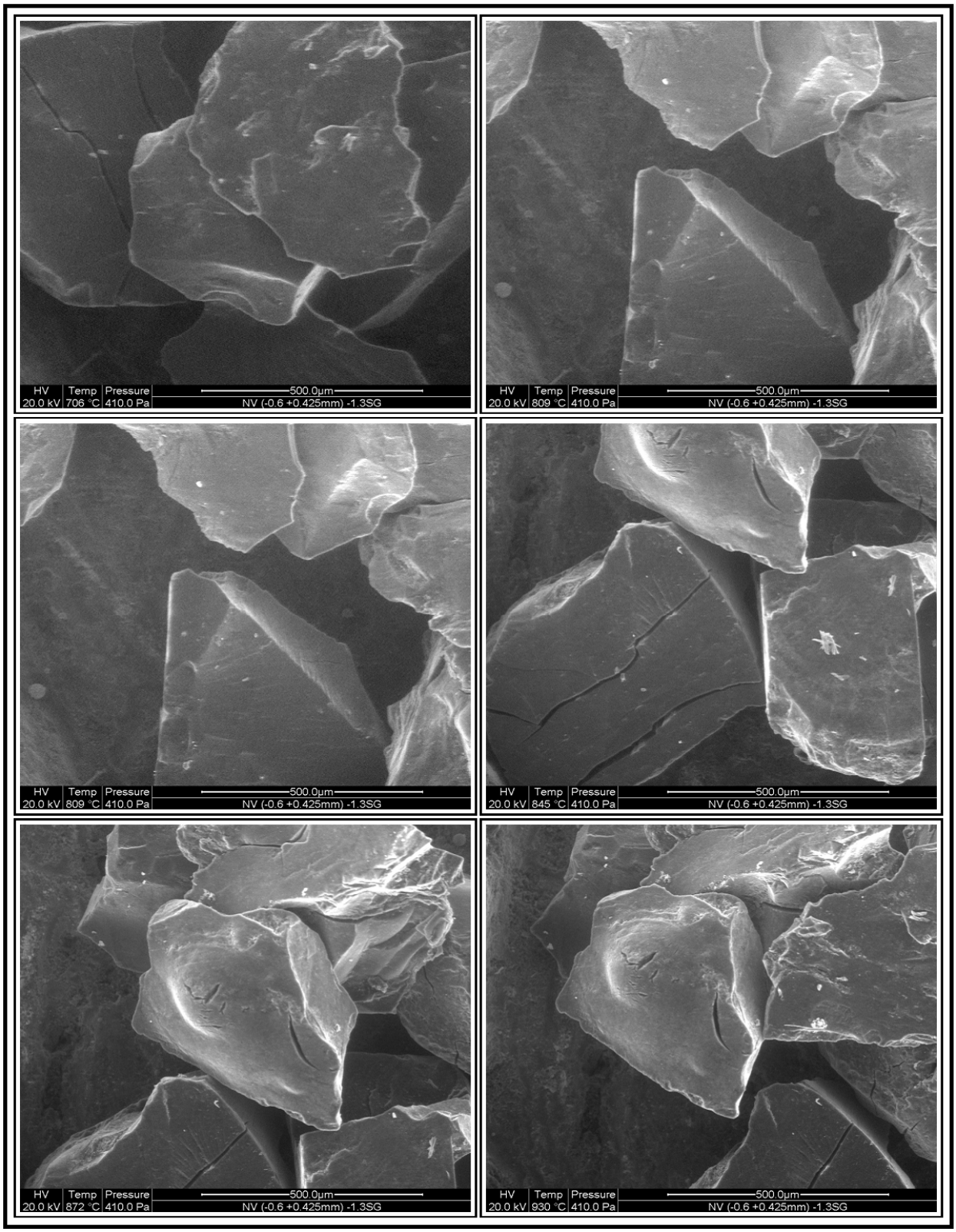

Figure 4.3.5(e): SEM image observation for heating of the NV vitrinite coal.

The view is moved slightly upward to focus on the particle which was in centre view when heating started. This particle shows slight plastic deformation with a few cracks. At 873°C this particle jumps to the right and two other particles enter from the top left and top right hand corners while the particle at the bottom right hand corner moves out of view. The particle shows no further movement up to 930°C when heating is suspended. Good separation of this maceral fraction is observed as most particles show clear clean cracks with little plastic behaviour which is consistent with the behaviour expected from a coal with this low grade.

4.3.6. Discussion of SEM results

The SEM results correspond with the TGA results showing no movement during the first stage of heating when water evaporates from the particles. The first real sign of movements is observed between 350 and 450°C (or even slightly higher) when the more aggressive primary devolatilisation initiates. This corresponds to findings by others as described in paragraphs 2.4.2 to 2.4.6.

From the visual results obtained during the course of these experiments no movement in any particles were observed below a temperature of 260°C except for barely noticeable movement in the NV particles at temperatures higher than 160°C (which can be attributed to water evolution and slight thermal expansion).

This experiment concurs with the findings from paragraph 4.2.6 were the maximum temperature at which thermal drying should be performed must preferably be kept below 160°C and definitely below 260°C to limit any effect the heat may have on the physical and chemical properties of the coal.

4.4. Proximate analysis results

The proximate analysis results are presented in the form of graphs. The experimental data as well as standard deviations on the data are presented in Appendix C. It was found that all deviations fall within the ISO tolerances discussed in chapter 3.

The proximate analyses were conducted at temperatures of ambient room temperature, 105, 130, 160, 190, 220 and 250°C and atmospheric pressure. It was decided to keep the temperature intervals between the data points small to investigate and focus on the lower temperature range as both the TGA and SEM results indicated that no physical changes occur at temperatures below 260°C. These smaller temperature intervals will result in detailed graphs which can be used to validate or contradict the results and subsequent conclusions made from the TGA and SEM experiments.

The first set of graphs indicates the composition of the coal samples on a dry basis in terms of volatile matter, fixed carbon and ash at the pre-selected temperatures indicated above. It was decided to exclude moisture content from these results as all moisture which can be seen during these experiments was reabsorbed after thermal drying and are thus deemed irrelevant for the purpose of this study. Moisture content graphs are however displayed in appendix B and must be considered when transport and storage methods for the coal after the drying process are evaluated.

The second set of graphs indicates the changes which occur in the calorific value (LHV) of the coal samples as they are heated to the pre-selected temperatures indicated in the first paragraph of this section.

4.4.1. Proximate analysis results for the WB2 coal

In general the proximate analysis results for the WB2 coal indicated in Graph 4.4.1(a) substantiate the findings form the TGA and SEM experiments as no major change in composition can be observed.

Generally the only changes observed are the slight decrease in volatile content and increase in fixed carbon. The increase in fixed carbon is only a percentage increase and not an actual weight increase and can be attributed to the weight and resultant percentage decrease in volatile content.

It can also be seen that the vitrinite rich fraction (-1.3SG) shows the lowest ash content with an increase in ash content observed in the mixture fraction and another increase in the inertinite (+1.4SG) fraction's ash content. The virgin sample's (normal) ash content shows an average when compared to the separated fractions' ash content. A greater volatile content is also observed in the vitrinite (-1.3SG) fraction which decreases through to the inertinite (+1.4SG) fraction with the virgin sample (normal) again showing an average when compared to the volatile content of the separated fractions. The fixed carbon content in all samples remains fairly constant for the WB2 coal.

The calorific values of the WB2 coal indicated in Graph 4.4.1(b) corresponds to the analysis results indicated in Graph 4.4.1(a) in that no major changes are observed in the studied temperature range. Slight decreases in the calorific values of all samples are however observed in the last temperature increment but this deviation falls within an acceptable experimental tolerance range and can as a result not be attributed to a change caused by the higher drying temperature.

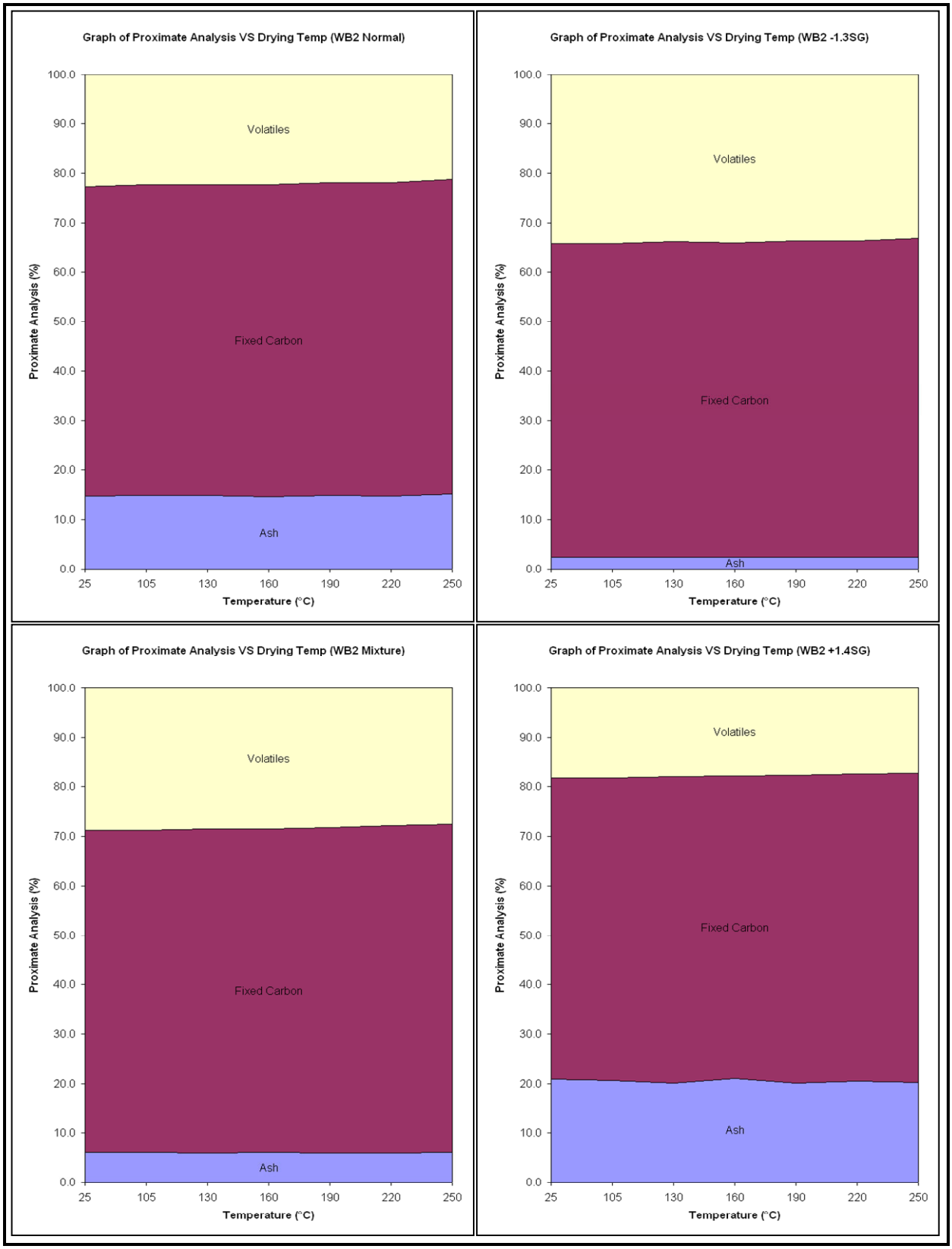

Graph 4.4.1(a): Proximate analysis results for the WB2 coal.

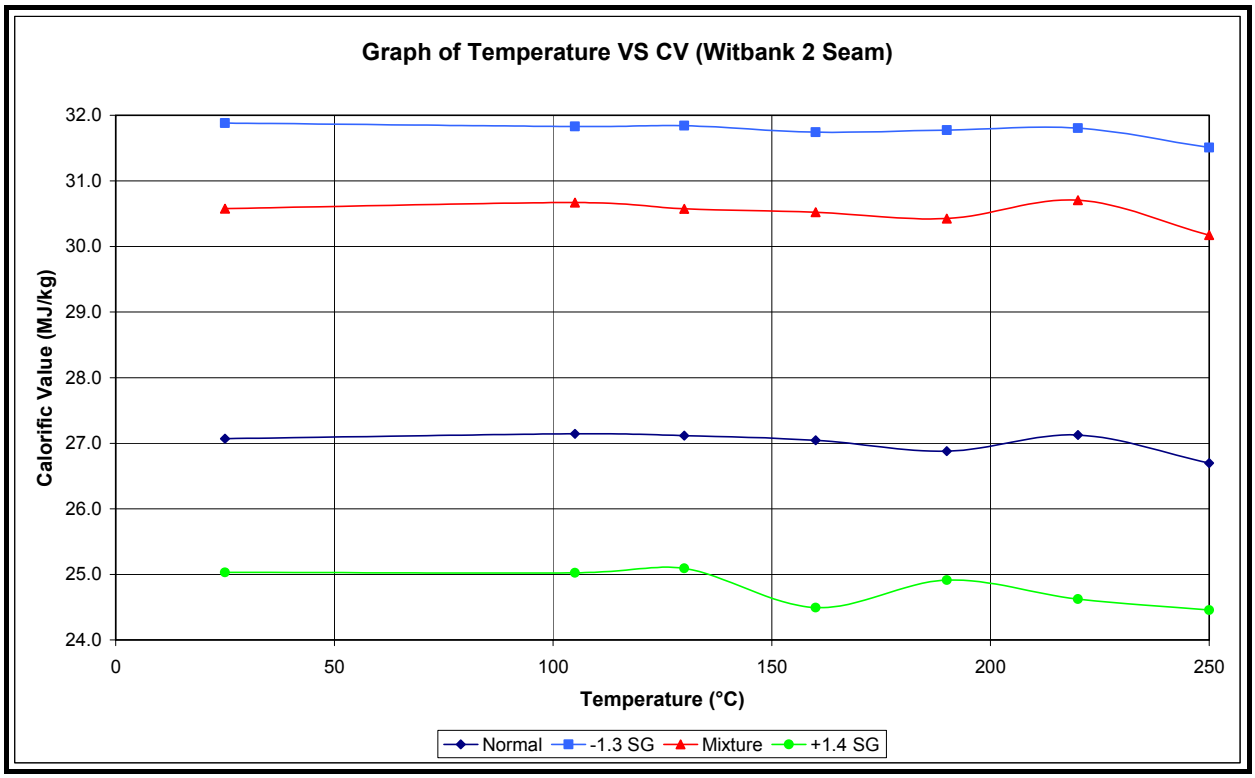

Graph 4.4.1(b): Calorific value results for the WB2 coal.

4.4.2. Proximate analysis results for the WB4 coal

In general the proximate analysis results for the WB4 coal indicated in Graph 4.4.2(a) substantiate the findings form the TGA and SEM experiments as no major change in composition can be observed. This also corresponds to and substantiates the results from the WB2 coal.

The only overall change observed is the slight decrease in volatile content and increase in fixed carbon. The increase in fixed carbon can again be attributed to the actual weight and resultant percentage decrease in volatile content as described for the WB2 coal.

The trends in the ash and volatile content results also correspond with the trends observed in the WB2 coal in that the vitrinite rich fraction (-1.3SG) shows the lowest ash content which increases through to the inertinite (+1.4SG) fraction's ash content. The virgin sample's (normal) ash content again shows an average when compared to the separated fractions' ash content. The volatile content decreases from the vitrinite (-1.3SG) sample through to the inertinite (+1.4SG) sample with an average observed for the virgin sample. The fixed carbon content varies for the separated samples; this can be attributed to the large amount of ash present in the virgin (normal) and inertinite (+1.4SG) samples in comparison to the ash content of the vitrinite (-1.3SG) and mixture samples. The slight variance in the ash content of the virgin

(normal) and inertinite (+1.4SG) samples can be attributed to experimental error and falls within an acceptable range.

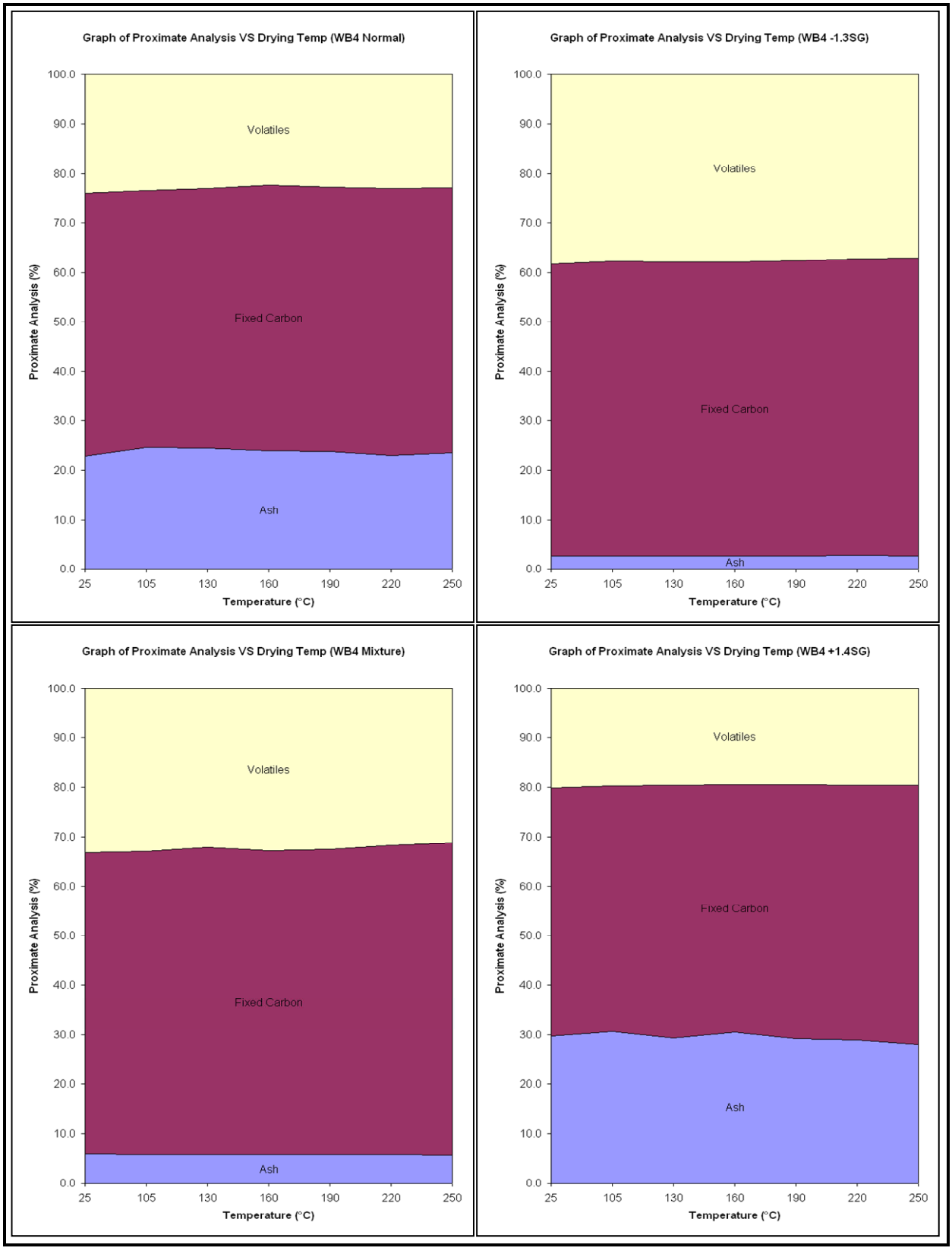

Graph 4.4.2(a): Proximate analysis results for the WB4 coal.

The calorific values of the WB4 coal indicated in Graph 4.4.2(b) corresponds to the analysis results indicated in Graph 4.4.2(a) in that no major changes are observed in the studied temperature range. A slight decrease in calorific value is again observed in the last temperature increment which falls within acceptable experimental tolerances.

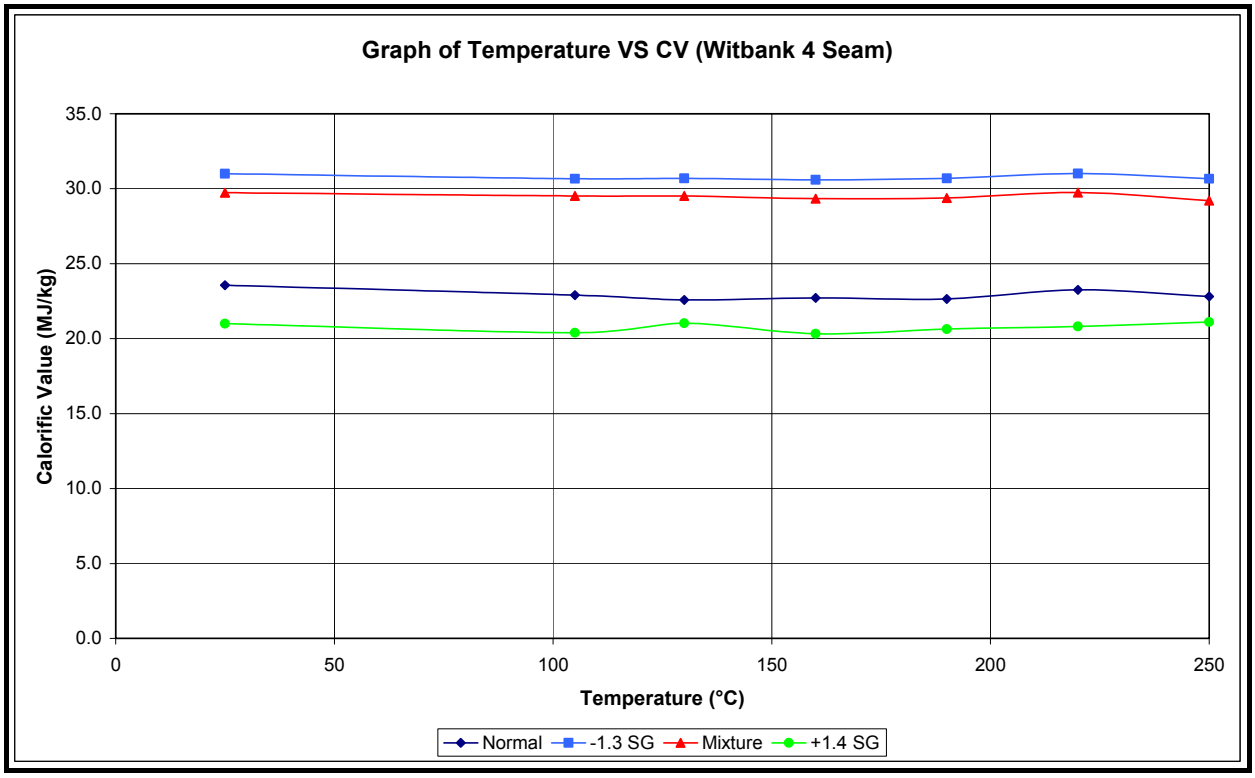

Graph 4.4.2(b): Calorific value results for the WB4 coal.

4.4.3. Proximate analysis results for the TS coal

In general the proximate analysis results for the TS coal indicated in Graph 4.4.3(a) substantiate the findings form the TGA and SEM experiments as no major change in composition can be observed and also correspond to the proximate analysis results obtained from the WB2 and WB4 coals.

Although minimal, again the only overall changes observed are the slight decrease in volatile content and increase in fixed carbon which can be attributed to the same reasons discussed for the WB2 and WB4 coals.

The trends observed in the ash content results also correspond with the trends observed in the proximate analysis results for the WB2 and WB4 coals. The volatile content however remains fairly constant for all samples while the fixed carbon content varies which correspond to observations made for the WB4 coal.

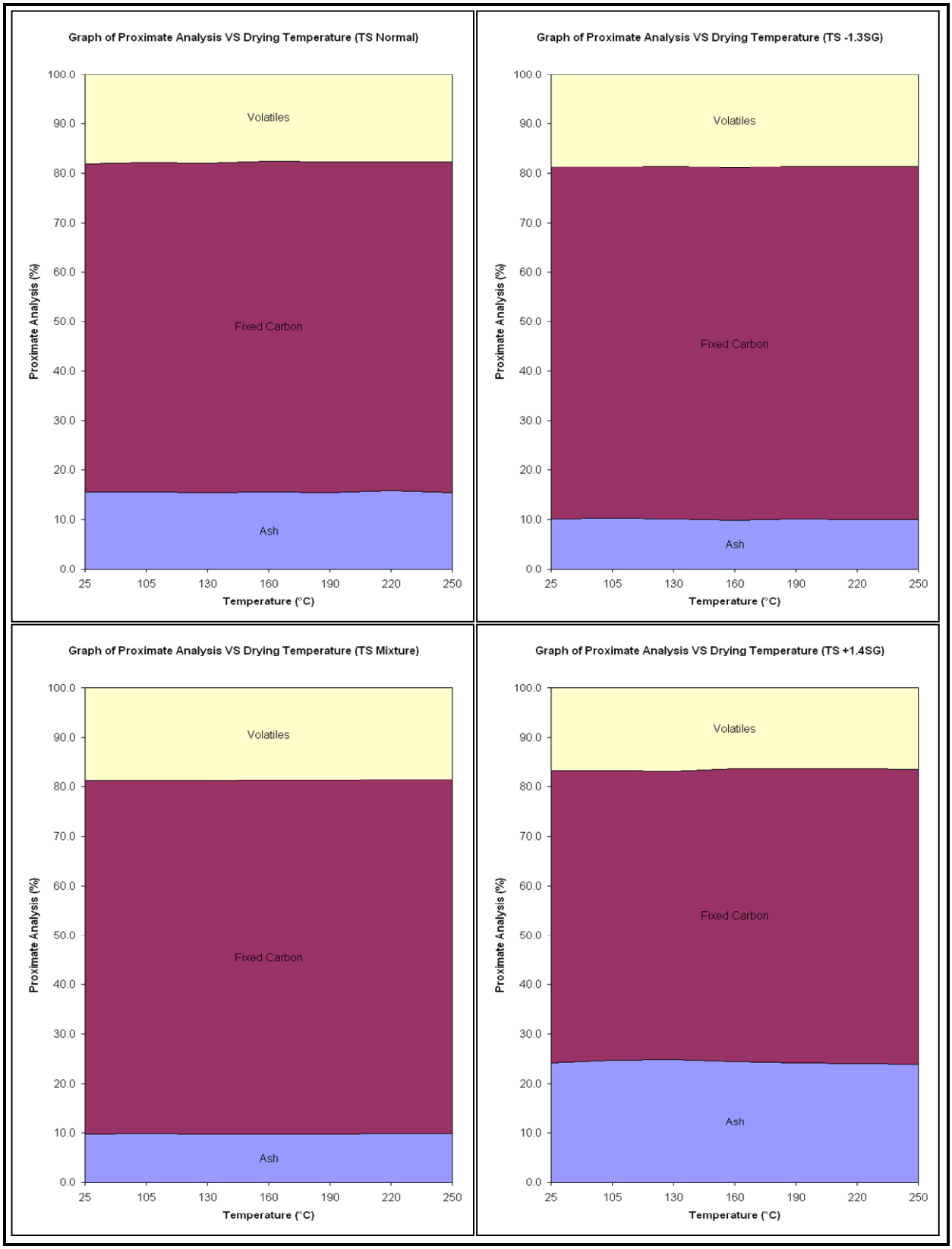

Graph 4.4.3(a): Proximate analysis results for the TS coal.

The calorific values of the TS coal indicated in Graph 4.4.3(b) corresponds to the proximate analysis results indicated in Graph 4.4.3(a) in that no major changes are observed in the studied temperature range. It is however observed that the mixture fraction has a slightly higher

calorific value than the vitrinite sample which differs from the other coals studied. This can be attributed to the fact that this coal is the highest ranked coal in South Africa and that the mixture fraction will be very pure, containing mostly vitrinite while the vitrinite rich fraction will contain both vitrinite and all of the exinite in the coal (Falcon & Snyman, 1986:25).

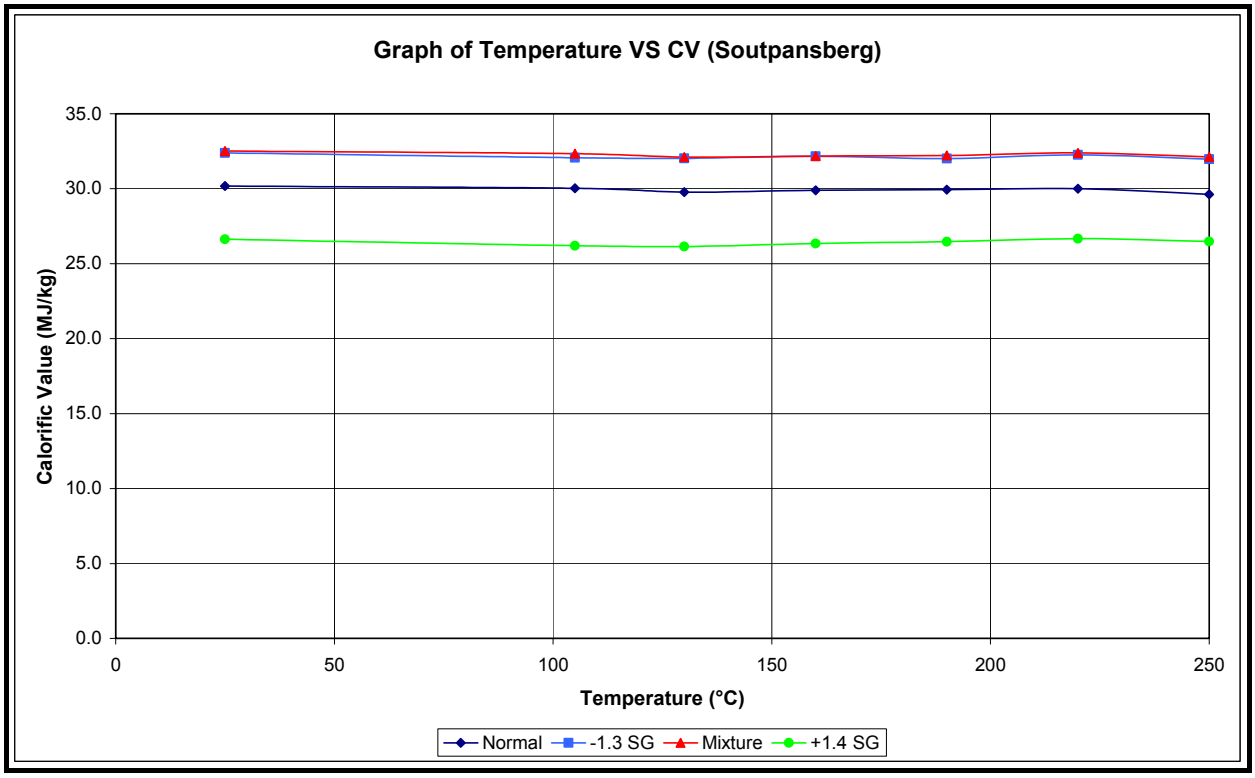

Graph 4.4.3(b): Calorific value results for the TS coal.

4.4.4. Proximate analysis results for the GG coal

In general the proximate analysis results for the GG coal indicated in Graph 4.4.4(a) substantiate the findings form the TGA and SEM experiments as no major change in composition can be observed; it also corresponds to the other proximate analysis results indicated above.

The only overall changes observed are the slight decrease in volatile content and resultant increase in fixed carbon.

The trends in the ash content results also correspond with the trends observed in the other proximate analysis results indicated above. The changes observed in the volatile content and fixed carbon content correspond to that seen in the WB2 coal where the volatile content decrease from the vitrinite (-1.3SG) fraction through to the inertinite fraction (+1.4SG) with the virgin (normal) sample showing an average while the fixed carbon content remains fairly constant for all samples tested.

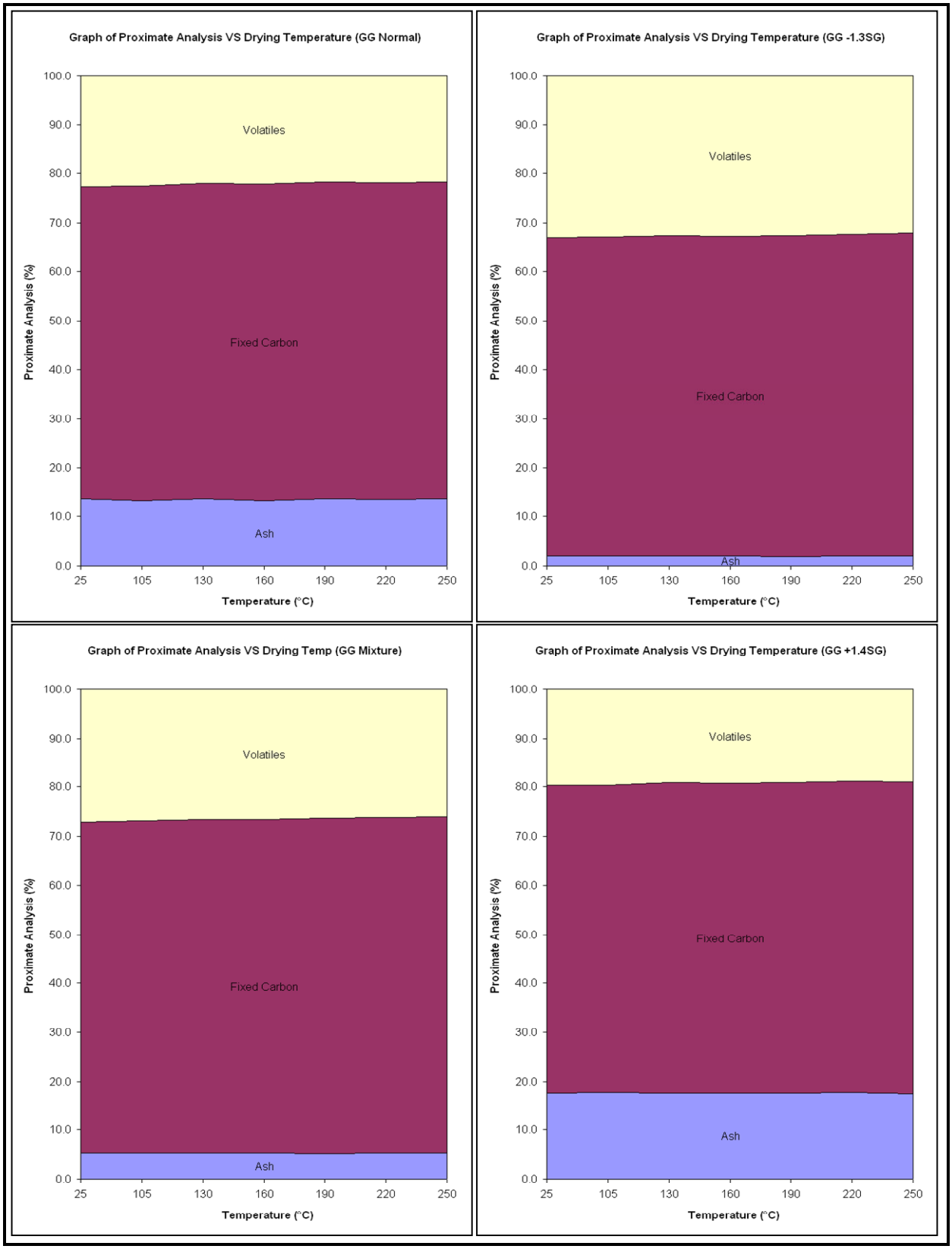

Graph 4.4.4(a): Proximate analysis results for the GG coal.

The calorific values of the GG coal indicated in Graph 4.4.4(b) corresponds to the analysis results indicated in Graph 4.4.4(a) in that no major changes is observed in the studied temperature range. A slight decrease in calorific value is however again observed in the last

temperature increment which falls within acceptable experimental tolerances. This corresponds to the trend observed for the other coals tested.

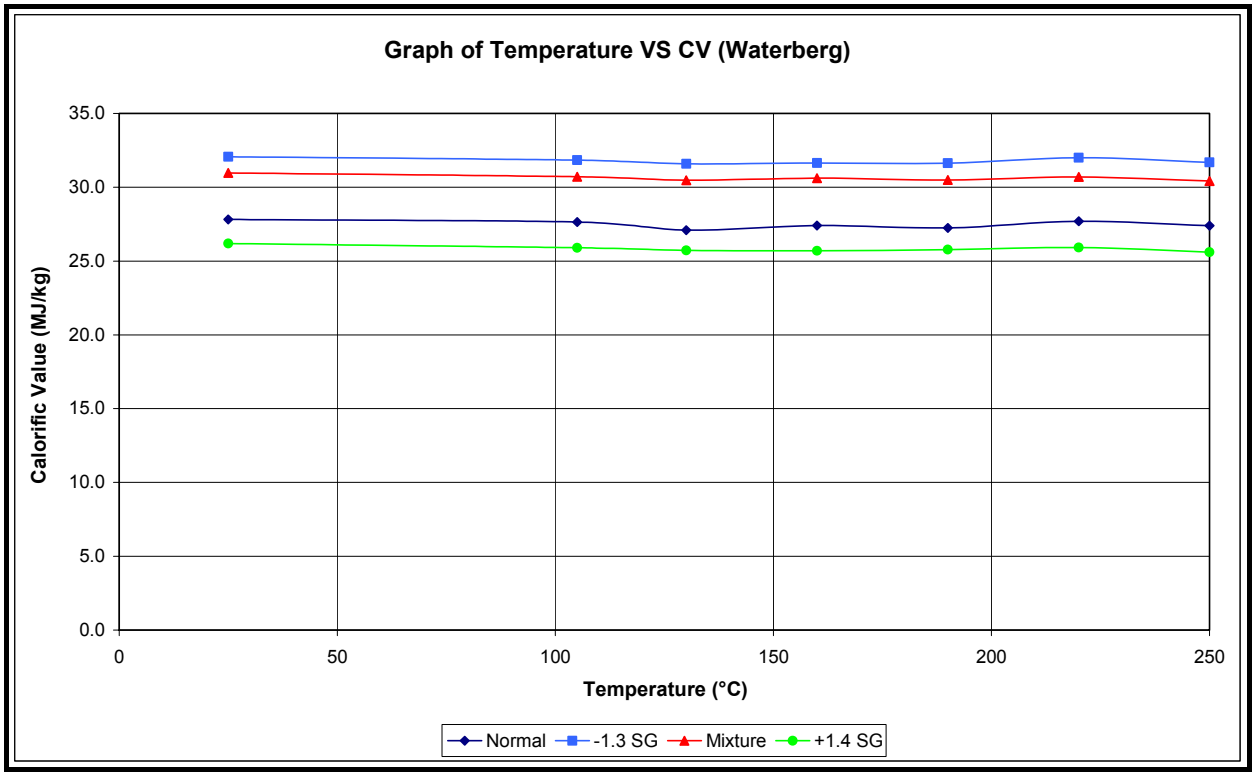

Graph 4.4.4(b): Calorific value results for the GG coal.

4.4.5. Proximate analysis results for the NV coal

In general the proximate analysis results for the NV coal indicated in graph 4.4.5(a) substantiate the findings form the TGA and SEM experiments as no major change in composition can be observed; it also corresponds to the other proximate analysis results indicated above.

The only overall changes observed are the slight decrease in volatile content and increase in fixed carbon in the vitrinite rich (-1.3SG) and mixture samples. The reason that these changes are not clearly visible in the virgin (normal) and inertinite rich (+1.4SG) samples is that the ash content are dominant on these graphs and changes in the other properties are as a result almost unnoticeable.

The trends in the ash content results correspond with the trends observed in the proximate analysis results of the other coals indicated above while the changes in volatile content correspond to that seen in the WB2 and GG coals. The changes in fixed carbon content correspond to that observed for the WB4 and TS coals; these can be attributed to the large change in ash content between the samples.

The variance in ash content of the virgin sample can be attributed to experimental error.

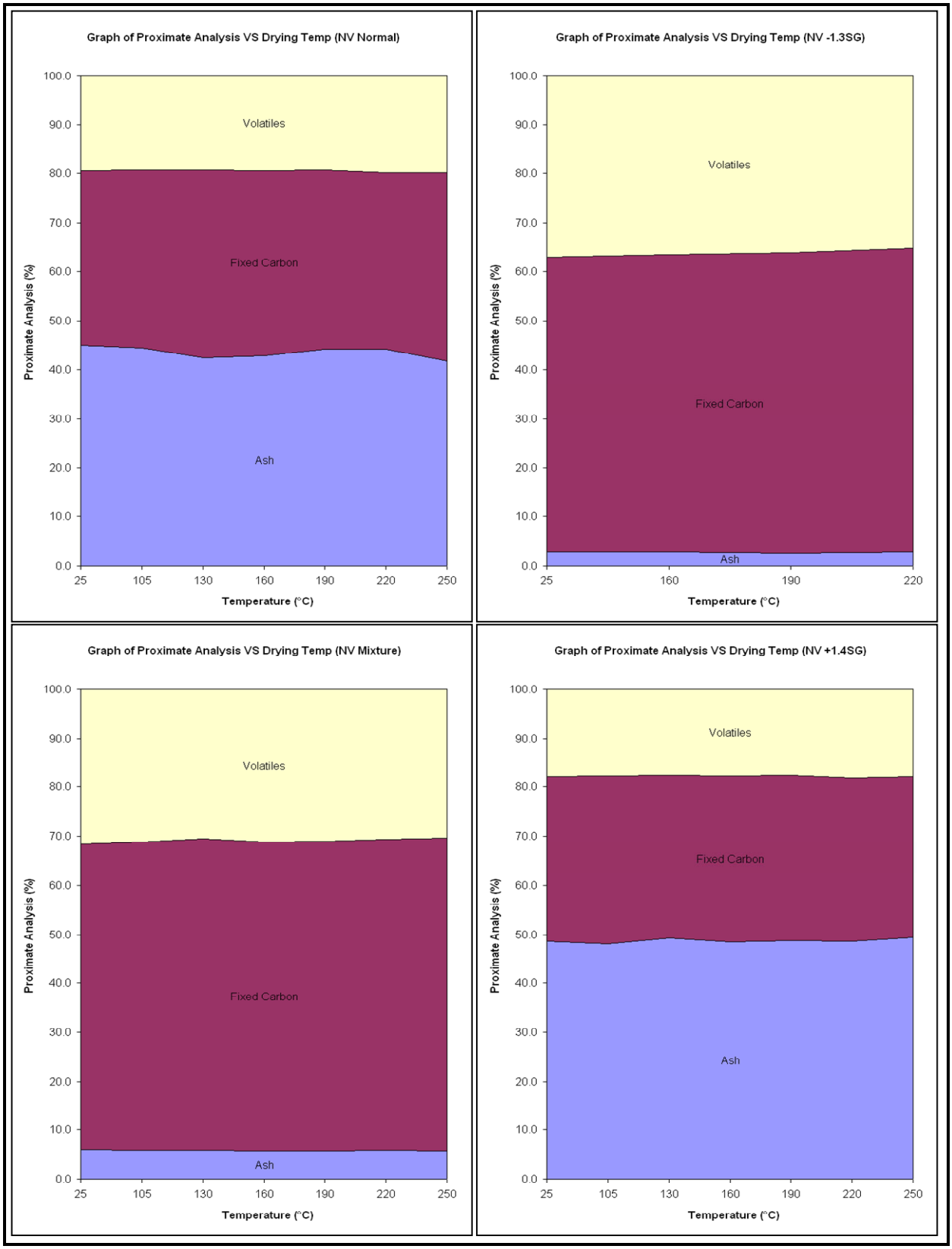

Graph 4.4.5(a): Proximate analysis results for the NV coal.

The calorific values of the NV coal indicated in Graph 4.4.5(b) corresponds to the analysis results indicated in Graph 4.4.5(a) in that no major changes is observed in this temperature range. The very low calorific value observed in the virgin (normal) and inertinite (+1.4SG)

samples can be attributed to the very high ash content associated with these fractions. A slight decrease in calorific value for the mixture and inertinite (+1.4SG) fractions is again observed in the last temperature increment which corresponds to the trend observed for the other coals.

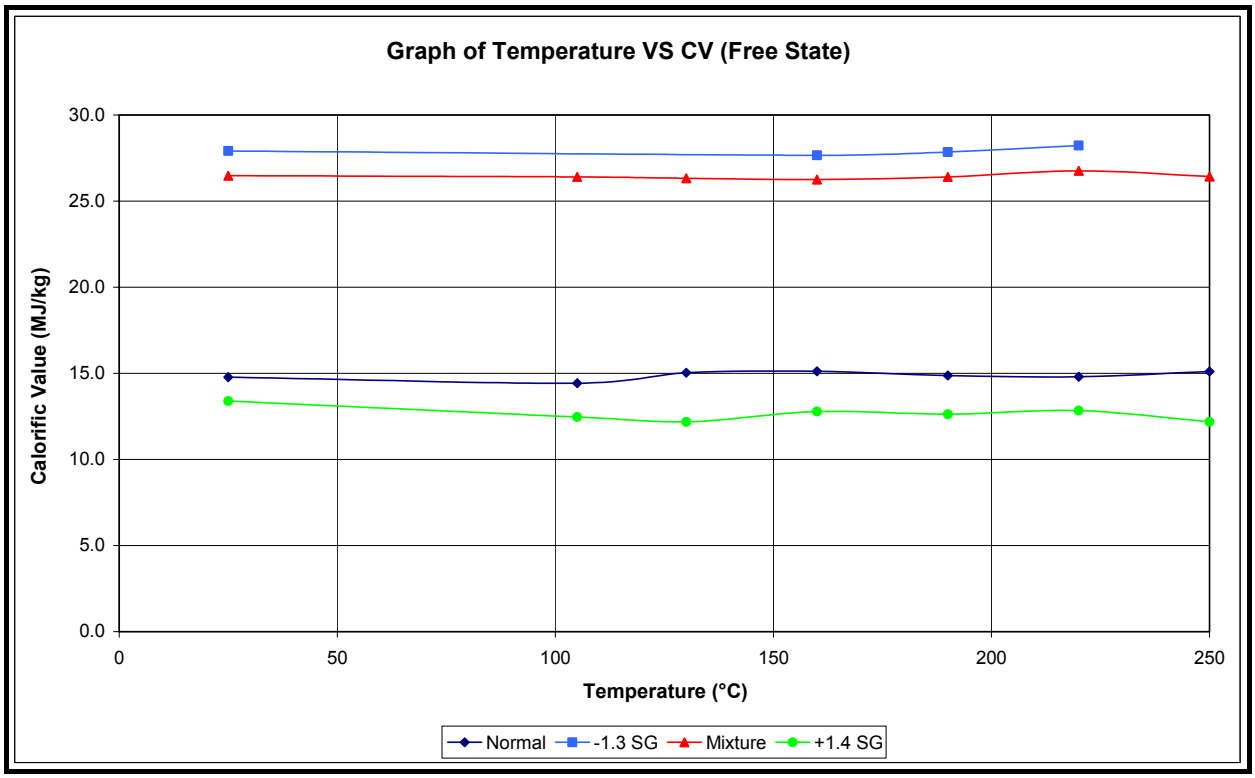

Graph 4.4.5(b): Calorific value results for the NV coal.

4.4.6. Discussion of proximate analysis results

In general the proximate analysis results correspond to the results obtained in the TGA and SEM experiments.

Though not significant enough to dictate a maximum drying temperature, the proximate analysis results do indicate that an almost unnoticeable amount of volatiles evaporate with the moisture from the coal particles up to the maximum experimental temperature of 250°C. This small loss in volatiles increases linearly with an increase in drying temperature and should be considered when a maximum drying temperature is selected.

The calorific value results indicate that the slight loss in volatiles does not affect the calorific value of the coal noticeably. The coal does however lose the calorific value stored inside the mass of volatiles which evolve when the coal is thermally dried.

To limit the loss of these volatiles and energy associated with the volatiles, the proximate analysis results also dictate that the drying temperature must be kept relatively low which is in agreement with the 150°C maximum drying temperature recommended in paragraph 4.2.6.

4.5. Mercury intrusion results

It was decided to conduct mercury intrusion (or often called mercury porosimetry) experiments on some of the samples to verify the results obtained in the TGA and SEM experiments as well as the proximate analysis.

Due to limitations regarding the availability of the porosimeter and the fact that these experiments were only done to supplement the other experimental results, it was decided to let a final year engineering student, Mr. Coenraad de Bruin (De Bruin, 2005:42–43), conduct these experiments on only three of the five coal samples selected for this study. The three samples selected for this purpose were the Witbank 2 seam (WB2), the Witbank 4 seam (WB4) and the Free State (NV) coal samples. Experimental data and repeatability are shown in Appendix D.

The experiments were done at temperatures of ambient room temperature, 105, 190, 250, 300, 350 and 400°C to verify the previous results which indicated that no physical changes occur in the lower temperature range (below 250°C).

Results obtained from the experiments are presented in the form of graphs where porosity (%), total pore area (m^2/g), median pore diameter (nm) and average pore diameter (nm) are plotted against temperature.

4.5.1. Mercury intrusion results for the WB2 coal

The WB2 results indicated in Graph 4.5.1 corresponds and verify the other experimental data and supplies additional insight into what happens to the coal structure as it is heated.

All tested properties of the WB2 coal samples remain fairly constant throughout the lower temperature range up to 250°C where after the porosity of the vitrinite rich fraction starts to increase slightly at 300°C. This increase is more substantial at 350°C and continues up to 400°C which is in exact agreement with the movements noticed during the SEM experiments.

The mixture sample remains unchanged up to about 300°C where only a slight increase is noticed with a more substantial increase to 400°C while the inertinite fraction only shows an increase in porosity at 400°C. This also corresponds to the movements observed during the SEM experiments with the SEM temperatures trailing slightly to the mercury intrusion temperatures. This can be attributed to initial unnoticeable changes that occur on a molecular level and as a result goes unnoticed during the SEM experiments as well as the fact that SEM drying occur at vacuum conditions while drying for the mercury intrusion is done under atmospheric conditions.

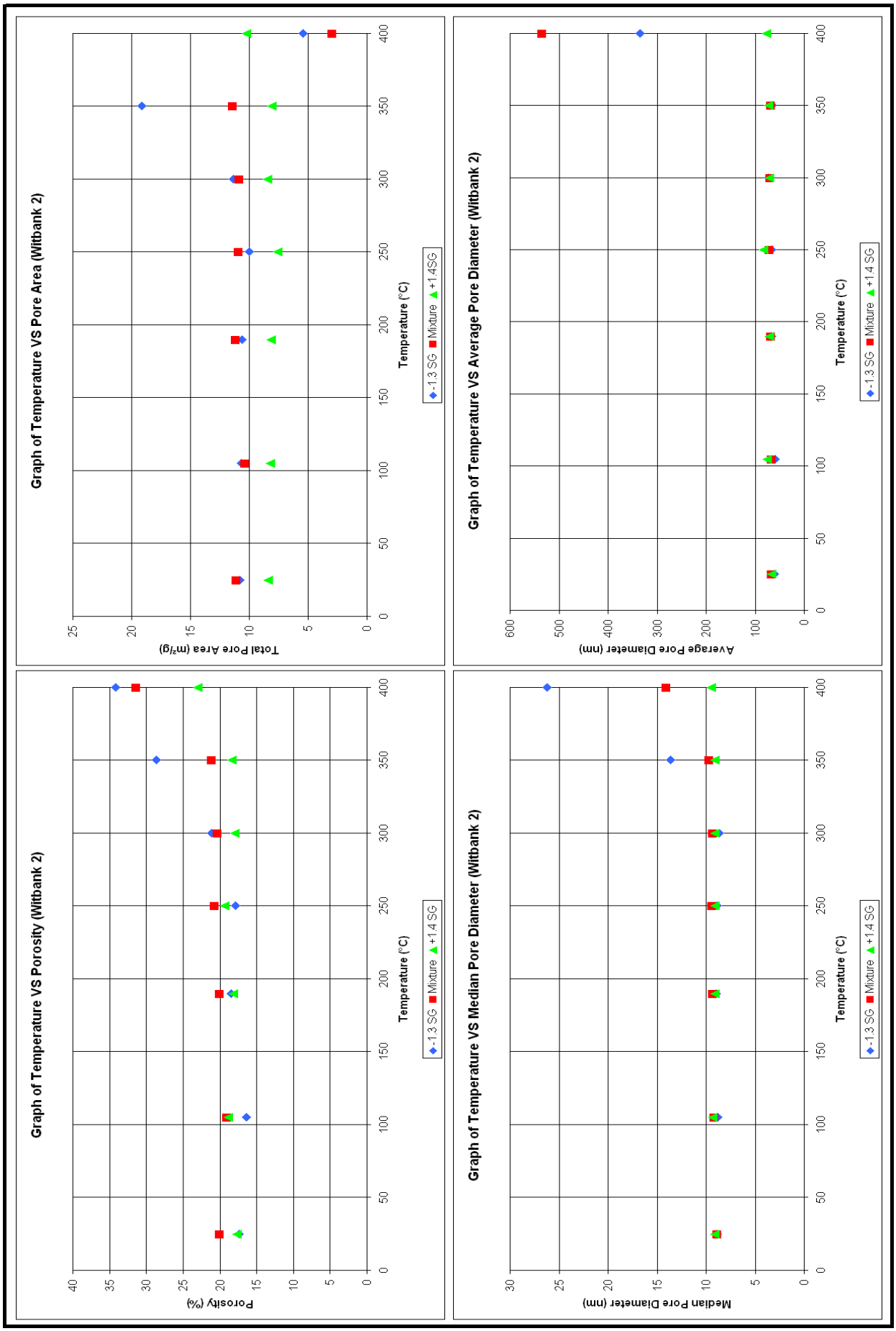

Graph 4.5.1: Mercury intrusion results for the WB2 coal.

When the pore area is considered, slight changes in the vitrinite fraction is observed at 300°C with an initial increase at 350°C and then a decrease as the pores collapse to 400°C. The mixture fraction shows a collapse of pores and decrease in porosity at 400°C. This can also be attributed to the huge increase in average pore diameter and lesser increase in median pore diameter as larger pores will lead to smaller surface area if these larger pores 'swallow' some of the smaller pores. The inertinite fraction shows a slight increase in pore area indicating that more pores form in this fraction during heating.

When the pore diameters are investigated it can be seen that the median diameter of the pores start to increase for the vitrinite rich fraction from 350°C and continues up to 400°C. The mixture fraction only shows an increase at 400°C while the inertinite rich fraction shows no change. This indicates that most of the pores stay unchanged up to 300°C with an increase in size for some of the pores from 350°C.

If the average pore diameter is considered it is found that changes only occur at 400°C with the vitrinite and mixture fractions. It is noticed that the mixture shows a larger increase in average pore diameter than the vitrinite which can be attributed to the planes between the vitrinite and inertinite in this fraction starting to part. This is also the reason that the mixture fraction shows a larger overall decrease in pore area than the vitrinite fraction.

The very large change in the average pore diameter versus the median pore diameter can be attributed to the formation of the cracks seen during the SEM experiments as only a few large cracks will increase the average pore size dramatically but show little effect on the median pore diameter.

4.5.2. Mercury intrusion results for the WB4 coal

The WB4 results indicated in Graph 4.5.2 corresponds and verify the other experimental data indicated in the previous paragraphs.

All tested properties of the WB4 coal samples remain fairly constant throughout the lower temperature range up to 300°C when the porosity of the vitrinite fraction shows a slight increase. A decrease is then noticed at 350°C with a substantial increase at 400°C which is in agreement with the movements noticed during the SEM experiments.

The porosity of the mixture and inertinite samples remain unchanged up to 350°C and only increases (inertinite to a lesser extent) at 400°C. This also corresponds to the movements observed during the SEM experiments.

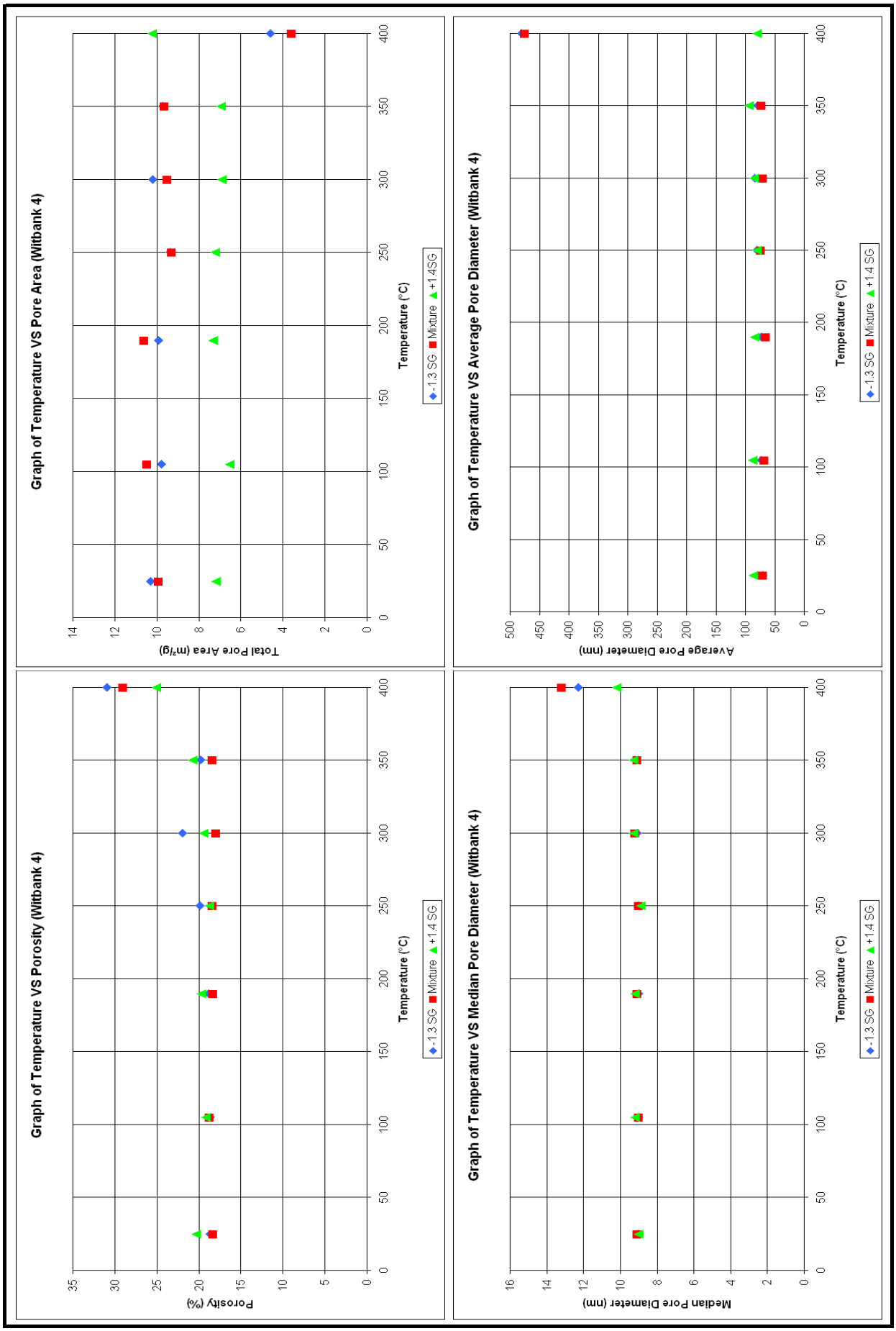

Graph 4.5.2: Mercury intrusion results for the WB4 coal.

The pore area for all fractions remains fairly constant up to a temperature of 350°C with a decrease in the pore area of the vitrinite and mixture at 400°C. The mixture fraction again shows a larger decrease than the vitrinite fraction. The inertinite fraction shows an increase in pore area, again indicating the formation of more pores as the sample is heated.

When the pore diameters are investigated it can be seen that the median diameter of the pores start to increase for all fractions at 400°C. The mixture fraction shows the largest increase followed by the vitrinite fraction. This indicates that most of the pores stay unchanged up to 350°C with an increase in size for most of the pores at 400°C.

If the average pore diameter is considered it is found that changes only occur at 400°C with the vitrinite and mixture fractions. It is noticed that the mixture and vitrinite fraction shows a similar increase in average pore diameter. The inertinite fraction remains unchanged at 400°C indicating that no surface cracks started to form yet while the very large change in the average pore diameter of the vitrinite and mixture fractions in comparison to the median pore diameter can be attributed to the formation of these cracks.

4.5.3. Mercury intrusion results for the NV coal

The NV results indicated in Graph 4.5.3 correspond well and verify the other experimental data indicated in the previous paragraphs.

The tested properties of the NV coal samples remain fairly constant throughout the lower temperature range with very little change, even at 400°C. The porosity of the vitrinite fraction remains constant with an increase at 400°C. The mixture fraction shows a slight increase at 400°C while the porosity of the inertinite fraction remains unchanged. This is in agreement with the movements noticed during the SEM experiments.

The pore area for all fractions remains fairly constant up to a temperature of 350°C with a slight decrease in the pore area of the vitrinite and mixture fractions up to this temperature. The vitrinite fraction shows a drop in pore area at 400°C while the other fraction's pore area remains constant.

When the pore diameters are investigated it can be seen that the median diameter of the pores show a slight increase at 400°C.

The average pore diameter also remains unchanged with only the vitrinite fraction showing a dramatic increase at 400°C.

These 'uneventful' results can be attributed to the low reactivity associated with this low rank coal.

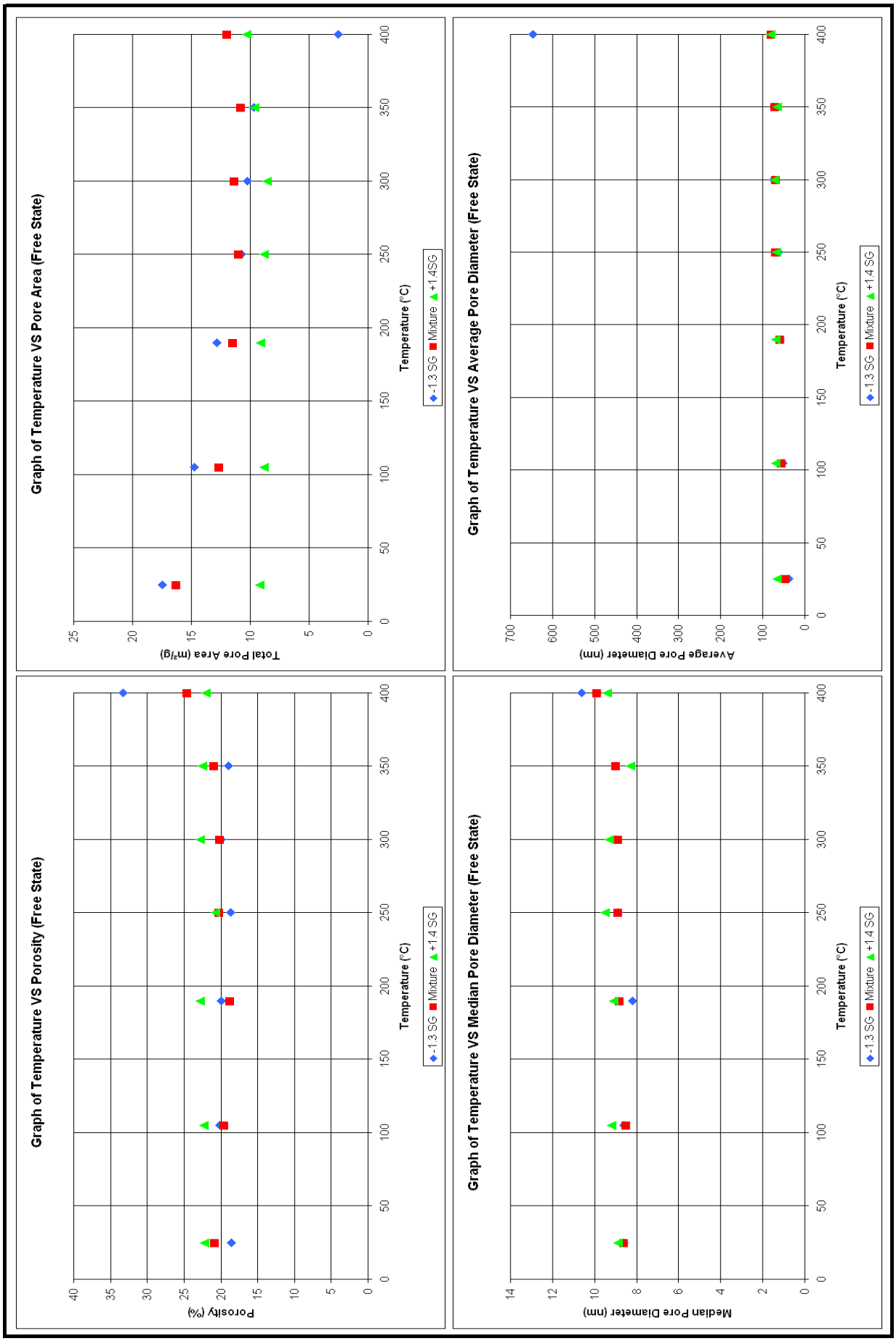

Graph 4.5.3: Mercury intrusion results for the NV coal.

4.5.4. Discussion of mercury intrusion results

The mercury intrusion results correspond to the findings in the TGA and SEM experiments as well as the proximate analysis, showing, that depending on the rank and reactivity of the coal, structural changes only start to occur at temperatures above 250°C.

The results indicate:

- That porosity in general increase above this temperature.
- That the pore area of the vitrinite and mixture fractions decrease whiles the pore area of the inertinite fraction increase above this temperature.
- The median pore diameter for all fractions increases slightly.
- The average pore diameter increases dramatically for both the vitrinite and mixture fractions while the inertinite's average pore diameter remains constant.

From this it can be concluded that some of the pores of the more plastic vitrinite and mixture fractions became bigger and swallow some of the smaller pores to form a few very large pores which would explain:

- The excessive increase in average pore diameter.
- Slight increase in median pore diameter, caused by the larger pores but limited by the huge amount of smaller pores.
- Decrease in pore area as a few larger pores 'swallowing' a lot of smaller pores resulted in the decrease in pore area.
- Increase in porosity caused by an increase in open area as a result of the larger pores.

It can also concluded that the harder and more structured inertinite also shows an increase in pore diameter if the median pore diameter is considered but do not swallow neighbouring pores as the average pore diameter remains fairly constant. The increase in pore area is as a result of the increase in median pore diameter; the individual pores physically have a larger surface area because of the swelling but no pores are destroyed as they are swallowed because of the plastic behaviour associated with the vitrinite and mixture samples.

Chapter 5 Plant Proposal

This chapter is dedicated to the proposal of a thermal drying plant. Both the literature discussed in chapter 2 as well as the experimental results in chapter 4 will be evaluated in this proposal as to allow the development of a technically and economically feasible thermal drying plant.

5.1. Feasibility of a thermal drying plant

A few aspects must be considered when a thermal drying plant / process is developed which is not limited to the experimental results discussed in chapter 4. Among others a suitable dryer must be selected and a method to transport the dried coal must be investigated.

If the industrial thermal dryers discussed in chapter 2.7 are considered it is found that most of them will not be suitable for the large scale thermal drying of coal. The application of these dryers is briefly discussed below:

1. Cabinet dryers are not suitable for a large scale drying operation and are more suitable for lab scale drying.
2. Calciners are associated with calcination reactions and are not applicable here. The technology is however very similar to rotary dryers which will be discussed in point 8.
3. Conveyor dryers normally handle larger particles than the fine coal discard investigated in this study. The fine coal might block the perforated belt and cause problems. The heating medium is also passed through the fine coal to establish heating which might lead to excessive dust generation and increase the risk of a dust explosion. This technology is thus not considered suitable for the drying of fine coal.
4. Flash dryers seem like a suitable drying method. This technology however also leads to excessive dust generation resulting in the use of secondary dust collection units, increasing the risk of a dust explosion.
5. Fluidized bed dryers have the same advantages and disadvantages associated with flash dryers.

6. Indirect dryers offer the first practical solution. As the heating medium is in indirect contact with the coal, the coal is not exposed to high gas velocities which will inadvertently cause dust generation. The coal can also be dried within an inert atmosphere which will be easy to maintain as the inert gas's primary function will not be heating which causes the high gas velocities in the other drying processes.
7. Infrared dryers also seem like a suitable technology. The disadvantage of this technology however lies in the fact that it employs electricity or gas to generate the energy required for drying. An indirect dryer which utilizes some of the coal product as energy source to generate steam would therefore result in a more economical dryer.
8. Rotary dryers also offer low velocity air contact, reducing dust generation. The heated air used for drying can be replaced by an inert gas which will reduce oxidation and the risk of dust explosions.
9. Specialized dryers such as microwave dryers seem like a suitable technology. Chances are however that the coal's molecular structure might react to the microwaves which will lead to structural deterioration. This technology also utilizes electricity as energy source, posing the same disadvantage as infrared dryers.
10. Spray dryers are not recommended as the large variance in coal particle size may cause the spray nozzles to block. Due to the high drying air velocities associated with these dryers they are also prone to dust explosions.

The experimental results in chapter 4 indicated that the drying temperature should be kept below 200°C but preferably below 150°C; a dryer must therefore be selected which conform to this specification. For the purpose of this proposal it was decided to combine an indirect dryer and a rotary dryer in a single stage drying application as both of these can be used on a large scale and the use of these technologies will result in minimal dust generation.

A small portion of the coal product will be combusted in a boiler to generate steam which will be used to dry the coal indirectly while the combusted gas will be used to dry the coal directly and also blanket the coal in an inert atmosphere, preventing the possibility of oxidation, spontaneous combustion and a dust explosion. The temperature of the dryer can also be controlled better by combining these two methods as the amount of coal fed to the boiler and the pressure at which the boiler is maintained will control both the outlet temperatures of the combusted coal gas and saturated steam. A calculation indicating the fraction of the dried coal product needed to supply the energy required to dry the wet coal fed to the plant is shown in paragraph 5.3.

After the coal is dried, it is recommended to pelletize the fine coal using a press pelletizer which will resolve any further dust generation and transport problems. It is also suspected that the hot

coal ejected from the thermal drying process will pelletize with greater ease than coal dried by means of a mechanical drying process as the coal's temperature is closer to the plastic state observed during the SEM experiments.

The coal can then be stored in a hopper or other isolated environment where it can be cooled down while being exposed to an inert atmosphere before transported to the client. This will reduce the risk of spontaneous combustion and oxidation by depleting the coal surface from oxygen while it is still hot.

5.2. Development of a thermal drying process

Figure 5.2 shows a simplified flow diagram of the thermal drying plant proposed. In this plant the wet fine coal which is normally discarded will be fed to the proposed thermal dryer (DRY-01). The dried coal (DRY-02) will be fed to a press pelletizer where all fine coal will be pelletized into larger coal particles. The pelletized coal particles (PEL-01) will now be fed to a hopper where it will be cooled under inert conditions.

From the hopper the larger part of the coal pellets are fed as product (PRD-01) to be transported to the client while a smaller fraction (BLR-01) (as calculated in paragraph 5.3) will be combusted in a boiler to generate the steam required (STM-01) to operate the thermal dryer.

The combusted coal gas from the boiler (COM-01) is fed through a blower (COM-02) and split into two streams.

The first stream (COM-03) is fed hot to the inside of the dryer to be in direct contact with the coal with a dual purpose; to aid in drying the wet coal feed (DRY-01) as well as to ensure that an inert atmosphere blankets the coal to prevent oxidation, spontaneous combustion and a dust explosion.

The second stream (COM-04) is fed to a heat exchanger where it is cooled down to atmospheric temperature before it (COM-05) is passed through the hopper containing the pelletized coal product (PEL-01) to both cool down the hot product from the pelletizer and to prevent oxidation, spontaneous combustion and a dust explosion during the cooling process.

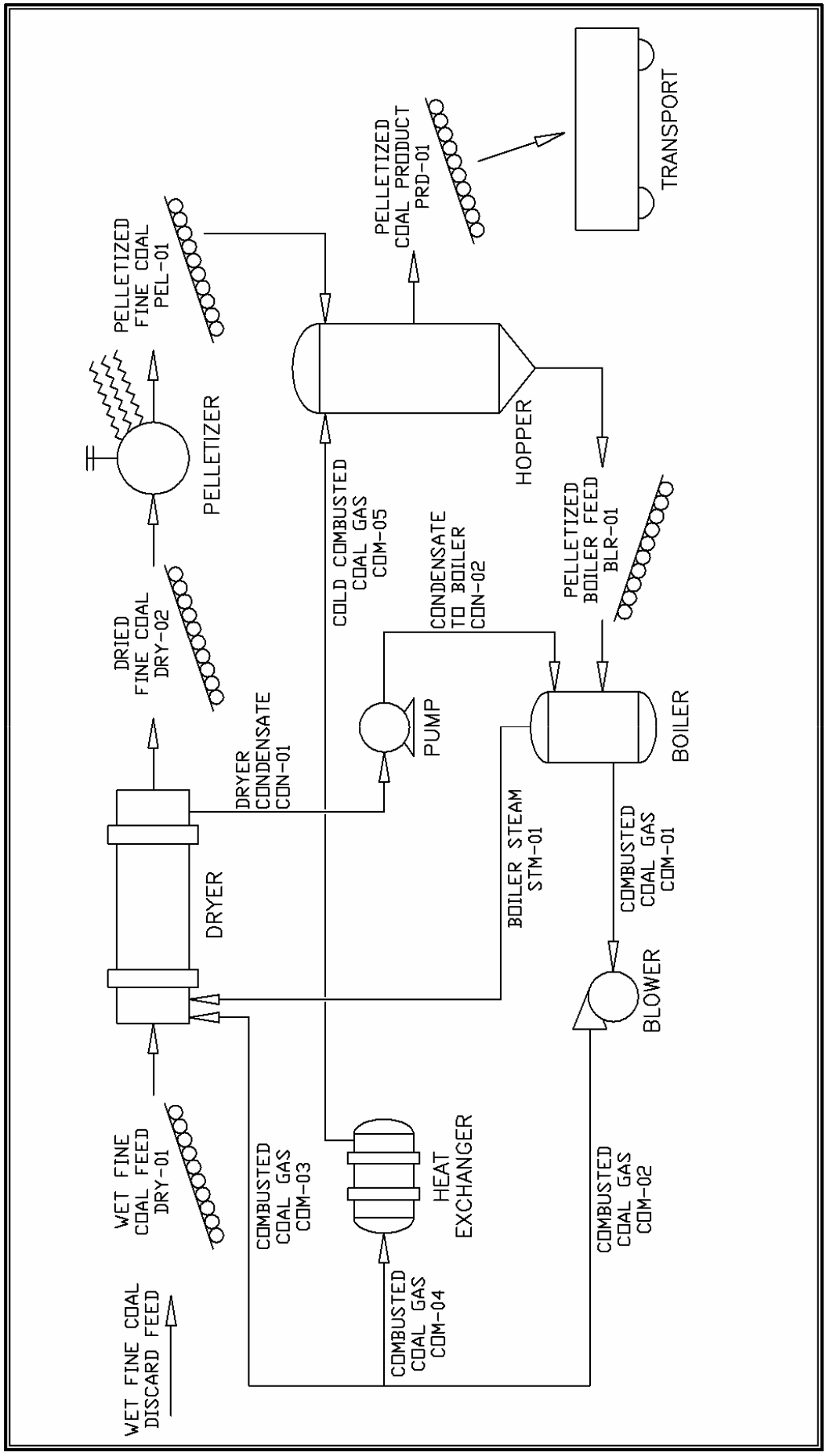

Figure 5.2: Simplified thermal drying plant flow diagram.

5.3. Calculation of energy requirement

To determine the economical feasibility of a thermal drying process the energy requirement of such a process must be evaluated. If it is found that the bulk of the pelletized coal product must be combusted to generate enough heat to dry the wet coal the process will not be feasible. For this calculation the following assumptions were made:

a) The discarded coal slurry fed to the thermal drying plant will have a moisture content of 35%.
b) For the purpose of this calculation the Free State coal sample was selected as it has the highest ash content and lowest calorific value of all the coals tested in this study. For calculation purposes the Heat Capacity of the volatiles as well as the carbon content of the coal was considered to be the same as that of pure carbon.
c) The fractional composition of ash and carbon / volatiles was back calculated using the values determined during the proximate analysis as indicated in Table C.5.1 and the moisture content of the coal indicated in (a) above.
d) A mass basis of 1kg wet coal feed was selected for calculation purposes.
e) The inlet temperature of the wet coal feed was assumed to be 25°C with the boiling point of the coal's moisture at 100°C and the outlet temperature of both the dried coal product and vaporized moisture at 150°C as per the recommendations from chapter 4.
f) The boiler efficiency was assumed to be 75% (Council of Industrial Blowers, 2003:5). The rest of the thermal drying system's energy efficiency, including the dryer was assumed to be the same as the boiler and was selected as 75%.

The variables in the thermal drying system were thus defined as:

Defined Variables:

$x_{H2O} := 0.35$	Fraction of moisture in fine Coal
$x_C := 0.357$	Fraction of Carbon / Vols in NV Coal (Calculated from Table B.5.1 in Appendixes)
$x_{Ash} := 0.293$	Fraction of Ash in NV Coal (Calculated from Table B.5.1 in Appendixes)
$m := 1kg$	Mass basis for energy calculation
$T_{in} := (25 + 273.15)K$	Inlet temperature of Coal

$T_{out} := (150 + 273.15)K$ Outlet temperature of Coal

$T_{boil} := (100 + 273.15)K$ Boiling temperature of Water

$y_{boiler} := 0.75$ Boiler efficiency
(Council of Industrial Boiler Owners, 2003:5)

$y_{system.loss} := 0.75$ System losses - assume same as for boilers

The physical properties of the coal and steam needed for the calculation are defined below:

Properties:

$Cp_{H2O} := 4.217 \frac{kJ}{kg \cdot K}$ Heat Capacity of Water at 100ºC
(Incropera & De Wit, 1996:846)

$Cp_{Steam.373.15} := 2.029 \frac{kJ}{kg \cdot K}$ Heat Capacity of Steam at 100ºC
(Incropera & De Wit, 1996:846)

$Cp_{Steam.420} := 2.291 \frac{kJ}{kg \cdot K}$ Heat Capacity of Steam at 150ºC
(Incropera & De Wit, 1996:847)

$\Delta H_{H2O} := 2257 \frac{kJ}{kg}$ Heat of Vaporization of Water at 100ºC
(Incropera & De Wit, 1996:846)

$Cp_{Coal} := 1.26 \frac{kJ}{kg \cdot K}$ Heat Capacity of Coal at 300K
(Incropera & De Wit, 1996:837)

$Cp_{Ash.300} := 0.745 \frac{kJ}{kg \cdot K}$ Heat Capacity of SiO_2 at 300K
(Incropera & De Wit, 1996:832)

$Cp_{Ash.400} := 0.885 \frac{kJ}{kg \cdot K}$ Heat Capacity of SiO_2 at 400K
(Incropera & De Wit, 1996:832)

$E_{Coal} := 14.8 \frac{MJ}{kg}$ Calorific Value of NV Coal at 25°C
(Table B.5.1 in Appendixes)

The calculation to determine the overall system efficiency using the values specified above is shown below:

Calculation of Energy to Heat Coal from 25°C to 150°C:

$E_{H2O} := x_{H2O} \cdot m \cdot Cp_{H2O} \cdot (T_{boil} - T_{in})$ Energy required to heat coal moisture up to boiling point (100°C).

$E_{H2O} = 110.696\,kJ$

$E_{vap} := x_{H2O} \cdot m \cdot \Delta H_{H2O}$ Energy required to vaporize coal moisture at boiling point (100°C).

$E_{vap} = 789.95\,kJ$

$$E_{Steam} := x_{H2O} \cdot m \cdot \left(\frac{Cp_{Steam.373.15} + Cp_{Steam.420}}{2} \right) \cdot (T_{out} - T_{boil})$$

$E_{Steam} = 37.8\,kJ$ Energy required to superheat coal moisture from boiling point (100°C) to 150°C.

$E_C := x_C \cdot m \cdot Cp_{Coal} \cdot (T_{out} - T_{in})$ Energy required to heat coal carbon and volatiles from 25°C to 150°C.

$E_C = 56.227\,kJ$

$$E_{Ash} := x_{Ash} \cdot m \cdot \left(\frac{Cp_{Ash.300} + Cp_{Ash.400}}{2} \right) \cdot (T_{out} - T_{in})$$

$E_{Ash} = 29.849\,kJ$ Energy required to heat coal ash from 25°C to 150°C.

$E_{Coal.required} := E_{H2O} + E_{vap} + E_{Steam} + E_C + E_{Ash}$

$E_{Coal.required} = 1.025 \times 10^3\,kJ$ Total energy required to heat coal and vaporize moisture from 25°C to 150°C.

$$Eff := \frac{E_{Coal} \cdot m - E_{Coal.required}}{E_{Coal} \cdot m}$$ Overall efficiency of Thermal Drying Plant

$Eff = 93.078\,\%$

It is found that less than 7% of the pelletized coal product of the low grade Free State coal must be combusted in the boiler to supply the required heat to dry the wet coal feed. If the Soutpansberg coal is considered, which showed the highest calorific value and lowest ash content, it is found that only 3.5% of the total coal product must be combusted to supply the required heat to dry the wet coal feed.

Furthermore, this energy is ‘free’ as it is generated from the pelletized coal which will be discarded if a drying process is not used which differs from a mechanical drying process where the energy for drying is supplied from electricity.

The only electrical energy needed to run this plant would be the electrical requirement of the conveyors, pelletizer, blower and pump which will be minimal compared to the heating requirement.

Chapter 6 Conclusions

In this chapter conclusions about the results obtained will be made, as well as recommendations for future work.

6.1. Introduction

This chapter will summarise the findings of this study in the form of two paragraphs.

Firstly the experimental results from chapter 4 will be discussed and concluded in light of the objectives stated in paragraph 1.2.

Secondly, future research which must be conducted to determine the feasibility of a thermal drying plant and accurately model the dryer proposed in chapter 5 will be discussed.

6.2. Conclusions and discussion

The objectives stated in paragraph 1.2 will be discussed and concluded in this paragraph.

1. This first section will focus on discussing the experimental results from chapter 4.

    a) The TGA **mass loss** curve indicates that all maceral fractions from the five coal samples tested loose mass at a fairly constant rate up to 150°C where after the rate of mass loss decreases up to about 200°C. Between 200 and 350°C almost no mass loss can be observed where after primary devolatilisation initiates starting between 350 and 450°C.

    b) The SEM results indicated no **physical changes** in any of the coal macerals tested during the first stage of heating when water evaporates from the particles. The first real sign of change is observed between 350 and 450°C (or even slightly higher) when the more aggressive primary devolatilisation initiates. No movements were observed below temperatures of 260°C except for barely noticeable movement in the NV

particles at temperatures higher than 160°C which can be attributed to water evolution and slight thermal expansion.

c) The only **change in chemical composition** indicated up to the maximum proximate analysis test temperature of 250°C is that an almost unnoticeable amount of volatiles evaporate with the moisture from the coal particles. This small loss in volatiles increases linearly with an increase in drying temperature and should be considered when a maximum drying temperature is selected.

The **calorific value** results indicate that the slight loss in volatiles do not noticeably affect the calorific value of the coal. The coal does however lose the energy associated with the small quantity of volatiles which evolve when the coal is thermally dried.

d) The mercury intrusion results indicate that depending on the rank and reactivity of the coal, **structural and porosity changes** only start to occur at temperatures above 250°C.

The pores of the more plastic vitrinite and mixture fractions become bigger and swallowed some of the smaller pores to form a few very large pores while the harder and more ridged inertinite also shows an increase in pore diameter but neighbouring pores are not swallowed.

2. When the above summery is considered the following conclusions and recommendations can be made regarding a optimum drying temperature:

a) Mass loss is constant up to a temperature of 150°C and decrease up to 200°C where after limited loss is observed up to temperatures between 350 and 450°C when primary devolatilisation initiates. Limited loss in volatiles is observed up to a temperature of 250°C and although this small quantity should not dictate the optimum drying temperature, this should be limited and the drying temperature should therefore be kept as low as possible. When the evolution of water and volatiles is considered it is recommended that an optimum drying temperature of 150°C is selected; up to this temperature the rate of mass loss is fairly constant and only decrease from here. Limited loss in volatiles will also occur at this relatively low temperature.

b) The change in calorific value is insignificant but as stated above, the small loss in volatile mater will result in a small loss of energy, again stressing that the drying temperature should be kept relatively low. Considering this, 150°C can again be selected as the optimum drying temperature.

c) No structural changes or damage is observed below temperatures of 250°C, making the factors discussed above dominant in determining the optimum drying temperature.

An optimum drying temperature of 150°C is therefore recommended, not only because of the reasons stated above but also because a relatively high temperature driving force of 50°C will exist between the drying temperature and the boiling point of water which will result in relatively small dryers, keeping capital investment down. Heating to higher temperatures will also result in a waste of energy; limiting the drying temperature at 150°C would therefore limit operational costs.

3. A thermal drying plant operating under inert conditions is proposed in chapter 5. It was found that a relatively small quantity of between 3.5 and 7% of the product coal will have to be combusted to satisfy both the heating requirement of the plant and sustain the inert atmosphere required for drying. The proposed plant will produce a pelletized coal product, eliminating any further dust generation issues which might arise.

6.3. Recommendations for further research

Recommendations for research which must still be conducted to successfully implement the proposed thermal drying plant in industry are listed below.

1) Experimental data must be gathered from a lab scale thermal dryer built to the specifications proposed in chapter 5 in order to accurately model and size industrial scaled dryers.

2) An investigation must be launched to select an optimal pelletizer for the purpose of pelletizing the heated fine coal.

3) Methods to ensure that the heated fine coal is exposed to as little oxygen as possible from the inlet of the dryer through the pelletizing process up to the stage where the pelletized product is cooled in the storage hopper must be investigated to limit oxidation, spontaneous combustion and the probability of a dust explosion.

4) The studies indicated above must be combined in a financial feasibility study to determine if the proposed thermal drying plant will be feasible.

APPENDIX A: SEM sample photos

It was decided to show and discuss the SEM sample photos in this appendix as it does not depict supplementary information over and above the information obtained from the SEM experiments themselves. They do however correspond to, and show that, the changes that are seen during the SEM experiments are visible to the naked eye after the samples are removed from the SEM.

The photos will be shown in the same order in which the SEM experiments were discussed in paragraph 4.3. Each photo will show an unheated sample of the specified coal on the left hand side and the sample exposed to the maximum SEM temperature during the experiment (approximately 900°C) on the right hand side.

The SEM photos are in agreement with the SEM results discussed in paragraph 4.3. It is observed that very little change occur in the inertinite samples, some plastic deformation is observed in the mixture samples and extensive of plastic deformation is seen in the vitrinite samples.

Figure A.1.1: SEM WB2 inertinite experimental coal sample.

Figure A.1.2: SEM WB2 mixture experimental coal sample.

Figure A.1.3: SEM WB2 vitrinite experimental coal sample.

Figure A.2.1: SEM WB4 inertinite experimental coal sample.

Figure A.2.2: SEM WB4 mixture experimental coal sample.

Figure A.2.3: SEM WB4 vitrinite experimental coal sample.

Figure A.3.1: SEM TS inertinite experimental coal sample.

Figure A.3.2: SEM TS mixture experimental coal sample.

Figure A.3.3: SEM TS vitrinite experimental coal sample.

Figure A.4.1: SEM GG inertinite experimental coal sample.

Figure A.4.2: SEM GG mixture experimental coal sample.

Figure A.4.3: SEM GG vitrinite experimental coal sample.

Figure A.5.1: SEM NV inertinite experimental coal sample.

Figure A.5.2: SEM NV mixture experimental coal sample.

Figure A.5.3: SEM NV vitrinite experimental coal sample.

APPENDIX B: Moisture content graphs

It was decided to discuss the proximate analysis moisture content graphs in the appendixes as all moisture inside the coal particles was reabsorbed after thermal drying. These graphs are thus not relevant to the results pertaining to the physical changes that occur inside the coal particles during thermal drying. It was excluded from the proximate analysis graphs discussed in chapter 4 as it might result in false trends observed in the other properties discussed. It is however important information to consider when an industrial thermal drying method is developed as moisture re-absorption might affect the feasibility of a thermal drying process.

The moisture content graphs are displayed below in the same order in which they were discussed in chapter 4. A short discussion of all results will be done afterwards.

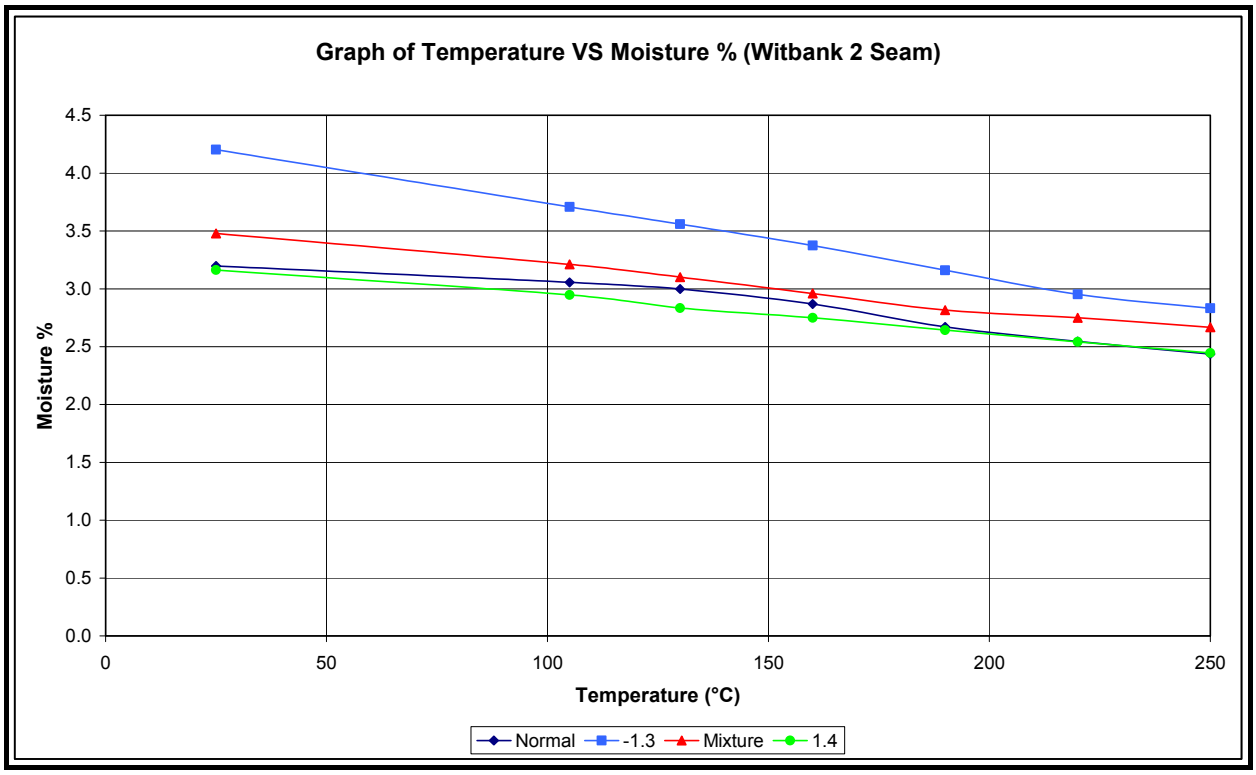

Graph B.1: Proximate analysis moisture content results for the WB2 coal.

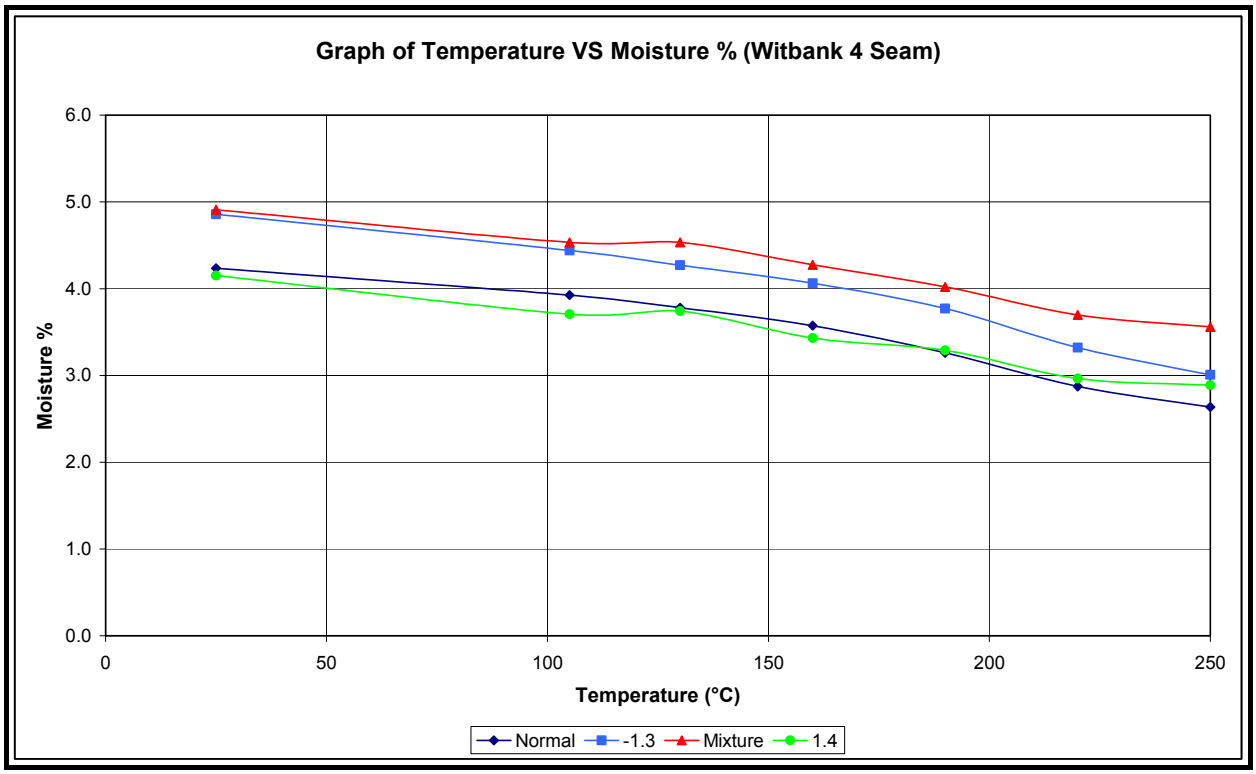

Graph B.2: Proximate analysis moisture content results for the WB4 coal.

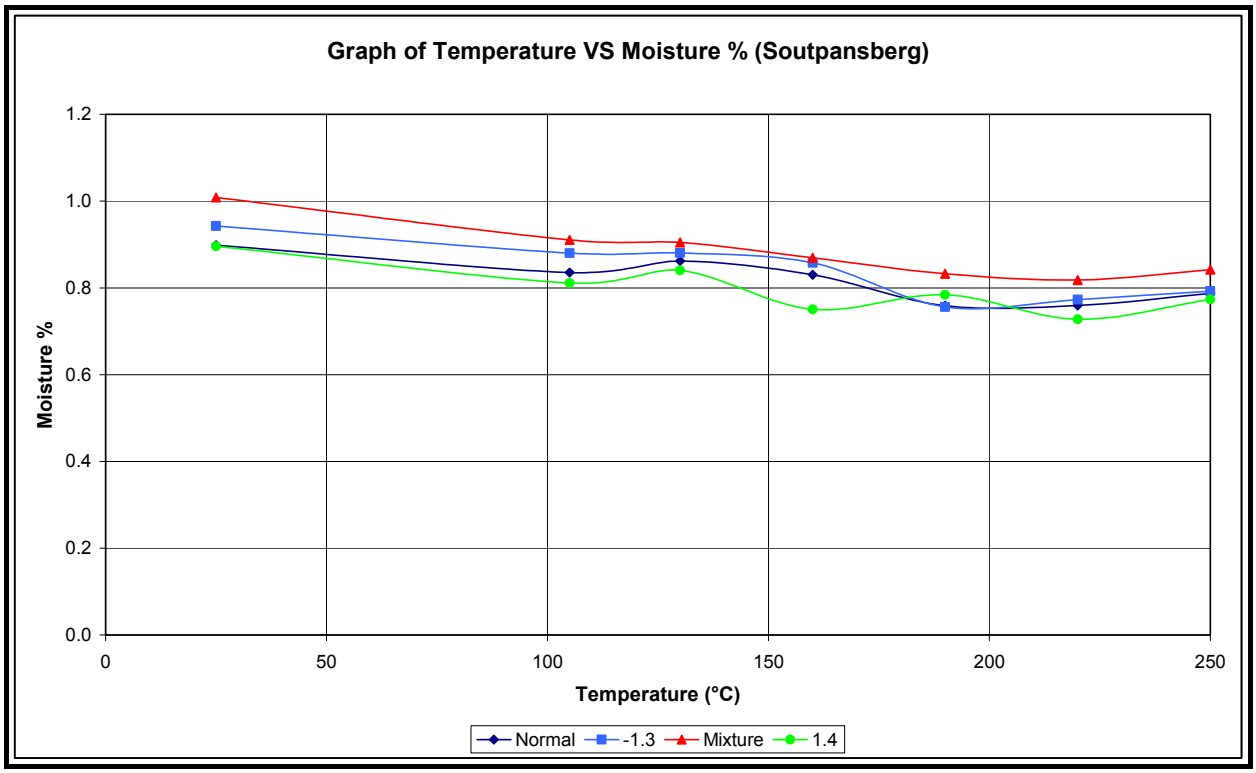

Graph B.3: Proximate analysis moisture content results for the TS coal.

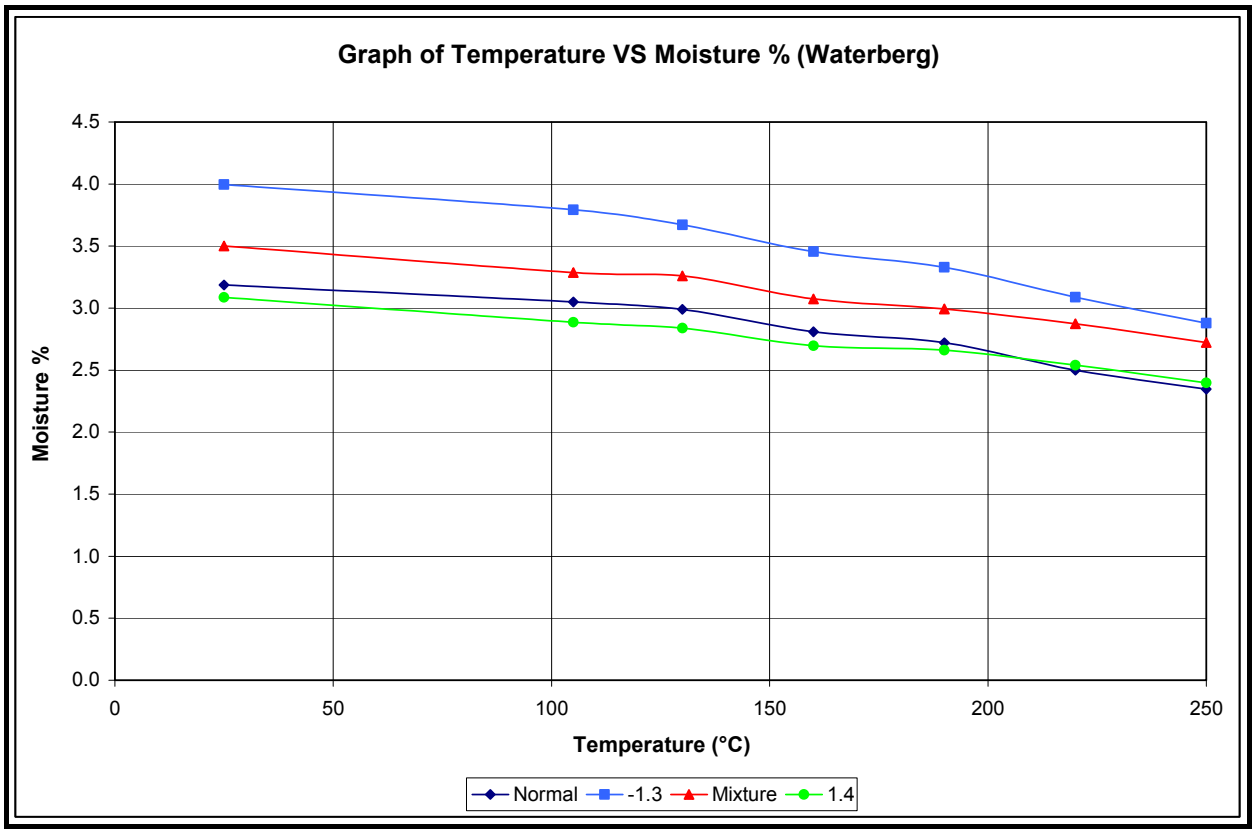

Graph B.4: Proximate analysis moisture content results for the GG coal.

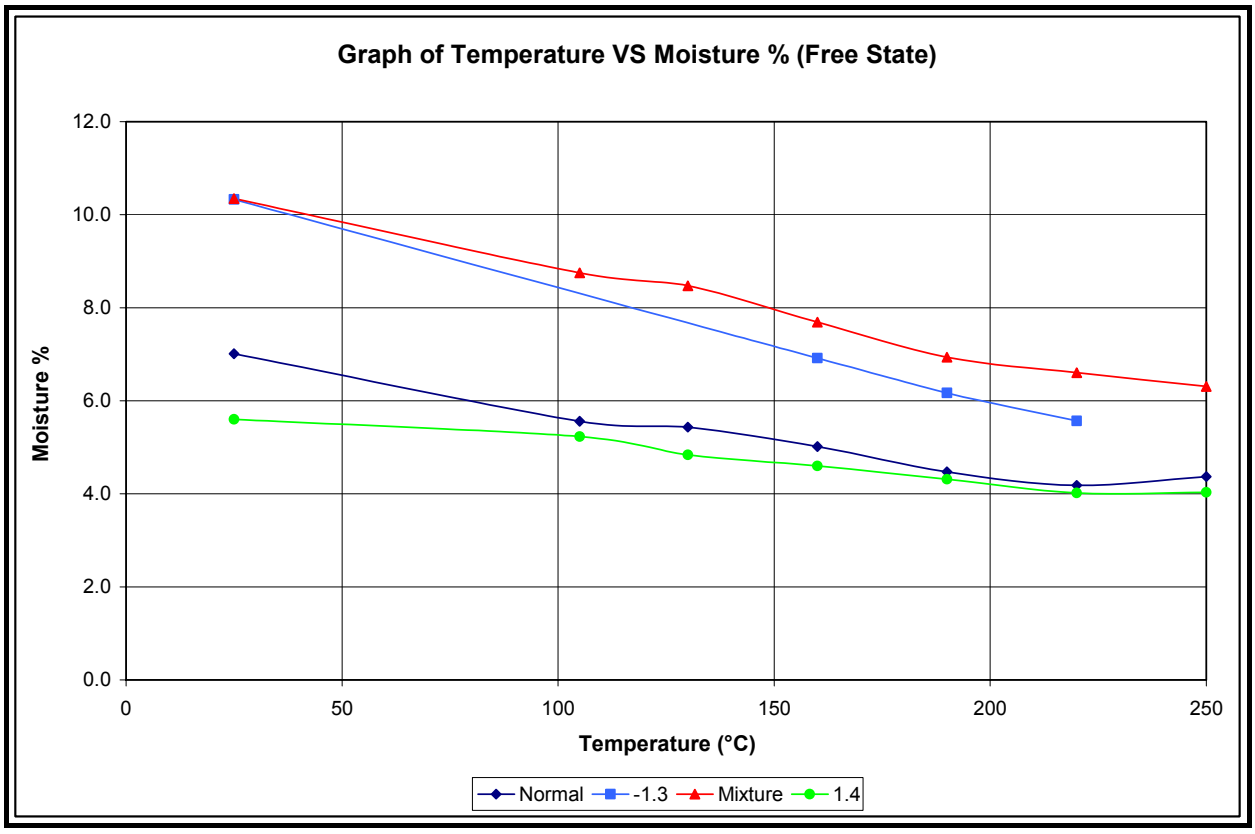

Graph B.5: Proximate analysis moisture content results for the NV coal.

All of the coal samples tested reveal a decrease in moisture content with an increase in drying temperature. This is in agreement with the findings of Van der Merwe & Campbell (2002:417-420). It can also be seen that the vitrinite and mixture samples have higher moisture contents than the inertinite samples indicating that the moisture in dried samples are not as much associated with the porosity of the samples but rather the total pore area of the samples – all porosity experiments revealed that the inertinite fraction has got a higher porosity than the vitrinite and mixture samples but a lower total pore area.

This might also explain why the virgin sample's moisture content cross to below the inertinite sample's moisture content for the WB2 and WB4 samples as the virgin sample was not exposed to the zinc chloride solution for density separation. The surface, which is the controlling factor for moisture re-absorption, was thus not exposed to the zinc and chlorine ions which would bind to the free radicals on the surface of the vitrinite, mixture and inertinite samples making them more hydrophilic.

APPENDIX C: Tabulated proximate analysis results

This appendix contains all the tabulated proximate analysis results displayed in paragraph 4.4 and appendix B. These results were calculated on a 'wet basis' from the raw data collected according to the specifications and formulas discussed in paragraph 3.2.4.2. The tabulated results will be displayed in the same order in which they were discussed in chapter 4.

The standard deviations on these values (as a measure of repeatability) are also shown. The moisture analysis was conducted two times, the volatile analysis four times, the ash analysis two times and the calorific value analysis three times for each sample except for the Free State vitrinite as too little sample was available to do repeatability on this fraction.

Witbank 2 Seam Proximate Analysis Results: Normal					
Temp (˚C)	Moisture (%)	Volatiles (%)	Fixed Carbon (%)	Ash (%)	CV (MJ/kg)
25	3.2 ± 0.1	21.9 ± 0.3	60.6 ± 0.6	14.3 ± 0.2	27.1 ± 0.1
105	3.1 ± 0.1	21.6 ± 0.2	60.9 ± 0.4	14.4 ± 0.0	27.1 ± 0.1
130	3.0 ± 0.0	21.6 ± 0.3	61.0 ± 0.5	14.4 ± 0.2	27.1 ± 0.1
160	2.9 ± 0.0	21.7 ± 0.2	61.2 ± 0.6	14.2 ± 0.4	27.0 ± 0.1
190	2.7 ± 0.1	21.3 ± 0.2	61.6 ± 0.3	14.4 ± 0.0	26.9 ± 0.1
220	2.5 ± 0.1	21.4 ± 0.2	61.7 ± 0.4	14.4 ± 0.1	27.1 ± 0.1
250	2.4 ± 0.1	20.7 ± 0.4	62.0 ± 0.5	14.8 ± 0.0	26.7 ± 0.2

Table C.1.1: Proximate analysis results for the WB2 virgin coal sample.

Witbank 2 Seam Proximate Analysis Results: -1.3 SG					
Temp (˚C)	Moisture (%)	Volatiles (%)	Fixed Carbon (%)	Ash (%)	CV (MJ/kg)
25	4.2 ± 0.1	32.8 ± 0.2	60.7 ± 0.4	2.3 ± 0.0	31.9 ± 0.0
105	3.7 ± 0.1	32.9 ± 0.3	61.1 ± 0.4	2.3 ± 0.0	31.8 ± 0.2
130	3.6 ± 0.0	32.7 ± 0.1	61.4 ± 0.1	2.3 ± 0.0	31.8 ± 0.0
160	3.4 ± 0.1	32.9 ± 0.3	61.4 ± 0.4	2.3 ± 0.1	31.7 ± 0.1
190	3.2 ± 0.0	32.6 ± 0.3	61.8 ± 0.3	2.3 ± 0.0	31.8 ± 0.0
220	3.0 ± 0.0	32.6 ± 0.2	62.1 ± 0.3	2.3 ± 0.0	31.8 ± 0.2
250	2.8 ± 0.1	32.2 ± 0.2	62.6 ± 0.4	2.3 ± 0.0	31.5 ± 0.1

Table C.1.2: Proximate analysis results for the WB2 vitrinite coal sample.

Witbank 2 Seam Proximate Analysis Results: Mixture					
Temp (˚C)	Moisture (%)	Volatiles (%)	Fixed Carbon (%)	Ash (%)	CV (MJ/kg)
25	3.5 ± 0.1	27.8 ± 0.2	63.0 ± 0.4	5.7 ± 0.0	30.6 ± 0.1
105	3.2 ± 0.1	27.9 ± 0.3	63.2 ± 0.3	5.8 ± 0.0	30.7 ± 0.0
130	3.1 ± 0.0	27.6 ± 0.1	63.6 ± 0.2	5.7 ± 0.1	30.6 ± 0.0
160	3.0 ± 0.0	27.7 ± 0.2	63.6 ± 0.3	5.7 ± 0.0	30.5 ± 0.1
190	2.8 ± 0.0	27.4 ± 0.3	64.1 ± 0.3	5.7 ± 0.0	30.4 ± 0.1
220	2.8 ± 0.0	27.1 ± 0.2	64.4 ± 0.3	5.7 ± 0.0	30.7 ± 0.2
250	2.7 ± 0.1	26.8 ± 0.1	64.7 ± 0.3	5.8 ± 0.1	30.2 ± 0.0

Table C.1.3: Proximate analysis results for the WB2 mixture coal sample.

Witbank 2 Seam Proximate Analysis Results: +1.4 SG					
Temp (˚C)	Moisture (%)	Volatiles (%)	Fixed Carbon (%)	Ash (%)	CV (MJ/kg)
25	3.2 ± 0.1	17.5 ± 0.3	59.0 ± 0.6	20.3 ± 0.2	25.0 ± 0.1
105	2.9 ± 0.0	17.7 ± 0.2	59.3 ± 0.2	20.1 ± 0.0	25.0 ± 0.1
130	2.8 ± 0.0	17.4 ± 0.3	60.2 ± 0.3	19.6 ± 0.0	25.1 ± 0.1
160	2.8 ± 0.0	17.3 ± 0.3	59.4 ± 0.4	20.6 ± 0.1	24.5 ± 0.1
190	2.6 ± 0.0	17.2 ± 0.2	60.5 ± 0.3	19.6 ± 0.0	24.9 ± 0.1
220	2.5 ± 0.1	17.0 ± 0.2	60.4 ± 0.5	20.1 ± 0.1	24.6 ± 0.0
250	2.4 ± 0.1	16.9 ± 0.2	60.9 ± 0.5	19.8 ± 0.2	24.5 ± 0.1

Table C.1.4: Proximate analysis results for the WB2 inertinite coal sample.

Witbank 4 Seam Proximate Analysis Results: Normal					
Temp (˚C)	Moisture (%)	Volatiles (%)	Fixed Carbon (%)	Ash (%)	CV (MJ/kg)
25	4.2 ± 0.0	22.9 ± 0.3	50.9 ± 0.5	21.9 ± 0.1	23.6 ± 0.1
105	3.9 ± 0.0	22.5 ± 0.3	50.1 ± 0.4	23.5 ± 0.1	22.9 ± 0.3
130	3.8 ± 0.0	22.0 ± 0.3	50.8 ± 0.5	23.4 ± 0.2	22.6 ± 0.0
160	3.6 ± 0.0	21.5 ± 2.0	51.9 ± 2.3	23.0 ± 0.2	22.7 ± 0.3
190	3.3 ± 0.0	22.0 ± 0.4	51.9 ± 0.9	22.9 ± 0.5	22.6 ± 0.2
220	2.9 ± 0.0	22.3 ± 0.2	52.6 ± 0.4	22.2 ± 0.2	23.3 ± 0.2
250	2.6 ± 0.0	22.2 ± 0.3	52.3 ± 0.4	22.8 ± 0.0	22.8 ± 0.3

Table C.2.1: Proximate analysis results for the WB4 virgin coal sample.

Witbank 4 Seam Proximate Analysis Results: -1.3 SG					
Temp (˚C)	Moisture (%)	Volatiles (%)	Fixed Carbon (%)	Ash (%)	CV (MJ/kg)
25	4.9 ± 0.0	36.4 ± 0.1	56.2 ± 0.2	2.6 ± 0.0	31.0 ± 0.2
105	4.4 ± 0.0	36.1 ± 0.4	56.9 ± 0.5	2.6 ± 0.1	30.7 ± 0.2
130	4.3 ± 0.1	36.3 ± 0.1	56.9 ± 0.2	2.6 ± 0.0	30.7 ± 0.1
160	4.1 ± 0.0	36.4 ± 0.2	57.0 ± 0.3	2.6 ± 0.1	30.6 ± 0.0
190	3.8 ± 0.1	36.2 ± 0.3	57.4 ± 0.4	2.6 ± 0.1	30.7 ± 0.0
220	3.3 ± 0.1	36.1 ± 0.2	58.0 ± 0.4	2.6 ± 0.1	31.0 ± 0.2
250	3.0 ± 0.1	36.1 ± 0.3	58.4 ± 0.4	2.6 ± 0.1	30.7 ± 0.0

Table C.2.2: Proximate analysis results for the WB4 vitrinite coal sample.

Witbank 4 Seam Proximate Analysis Results: Mixture					
Temp (˚C)	Moisture (%)	Volatiles (%)	Fixed Carbon (%)	Ash (%)	CV (MJ/kg)
25	4.9 ± 0.0	31.5 ± 0.2	58.1 ± 0.2	5.5 ± 0.0	29.7 ± 0.1
105	4.5 ± 0.0	31.4 ± 0.2	58.7 ± 0.3	5.5 ± 0.1	29.5 ± 0.1
130	4.5 ± 0.0	30.6 ± 0.3	59.4 ± 0.3	5.4 ± 0.0	29.5 ± 0.1
160	4.3 ± 0.1	31.3 ± 0.2	58.9 ± 0.3	5.5 ± 0.0	29.4 ± 0.1
190	4.0 ± 0.0	31.1 ± 0.2	59.4 ± 0.3	5.4 ± 0.0	29.4 ± 0.0
220	3.7 ± 0.0	30.5 ± 0.4	60.2 ± 0.6	5.5 ± 0.1	29.8 ± 0.1
250	3.6 ± 0.0	30.1 ± 0.1	60.9 ± 0.3	5.4 ± 0.1	29.2 ± 0.1

Table C.2.3: Proximate analysis results for the WB4 mixture coal sample.

Witbank 4 Seam Proximate Analysis Results: +1.4 SG												
Temp (˚C)	Moisture (%)			Volatiles (%)			Fixed Carbon (%)			Ash (%)			CV (MJ/kg)		
25	4.2	±	0.0	19.3	±	0.2	48.0	±	0.3	28.5	±	0.1	21.0	±	0.1
105	3.7	±	0.1	19.1	±	0.3	47.7	±	0.7	29.6	±	0.3	20.4	±	0.3
130	3.7	±	0.0	18.9	±	0.4	49.1	±	0.5	28.3	±	0.1	21.0	±	0.1
160	3.4	±	0.0	18.8	±	0.5	48.2	±	0.7	29.5	±	0.2	20.3	±	0.1
190	3.3	±	0.0	18.8	±	0.3	49.8	±	1.0	28.2	±	0.7	20.6	±	0.1
220	3.0	±	0.0	19.0	±	0.3	50.0	±	0.5	28.1	±	0.2	20.8	±	0.2
250	2.9	±	0.0	19.1	±	0.3	50.8	±	0.6	27.2	±	0.3	21.1	±	0.1

Table C.2.4: Proximate analysis results for the WB4 inertinite coal sample.

Soutpansberg Coal Proximate Analysis Results: Normal												
Temp (˚C)	Moisture (%)			Volatiles (%)			Fixed Carbon (%)			Ash (%)			CV (MJ/kg)		
25	0.9	±	0.1	17.8	±	0.1	65.8	±	0.2	15.4	±	0.0	30.2	±	0.1
105	0.8	±	0.0	17.7	±	0.2	66.1	±	0.4	15.4	±	0.2	30.0	±	0.1
130	0.9	±	0.1	17.7	±	0.3	66.2	±	0.5	15.2	±	0.1	29.8	±	0.1
160	0.8	±	0.0	17.3	±	0.2	66.4	±	0.3	15.4	±	0.1	29.9	±	0.1
190	0.8	±	0.0	17.5	±	0.3	66.4	±	0.6	15.3	±	0.2	29.9	±	0.1
220	0.8	±	0.0	17.5	±	0.3	66.1	±	0.4	15.7	±	0.1	30.0	±	0.2
250	0.8	±	0.1	17.6	±	0.3	66.4	±	0.5	15.3	±	0.1	29.6	±	0.0

Table C.3.1: Proximate analysis results for the TS virgin coal sample.

Soutpansberg Coal Proximate Analysis Results: -1.3 SG												
Temp (˚C)	Moisture (%)			Volatiles (%)			Fixed Carbon (%)			Ash (%)			CV (MJ/kg)		
25	0.9	±	0.0	18.5	±	0.2	70.5	±	0.5	10.0	±	0.3	32.4	±	0.1
105	0.9	±	0.0	18.5	±	0.1	70.5	±	0.4	10.2	±	0.2	32.1	±	0.3
130	0.9	±	0.0	18.4	±	0.1	70.7	±	0.2	10.0	±	0.0	32.0	±	0.2
160	0.9	±	0.0	18.6	±	0.3	70.8	±	0.3	9.7	±	0.0	32.2	±	0.0
190	0.8	±	0.0	18.4	±	0.3	70.9	±	0.3	10.0	±	0.0	32.0	±	0.0
220	0.8	±	0.0	18.4	±	0.2	70.9	±	0.4	9.9	±	0.1	32.3	±	0.1
250	0.8	±	0.0	18.4	±	0.3	71.0	±	0.4	9.9	±	0.0	32.0	±	0.1

Table C.3.2: Proximate analysis results for the TS vitrinite coal sample.

Soutpansberg Coal Proximate Analysis Results: Mixture												
Temp (˚C)	Moisture (%)			Volatiles (%)			Fixed Carbon (%)			Ash (%)			CV (MJ/kg)		
25	1.0	±	0.1	18.7	±	0.2	70.7	±	0.3	9.6	±	0.0	32.5	±	0.0
105	0.9	±	0.0	18.7	±	0.2	70.7	±	0.3	9.7	±	0.1	32.3	±	0.1
130	0.9	±	0.1	18.7	±	0.1	70.8	±	0.3	9.7	±	0.1	32.1	±	0.1
160	0.9	±	0.0	18.6	±	0.2	71.0	±	0.2	9.6	±	0.0	32.2	±	0.1
190	0.8	±	0.0	18.5	±	0.2	71.0	±	0.3	9.6	±	0.1	32.2	±	0.0
220	0.8	±	0.0	18.4	±	0.3	71.0	±	0.5	9.7	±	0.1	32.4	±	0.1
250	0.8	±	0.0	18.5	±	0.1	71.0	±	0.2	9.7	±	0.0	32.1	±	0.1

Table C.3.3: Proximate analysis results for the TS mixture coal sample.

Soutpansberg Coal Proximate Analysis Results: +1.4 SG												
Temp (˚C)	Moisture (%)			Volatiles (%)			Fixed Carbon (%)			Ash (%)			CV (MJ/kg)		
25	0.9	±	0.0	16.5	±	0.1	58.6	±	0.1	23.9	±	0.1	26.6	±	0.1
105	0.8	±	0.0	16.6	±	0.1	58.1	±	0.3	24.5	±	0.1	26.2	±	0.2
130	0.8	±	0.0	16.7	±	0.3	57.9	±	0.5	24.6	±	0.1	26.1	±	0.1
160	0.8	±	0.0	16.2	±	0.3	58.9	±	0.4	24.2	±	0.1	26.3	±	0.1
190	0.8	±	0.0	16.2	±	0.3	59.1	±	0.6	24.0	±	0.2	26.5	±	0.1
220	0.7	±	0.0	16.3	±	0.3	59.2	±	0.3	23.8	±	0.0	26.7	±	0.1
250	0.8	±	0.1	16.3	±	0.2	59.3	±	0.3	23.6	±	0.0	26.5	±	0.1

Table C.3.4: Proximate analysis results for the TS inertinite coal sample.

Waterberg Coal Proximate Analysis Results: Normal												
Temp (˚C)	Moisture (%)			Volatiles (%)			Fixed Carbon (%)			Ash (%)			CV (MJ/kg)		
25	3.2	±	0.0	21.9	±	0.2	61.7	±	0.3	13.2	±	0.0	27.8	±	0.1
105	3.0	±	0.1	21.8	±	0.2	62.3	±	0.4	12.8	±	0.0	27.6	±	0.1
130	3.0	±	0.1	21.3	±	0.3	62.5	±	0.4	13.2	±	0.0	27.1	±	0.1
160	2.8	±	0.0	21.5	±	0.4	62.7	±	0.4	12.9	±	0.0	27.4	±	0.0
190	2.7	±	0.0	21.1	±	0.3	62.9	±	0.4	13.3	±	0.1	27.2	±	0.0
220	2.5	±	0.0	21.2	±	0.3	63.2	±	0.5	13.1	±	0.2	27.7	±	0.0
250	2.3	±	0.1	21.2	±	0.3	63.2	±	0.4	13.3	±	0.1	27.4	±	0.1

Table C.4.1: Proximate analysis results for the GG virgin coal sample.

Waterberg Coal Proximate Analysis Results: -1.3 SG												
Temp (˚C)	Moisture (%)			Volatiles (%)			Fixed Carbon (%)			Ash (%)			CV (MJ/kg)		
25	4.0	±	0.1	31.8	±	0.2	62.4	±	0.3	1.9	±	0.0	32.1	±	0.1
105	3.8	±	0.1	31.7	±	0.2	62.6	±	0.3	1.9	±	0.0	31.8	±	0.1
130	3.7	±	0.0	31.4	±	0.2	63.0	±	0.3	1.9	±	0.1	31.6	±	0.1
160	3.5	±	0.0	31.7	±	0.3	63.0	±	0.3	1.9	±	0.0	31.6	±	0.1
190	3.3	±	0.0	31.5	±	0.3	63.3	±	0.3	1.8	±	0.0	31.6	±	0.1
220	3.1	±	0.0	31.5	±	0.4	63.5	±	0.5	1.9	±	0.1	32.0	±	0.1
250	2.9	±	0.1	31.2	±	0.2	64.0	±	0.3	1.9	±	0.0	31.7	±	0.1

Table C.4.2: Proximate analysis results for the GG vitrinite coal sample.

Waterberg Coal Proximate Analysis Results: Mixture												
Temp (˚C)	Moisture (%)			Volatiles (%)			Fixed Carbon (%)			Ash (%)			CV (MJ/kg)		
25	3.5	±	0.1	26.2	±	0.3	65.2	±	0.4	5.1	±	0.0	31.0	±	0.1
105	3.3	±	0.1	26.0	±	0.3	65.6	±	0.4	5.1	±	0.0	30.7	±	0.1
130	3.3	±	0.0	25.7	±	0.2	66.0	±	0.3	5.0	±	0.1	30.5	±	0.1
160	3.1	±	0.0	25.8	±	0.3	66.0	±	0.4	5.1	±	0.1	30.6	±	0.1
190	3.0	±	0.0	25.6	±	0.3	66.4	±	0.3	5.0	±	0.0	30.5	±	0.0
220	2.9	±	0.0	25.5	±	0.4	66.5	±	0.5	5.1	±	0.1	30.7	±	0.0
250	2.7	±	0.1	25.4	±	0.0	66.8	±	0.2	5.0	±	0.1	30.4	±	0.2

Table C.4.3: Proximate analysis results for the GG mixture coal sample.

Waterberg Coal Proximate Analysis Results: +1.4 SG												
Temp (˚C)	Moisture (%)			Volatiles (%)			Fixed Carbon (%)			Ash (%)			CV (MJ/kg)		
25	3.1	±	0.0	19.1	±	0.2	60.9	±	0.3	17.0	±	0.0	26.2	±	0.2
105	2.9	±	0.1	19.1	±	0.1	60.9	±	0.4	17.1	±	0.2	25.9	±	0.1
130	2.8	±	0.1	18.7	±	0.3	61.4	±	0.5	17.1	±	0.1	25.7	±	0.1
160	2.7	±	0.1	18.7	±	0.3	61.5	±	0.5	17.1	±	0.1	25.7	±	0.1
190	2.7	±	0.0	18.6	±	0.2	61.7	±	0.2	17.0	±	0.0	25.8	±	0.1
220	2.5	±	0.0	18.4	±	0.2	61.8	±	0.5	17.2	±	0.3	25.9	±	0.1
250	2.4	±	0.0	18.5	±	0.2	62.0	±	0.4	17.0	±	0.1	25.6	±	0.1

Table C.4.4: Proximate analysis results for the GG inertinite coal sample.

Free State Coal Proximate Analysis Results: Normal												
Temp (˚C)	Moisture (%)			Volatiles (%)			Fixed Carbon (%)			Ash (%)			CV (MJ/kg)		
25	7.0	±	0.1	18.1	±	0.2	33.0	±	0.4	41.9	±	0.1	14.8	±	0.1
105	5.6	±	0.0	18.2	±	0.2	34.3	±	0.7	42.0	±	0.4	14.4	±	0.3
130	5.4	±	0.2	18.3	±	0.4	36.2	±	1.1	40.1	±	0.4	15.0	±	0.1
160	5.0	±	0.1	18.4	±	0.2	35.9	±	0.8	40.7	±	0.5	15.1	±	0.1
190	4.5	±	0.1	18.4	±	0.2	34.9	±	0.5	42.2	±	0.2	14.9	±	0.1
220	4.2	±	0.1	18.9	±	0.3	34.5	±	0.9	42.4	±	0.5	14.8	±	0.2
250	4.4	±	0.1	18.9	±	0.4	36.7	±	1.3	40.0	±	0.8	15.1	±	0.2

Table C.5.1: Proximate analysis results for the NV virgin coal sample.

New Vaal Seam Proximate Analysis Results: -1.3 SG					
Temp (˚C)	Moisture (%)	Volatiles (%)	Fixed Carbon (%)	Ash (%)	CV (MJ/kg)
25	10.3	33.3	53.9	2.5	27.9
160	6.9	34.0	56.4	2.6	27.7
190	6.2	34.0	57.4	2.4	27.9
220	5.6	33.2	58.5	2.7	28.2

Table C.5.2: Proximate analysis results for the NV vitrinite coal sample.

Free State Coal Proximate Analysis Results: Mixture												
Temp (˚C)	Moisture (%)			Volatiles (%)			Fixed Carbon (%)			Ash (%)			CV (MJ/kg)		
25	10.3	±	0.1	28.4	±	0.2	55.9	±	0.4	5.4	±	0.0	26.5	±	0.1
105	8.7	±	0.1	28.5	±	0.5	57.3	±	0.6	5.4	±	0.0	26.4	±	0.2
130	8.5	±	0.2	28.0	±	0.5	58.1	±	0.7	5.4	±	0.0	26.3	±	0.1
160	7.7	±	0.0	28.8	±	0.5	58.2	±	0.5	5.4	±	0.0	26.3	±	0.1
190	6.9	±	0.2	28.9	±	0.2	58.8	±	0.5	5.3	±	0.1	26.4	±	0.1
220	6.6	±	0.1	28.7	±	0.3	59.2	±	0.4	5.5	±	0.0	26.8	±	0.0
250	6.3	±	0.1	28.5	±	0.2	59.8	±	0.3	5.4	±	0.0	26.4	±	0.0

Table C.5.3: Proximate analysis results for the NV mixture coal sample.

Free State Coal Proximate Analysis Results: +1.4 SG					
Temp (˚C)	Moisture (%)	Volatiles (%)	Fixed Carbon (%)	Ash (%)	CV (MJ/kg)
25	5.6 ± 0.0	16.8 ± 0.2	31.8 ± 0.4	45.8 ± 0.2	13.4 ± 0.2
105	5.2 ± 0.1	16.7 ± 0.3	32.4 ± 0.4	45.6 ± 0.1	12.5 ± 0.1
130	4.8 ± 0.1	16.7 ± 0.4	31.6 ± 0.6	46.9 ± 0.1	12.2 ± 0.1
160	4.6 ± 0.0	16.8 ± 0.3	32.4 ± 0.8	46.2 ± 0.4	12.8 ± 0.1
190	4.3 ± 0.1	16.8 ± 0.2	32.3 ± 0.4	46.6 ± 0.2	12.6 ± 0.1
220	4.0 ± 0.2	17.4 ± 0.2	31.9 ± 0.8	46.7 ± 0.4	12.8 ± 0.1
250	4.0 ± 0.1	17.1 ± 0.3	31.5 ± 0.5	47.4 ± 0.1	12.2 ± 0.2

Table C.5.4: Proximate analysis results for the NV inertinite coal sample.

APPENDIX D: Tabulated mercury intrusion results

This appendix contains all the tabulated mercury intrusion results displayed in paragraph 4.5. These results were calculated by the Autopore IV 9500 software after the experiments were done according to paragraph 3.2.5. The tabulated results will be displayed in the same order in which they were discussed in chapter 4.

Repeatability was done by repeating the experiment five times on the Free State Inertinite Sample before heating it; these results are shown in Table D.4.

Witbank 2 Seam Mercury Intrusion Results: -1.3 SG						
Temp (˚C)	Mass (g)	Stem Volume used (%)	Porosity (%)	Median Pore Diameter (nm)	Average Pore Diameter (nm)	Total Pore Area (m²/g)
25	1.015	40	17.336	8.9	60.4	10.784
105	1.091	42	16.437	8.8	59.5	10.679
190	1.101	48	18.467	9.0	67.1	10.646
250	1.240	51	17.855	8.9	67.2	9.982
300	1.110	56	21.117	8.7	73.1	11.356
350	0.816	62	28.671	13.6	65.4	19.111
400	0.806	89	34.152	26.2	334.5	5.458

Table D.1.1: Mercury intrusion results for the WB2 vitrinite coal sample.

Witbank 2 Seam Mercury Intrusion Results: Mixture						
Temp (˚C)	Mass (g)	Stem Volume used (%)	Porosity (%)	Median Pore Diameter (nm)	Average Pore Diameter (nm)	Total Pore Area (m²/g)
25	1.014	46	20.083	8.9	67.1	11.131
105	1.280	54	19.081	9.2	66.7	10.399
190	1.144	52	20.004	9.3	67.5	11.142
250	1.105	53	20.790	9.4	71.8	10.903
300	1.152	52	20.362	9.3	69.6	10.856
350	1.116	53	21.154	9.7	68.0	11.422
400	0.912	88	31.436	14.1	535.1	2.975

Table D.1.2: Mercury intrusion results for the WB2 mixture coal sample.

Witbank 2 Seam Mercury Intrusion Results: +1.4 SG						
Temp (˚C)	Mass (g)	Stem Volume used (%)	Porosity (%)	Median Pore Diameter (nm)	Average Pore Diameter (nm)	Total Pore Area (m²/g)
25	1.281	44	17.669	9.1	67.3	8.423
105	1.166	44	18.822	9.3	75.0	8.238
190	1.330	47	18.167	9.1	71.6	8.128
250	1.400	53	19.368	9.1	82.7	7.566
300	1.264	46	18.011	9.1	70.4	8.429
350	1.162	41	18.342	9.1	72.8	8.088
400	1.980	57	23.018	9.5	77.2	10.248

Table D.1.3: Mercury intrusion results for the WB2 inertinite coal sample.

Witbank 4 Seam Mercury Intrusion Results: -1.3 SG						
Temp (˚C)	Mass (g)	Stem Volume used (%)	Porosity (%)	Median Pore Diameter (nm)	Average Pore Diameter (nm)	Total Pore Area (m²/g)
25	0.994	44	18.694	9.0	70.5	10.287
105	1.041	45	18.680	9.0	73.2	9.799
190	1.015	45	18.882	9.0	73.1	9.938
250	1.103	51	19.834	9.0	80.7	9.385
300	0.991	52	21.929	9.1	84.3	10.214
350	1.113	52	19.808	9.2	79.2	9.727
400	0.674	90	30.952	12.3	480.7	4.601

Table D.2.1: Mercury intrusion results for the WB4 vitrinite coal sample.

Witbank 4 Seam Mercury Intrusion Results: Mixture						
Temp (˚C)	Mass (g)	Stem Volume used (%)	Porosity (%)	Median Pore Diameter (nm)	Average Pore Diameter (nm)	Total Pore Area (m²/g)
25	1.155	49	18.344	9.1	70.1	9.925
105	1.073	47	18.748	9.0	68.5	10.461
190	1.023	43	18.312	9.1	65.7	10.605
250	1.174	49	18.404	9.0	73.9	9.303
300	1.119	45	17.956	9.2	70.2	9.516
350	1.108	47	18.449	9.1	72.3	9.641
400	0.847	88	29.063	13.2	475.3	3.586

Table D.2.2: Mercury intrusion results for the WB4 mixture coal sample.

Witbank 4 Seam Mercury Intrusion Results: +1.4 SG						
Temp (˚C)	Mass (g)	Stem Volume used (%)	Porosity (%)	Median Pore Diameter (nm)	Average Pore Diameter (nm)	Total Pore Area (m²/g)
25	1.424	54	20.266	9.0	86.5	7.189
105	1.595	55	19.206	9.2	87.5	6.540
190	1.276	48	19.732	9.2	83.8	7.323
250	1.285	45	18.717	8.9	80.5	7.224
300	1.420	51	19.485	9.3	85.5	6.914
350	1.420	56	20.746	9.3	93.9	6.942
400	1.330	67	25.049	10.2	80.7	10.239

Table D.2.3: Mercury intrusion results for the WB4 inertinite coal sample.

Free State Coal Mercury Intrusion Results: -1.3 SG						
Temp (˚C)	Mass (g)	Stem Volume used (%)	Porosity (%)	Median Pore Diameter (nm)	Average Pore Diameter (nm)	Total Pore Area (m²/g)
25	0.955	39	18.542	8.6	38.8	17.441
105	1.142	53	20.178	8.6	52.2	14.783
190	1.088	50	19.971	8.2	59.2	12.809
250	1.058	43	18.681	8.9	62.1	10.734
300	0.952	44	19.988	9.0	73.9	10.244
350	0.960	42	18.934	9.0	73.8	9.721
400	0.982	92	33.255	10.6	646.3	2.521

Table D.3.1: Mercury intrusion results for the NV vitrinite coal sample.

Free State Coal Mercury Intrusion Results: Mixture						
Temp (˚C)	Mass (g)	Stem Volume used (%)	Porosity (%)	Median Pore Diameter (nm)	Average Pore Diameter (nm)	Total Pore Area (m²/g)
25	1.112	51	20.847	8.6	46.4	16.266
105	1.137	49	19.593	8.5	56.1	12.666
190	1.149	48	18.752	8.8	59.5	11.512
250	1.162	53	20.254	8.9	68.6	10.962
300	1.111	46	20.135	8.9	69.2	11.364
350	0.915	43	20.950	9.0	71.3	10.772
400	1.157	67	24.641	9.9	80.1	11.992

Table D.3.2: Mercury intrusion results for the NV mixture coal sample.

Free State Coal Mercury Intrusion Results: +1.4 SG						
Temp (˚C)	Mass (g)	Stem Volume used (%)	Porosity (%)	Median Pore Diameter (nm)	Average Pore Diameter (nm)	Total Pore Area (m²/g)
25	1.464	54	22.226	8.9	66.1	9.192
105	1.494	56	22.350	9.2	69.7	8.816
190	1.430	55	22.774	9.1	69.1	9.150
250	1.280	46	20.755	9.5	66.9	8.848
300	1.494	56	22.864	9.3	71.9	8.560
350	1.433	55	22.473	8.3	66.0	9.649
400	1.148	59	22.010	9.4	81.6	10.325

Table D.3.3: Mercury intrusion results for the NV inertinite coal sample.

Free State Coal Mercury Intrusion Standard Deviation: +1.4 SG						
Run	Mass (g)	Stem Volume used (%)	Porosity (%)	Median Pore Diameter (nm)	Average Pore Diameter (nm)	Total Pore Area (m²/g)
1	1.477	55	22.430	9.0	65.6	9.317
2	1.494	53	21.570	9.0	62.5	9.375
3	1.484	59	23.700	9.0	69.2	9.401
4	1.433	52	21.710	8.9	65.3	9.127
5	1.433	52	21.720	8.7	68.1	8.741
Average	1.464	54.200	22.226	8.920	66.140	9.192
σ	0.027	3.096	0.974	0.050	2.748	0.124
% Deviation	1.8%	5.7%	4.4%	0.6%	4.2%	1.3%

Table D.4: Mercury intrusion standard deviation results for the NV inertinite coal sample.

BIBLIOGRAPHY

AGARWAL, P.K., GENETTI, W.E. & LEE, Y.Y. 1986. Coupled drying and devolatilisation of wet coal in fluidized beds. *Chemical Engineering Science,* 41(9):2373-2383.

AGARWAL, P.K., & PEDLER, I. 1986. Drying, devolatilisation and volatile combustion for single coal particles: a pseudo steady state approach. *Fuel,* 65(5):640-643, May.

ALLARDICE, D.J. & EVANS, D.G. 1971a. The brown-coal/water system: Part 1, The effect of temperature on the evolution of water from brown coal. *Fuel,* 50(2):201-210, April.

ALLARDICE, D.G. & EVANS, D.G. 1971b. The brown coal/water system: Part 2. Water sorption isotherms on bed-moist Yallourn brown coal. *Fuel,* 50(3):236-253, July.

ARENILLAS, A., PEVIDA, C., RUBIERA, F., PALACIOS, J.M., NAVARRETE, R., DENOYEL, R., ROUQUEROL, J. & PIS, J.J. 2004. Surface characterization of synthetic coal chars made from model compounds. *Carbon,* 42(7):1345-1350.

ASIF, M. & MUNEER, T. 2007. Energy supply, its demand and security issues for developed and emerging economies. *Renewable & Sustainable Energy Reviews,* 11:1388-1413.

BALEK, V., MATUSCHEK, G., KETTRUP, A. & SYKOROVÁ, I. 1995. Chemical, petrographic and thermoanalytical characterization of two Northbohemian low rank coals. *Thermochimica Acta,* 263:141-157, Oct. 1.

BARIA, D.N. & HASAN, A.R. 1986. Steam/hot water drying of low rank coals. *Energy Progress,* 6(1):53-60, March.

BAXTER, L.L. 1992. Char fragmentation and fly ash formation during pulverized-coal combustion. *Combustion and Flame,* 90(2):174-184, Aug.

BENFELL, K.E., BEAMISH, B.B., & RODGERS, K.A. 1996. Thermogravimetric analytical procedures for characterizing New Zealand and Eastern Australian coals. *Thermochimica Acta,* 286:67-74, Feb. 27.

BJÖRKMAN, A. 2001. Projects on coal characterization. *Fuel,* 80(2):155-166, Jan.

BOIKO, E.A. 2000. Research on the thermal processing of brown coals of various oxidative ageing degree using the non-isothermal methods. *Thermochimica Acta,* 348(1-2):97-104, April 28.

BONGERS, G.D., JACKSON, W.R. & WOSKOBOENKO, F. 1998. Pressurised steam drying of Australian low-rank coals Part 1. Equilibrium moisture contents. *Fuel Processing Technology,* 57(1):41-54, Aug.

BRONSHTEIN, A.P., MAKAROV, G.N., AKOLOV, R.V. & GRIGOR'EV, N.P. 1979. Fuel: Evolution characteristics of gasses during pyrolysis of maceral concentrates of Russian coking coals. *Solid Fuel Chemistry,* 6:55.

BUTUZOVA, L. & KUCHER, R. 1979. Study of vitrinite and fusinite micro-components of Donetsk coal by derivatographic methods. *Chemistry of Solid Fuel,* 2:46

CARD, J.B.A. & JONES, A.R. 1995. A drop tube furnace study of coal combustion and unburned carbon content using optical techniques. *Combustion and Flame,* 101(4):539-547, June.

CARRAS, J.N. & YOUNG, B.C. 1994. Self-heating of coal and related materials: model, application and test methods. *Progress in Energy and Combustion Science,* 20(1):1-15.

CARR, R.M., KUMAGAI, H., PEAKE, B.M., ROBINSON, B.H., CLEMENS, A.H. & MATHESON, T.W. 1995. Formation of free radicals during drying and oxidation of a lignite and a bituminous coal. *Fuel,* 74(3):389-394, March.

CHEN, Z., AGARWAL, P.K. & AGNEW, J.B. 2001. Steam-drying of coal. Part 2. Modeling the operation of a fluidized bed drying unit. *Fuel,* 80(2):209-223, Jan.

CHEN, Z., WU, W. & AGARWAL, P.K. 2000. Steam-drying of coal. Part 1. Modeling the behavior of a single particle. *Fuel,* 79(8):961-973, June.

CHERN, J. & HAYHURST, A.N. 2004. Does a large coal particle in a hot fluidized bed lose its volatile content according to the shrinking core mode? *Combustion and Flame,* 139:208-221, Sep. 21.

CHERN, J. & HAYHURST, A.N. 2006. A model for the devolatilization of a coal particle sufficiently large to be controlled by heat transfer. *Combustion and Flame,* 146:553-571, Jun. 19.

CHU, J.C., LANE, A.M. & CONKILN, D. 1953. Evaporation of liquids into their superheated vapours. *Industrial and Engineering Chemistry,* 45(7):1586-1591, July.

COUNCIL OF INDUSTRIAL BOILER OWNERS. 2003. Energy efficiency & industrial boiler efficiency: An industry perspective. Mar 2003. http://cibo.org/pubs/whitepaper1.pdf Date of access: 6 Jul 2009.

DACOMBE, P., POURKASHANIAN, M., WILLIAMS, A. & YAP, L. 1999. Combustion-induced fragmentation behaviour of isolated coal particles. *Fuel,* 78(15):1847-1857, Dec.

DAS, T.K. 2001. Evolution characteristics of gasses during pyrolysis of maceral concentrates of Russian coking coals. *Fuel,* 80(4):489-500, March.

DE BRUIN, C.P. 2005. Thermal drying of South African coal III – Porosity analysis and TGA. Potchefstroom: North-West University. (Project – B.Eng) 42-43 p.

DROHAN, P.J.A. 1978. Shrinkage of Victorian brown coal upon thermal dewatering. Melbourne: University of Melbourne. (Thesis – M.Sc.) 57 p.

DRYTECH ENGINEERING. http://www.drytecheng.com/Drytech.htm. Date of access: 25 Jun. 2009

FALCON, R.M.S. & SNYMAN, C.P. 1986. An introduction to coal petrography: Atlas of petrographic constituents in the bituminous coals of South Africa. 1st ed. Johannesburg: The Geological Society of South Africa, 25 p.

FAVAS, G. & JACKSON, W.R. 2003a. Hydrothermal dewatering of lower rank coals. 1. Effects of process conditions on the properties of dried product. *Fuel,* 82(1):53-57, Jan.

FAVAS, G. & JACKSON, W.R. 2003b. Hydrothermal dewatering of lower rank coals. 2. Effects of coal characteristics for a range of Australian and international coals. *Fuel,* 82(1):59-69, Jan.

FAVAS, G., JACKSON, W.R. & Marshall, M. 2003. Hydrothermal dewatering of lower rank coals. 3. High-concentration slurries from hydrothermally treated lower rank coals. *Fuel,* 82(1):71-79, Jan.

GALE, T.K., BARTHOLOMEW, C.H. & FLETCHER, T.H. 1995. Decreases in the swelling and porosity of bituminous coals during devolatilisation at high heating rates. *Combustion and Flame,* 100(1-2):94-100, Jan.

GAVALAS, G.R. 1981. Analysis of char combustion including the effect of pore enlargement. *Combustion Science Technology,* 24:197-210.

GLASS, H.D. 1955. Differential thermal analysis of coking coals. *Fuel,* 34(3):253-268, July.

HALL, P.J. & LARSEN, J.W. 1991. Evidence of low-temperature second-order phase transitions in coal/solvent systems using differential scanning calorimetry. *Energy & Fuels,* 5(1):228-229, Jan.

HEIDENREICH, C.A. & ZHANG, D.K. 1999. Measuring the temperature response of large wet coal particles during heating. *Fuel,* 78(8):991-994, June.

HELBLE, J.J. & SAROFIM, A.F. 1989. Influence of char fragmentation on ash particle distributions. *Combustion and Flame,* 76(2):183-196, May.

INCROPERA, F.P. & DE WIT, D.P. 1996. Fundamentals of heat and mass transfer. 4th ed. New York: Willey*,* 886 p.

INTERNATIONAL ENERGY AGENCY. 2008. Key world energy statistics. IEA BOOKS, 6 & 24 p.

IORDANIDIS, A., GEORGAKOPOULOS, K., MARKOVA, K., FILIPPIDIS, A. & KASSOLI-FOURNARAKI, A. 2001. Application of TG-DTA to the study of Amynteon lignites, northern Greece. *Thermochimica Acta,* 371(1-2):137-141, April 26.

IWAI, Y., KOUJINA, Y., ARAI, Y., WATANABE, I., MOCHIDA, I. & SAKANISHI, K. 2002. Low temperature drying of low rank coal by supercritical carbon dioxide with methanol as entrainer. *The Journal of Supercritical Fluids,* 23(3):251-255, Aug.

JARVINEN, M.P., ZEVENHOVEN, R. & VAKKILAINEN, E.K. 2002. Auto-gasification of a biofuel. *Combustion and Flame,* 131(4):357-370, Dec.

JIMÉNEZ, A., IGLESIAS, M.J., LAGGOUN-DÉFARGE, F. & SUÁREZ-RUIZ, I. 1988. Study of physical and chemical properties of vitrinites. Inferences on depositional and coalification controls. *Chemical Geology,* 150(3-4):197-221, Sep.

JUNG, K. & STANMORE, B.R. 1980. Fluidized bed combustion of wet brown coal. *Fuel,* 59(2):74-80, Feb.

KARCZ, A. & PORADA, S. 1995. Formation of C_1-C_3 hydrocarbons during pressure pyrolysis and hydrogasification in relation to structural changes in coal. *Fuel,* 74(6):806-809, June.

KASATOCHKIN, V.I. & LARINA, N.K. 1975. Coal structure and properties. Moscow: Nedra, 159 p.

LI, X., MATUSCHEK, M., HERRERA, H., WANG, A. & KETTRUP, A. 2003. A study on combustion of Chinese coals by TA/MS. *Journal of Analytical and Applied Pyrolysis,* 67 (2):393-406, May.

LUCHT, L.M., LARSON, J.M. & PEPPAS, N.A. 1987. Macromolecular-structure and glass-transition temperature. *Energy Fuels,* 1:56.

MAHIDIN, OGAKI, Y., USUI, H. & OKUMA, O. 2003. The advantages of vacuum-treatment in the thermal upgrading of low-rank coals on the improvement of dewatering and devolatilisation. *Fuel Processing Technology,* 84(1-3):147-160, Nov.

MA, S., HILL, J.O. & HENG, S. 1989. A thermal analysis study of the combustion characteristics of Victorian brown coals. *Journal of Thermal analysis,* 35:1985-1996.

MURRAY, J.B. & EVANS, D.G. 1972. The brown-coal/water system: Part 3. Thermal dewatering of brown coal. *Fuel,* 51(4):290-296, Oct.

NDAJI, F.E., BUTTERFIELD, I.M. & THOMAS, K.M. 1997. Changes in the macromolecular structure of coals with pyrolysis temperature. *Fuel,* 76(2):169-177, Jan.

NDAJI, F.E. & THOMAS, K.M. 1995. The effects of oxidation on the macromolecular structure of coal. *Fuel,* 74(6):932-937, June.

NISHIOKA, M. 1994. Molecular mobility of high-volatile bituminous coals accompanying drying. *Fuel,* 73(1):57-62, Jan.

NUGROHO, Y.S., MCINTOSH, A.C. & GIBBS, B.M. 2000. Low-temperature oxidation of single and blended coals. *Fuel,* 79(15):1951-1961, Dec.

PENNER, S.S. 2006. Steps toward the hydrogen economy. *Energy,* 31:33-43.

PODDER, J., HOSSAIN, T. & MANNAN, Kh.M. 1995. An investigation into the thermal behaviour of Bangladeshi coals. *Thermochimica Acta,* 255:221-226, May 1.

POTTER, O.E. & KEOGH, A.J. 1981. Drying high-moisture coals before liquefaction or gasification. *Fuel Processing Technology,* 4(2-3):217-227, May.

RUSTSCHEV, D. 1976. Chemistry of solid fuel. L. Khimiya, 254 p.

SAHIMI, M. & TSOTSIS, T.T. 1988. Statistical modelling of gas-solid reaction with pore volume growth: Kinetic regime. *Chemical Engineering Science,* 43(1):113-121.

SAHU, S.G., SARKAR, P., CHAKRABORTY, N. & ADAK, A.K. 2010. Thermogravimetric assessment of combustion characteristics of blends of a coal with different biomass chars. *Fuel Processing Technology,* 91:369-378.

SARANCHUK, V., BUTUZIVA, L. & MINKOVA, V. 1993. Thermochemical destruction of brown coals. Naukova Dumka: Kiev, 222 p.

SAXENA, S.C. 1990. Devolatilisation and combustion characteristics of coal particles. *Progress in Energy and Combustion Science,* 16(1):55-94.

SERAGELDIN, M.A. & PAN, W. 1984. Coal analysis using thermogravimetry. *Thermochimica Acta,* 76(1-2):145-160, May 15.

SNYMAN, C.P. Red. 1996. Geologie vir Suid-Afrika. Pretoria: University of Pretoria, 608 p.

SOLOMON, P.R., FLETCHER, T.H. & PUGMIRE, R.J. 1993. Progress in coal pyrolysis. *Fuel,* 72(5):587-597, May.

SOTIRCHOS, S.V. & YU, H. 1985. Mathematical modelling of gas-solid reactions with solid product. *Chemical Engineering Science,* 40(11):2039-2052.

SPALDING, D.B. 1951. Combustion of fuel particles. *Fuel,* 30(6):121-130, June.

STIEGEL, G.J. & RAMEZAN, M. 2006. Hydrogen from coal gasification: An economical pathway to a sustainable energy future. *Coal Geology,* 65:173-190.

STREET, P.J., WEIGHT, R.P. & LIGHTMAN, P. 1969. Further investigations of structural changes occurring in pulverized coal particles during rapid heating. *Fuel,* 48(4):343-365, Oct.

STREZOV, V., LUCAS, J.A. & STREZOV, L. 2004. Experimental and modelling of the thermal regions of activity during pyrolysis of bituminous coals. *Journal of Analytical and Applied Pyrolysis,* 71(1):375-392, March.

SUUBERG, E.M., OTAKE, Y. & DEEVI, S. 1988. The macromolecular structure of coal – Its relationship to diffusion and reaction processes in coals. *American Chemistry Society and Division for Fuel Chemistry Preprints,* 33(1):387-394.

TAO, D., GROPPO, J.G. & PAREKH, B.K. 2000. Enhanced ultrafine coal dewatering using flocculation filtration processes. *Minerals Engineering,* 13(2):163-171, Feb.

TSAI, C.Y. & SCARONI, A.W. 1987. The structural changes of bituminous coal particles during the initial stages of pulverized-coal combustion. *Fuel,* 66(2):200-206, Feb.

ÜNAL, S., WOOD, D.G. & HARRIS, I.J. 1992. Effects of drying methods on the low temperature reactivity of Victorian brown coal to oxygen. *Fuel,* 71(2):183-192, Feb.

VAN DER MERWE, D. & CAMPBELL, Q.P. 2002. An investigation into the moisture absorption properties of thermally dried South African fine coal. *The Journal of The South African Institute of Mining and Metallurgy,* 102(7):417-420, October.

VAN DER WALT, P.J. 1984. Coal washing in South Africa. Johannesburg: University of the Witwatersrand. 1-22 p.

VAN KREVELEN, D.W. 1993. Coal. 3rd ed. Amsterdam: Elsevier. 549-600 p.

WAKEMAN, R.J. 1984. Dewatering of filter cakes: Vacuum and pressure dewatering. Devon. U.K. : University of Exeter. 420p.

WENZEL, L. & WHITE, R.R. 1951. Drying granular solids in superheated steam. *Industrial Engineering Chemistry,* 43(8):1829-1837, Aug.

WILDEGGER-GAISSMAIER, A.E. & AGARWAL, P.K. 1990. Drying and devolatilisation of large coal particles under combustion conditions. *Fuel,* 69(1):44-52, Jan.

WINTER, F., PRAH, M.E. & HOFBAUER, H. 1997. Temperatures in a fuel particle burning in a fluidized bed: The effect of drying, devolatilisation, and char combustion. *Combustion and Flame,* 108(3):302-314, Feb.

WOON, T.S. 1980. Oil slurry dewatering of brown coal lithotypes. Australia: University of Melbourne. (Thesis – M.Eng.Sc.).

WU, Z., XU, L., WANG, Z. & ZHANG, Z. 1998. Catalytic effects on the ignition temperature of coal. *Fuel,* 77(8):891-893, June.

YU, J., STREZOV, V., LUCAS, J. & WALL, T. 2003. Swelling behaviour of individual coal particles in the single particle reactor. *Fuel,* 82(15-17):1997-1987, Oct.-Dec.

YUN, Y. & SUUBERG, E.M. 1993. New applications of differential scanning calorimetry and solvent swelling for studies of coal structure: prepyrolysis structural relaxation. *Fuel,* 72(8):1245-1254, Aug.

YOSHIDA, T. & HYÕDÕ, T. 1970. Evaporation of water in air, humid air and superheated steam. *Industrial and Engineering Chemistry Process Design and Development,* 9(2):207-214.